Alma Mater Studiorum – Università di Bologna

DOTTORATO DI RICERCA IN

ONCOLOGIA, EMATOLOGIA E PATOLOGIA

Ciclo 34

Settore Concorsuale: 06/A2 - PATOLOGIA GENERALE E PATOLOGIA CLINICA

Settore Scientifico Disciplinare: MED/04 - PATOLOGIA GENERALE

CYTOTOXIC EFFECT OF IMMUNOTOXINS IN 2D AND 3D MODELS OF SARCOMA

Presentata da: Dott.ssa Giulia Calafato

Coordinatore Dottorato

Prof.ssa Manuela Ferracin

Supervisore

Prof. Andrea Bolognesi

Esame finale anno 2022

Abstract

Sarcomas are one of the most common types of cancer in children and comprise more than 50 heterogeneous histotypes. The standard therapeutic regimen, which includes surgery, chemotherapy and radiotherapy, does not often prove to be decisive. To improve patient outcome, alternative therapeutic strategies are being evaluated. Among these, RIP-containing immunotoxins (ITs) represent an innovative approach because of their high tumor specificity and cytotoxicity. Recently, in order to evaluate the efficacy of new drugs and develop personalized therapeutic protocols, three-dimensional models (i.e. spheroids and organoids) are emerging as valid tools in cancer research. My PhD project aimed to evaluate the cytotoxic effect of specific ITs, Tf-SO6, αEGFR1-Ocy and αHer2-Ocy, directed against TfR1, EGFR1 and Her2, in 2D (adherent cells) and 3D models (spheroids and organoids) of sarcoma. The results obtained showed that TfR1, EGFR1 and Her2 are highly expressed in our sarcoma models, and could be a possible target for immunotherapy. All tested ITs showed high specific cytotoxicity in 2D and 3D models, with IC_{50} values in nM range. Caspase 3/7 are highly activated after IT treatments in all cell models, but with different timing.

Index

Chapter 1 – Introduction

1.1 Ribosome-inactivating proteins (RIPs)

1.1.1   General properties

The term Ribosome-Inactivating Proteins (RIPs), introduced for the first time by Prof. Fiorenzo Stirpe, refers to a family of toxins able to irreversibly inactivate eukaryotic ribosomes [1]. Acting as RNA *N*-glycosylases (EC 3.2.2.22), RIPs can remove one or more adenines from 28S rRNA, thus irreversibly blocking cell protein synthesis, leading to cell death [2, 3]. Subsequently, it has been reported that RIPs can act on other polynucleotide substrates such as DNA, non-ribosomal RNAs, poly(A) and other substrates [4]. Moreover, it has been showed that RIPs can also remove adenine on poly(ADP-ribosyl)ated substrates, justifying the denomination of adenine:polynucleotide glycosylases [5]. RIPs are largely present in different plant families, as well as in some fungal and bacterial species [6]. Despite their biological activity has been studied for many years, the physiological role of RIPs in plants is not completely understood; nevertheless, some hypothesize that they could have a role in plant defense against biotic and abiotic stressors [7, 8]. Among those plant toxins already characterized, the most known are saporin, ricin, abrin, ebulin, nigrin, trichosanthin and volkensin. Shiga and Shiga-like toxins are bacterial RIPs produced as virulence particle by gram-negative pathogenic bacteria, to support their survival, as well as replication in the host organisms [9, 10]. RIPs are also present in different types of fungal species, such as *Calvatia caelata*, *Hypsizigus marmoreus*, *Flammulina velutipes*, *Lyophyllum shimeiji*, and *Pleurotus tuber-regium*, from which toxins have been purified [11, 12]. α-sarcin, isolated from *Aspergillus giganteus,* represents one of the best characterized mushroom RIPs. Injection, inhalation or ingestion of some of these toxins can be poisonous for human and animals leading to irreversible inhibition of cellular protein synthesis with presence of inflammation and acute necrosis of intoxicated tissues [13]. For their ability to act on multiple molecular targets, RIPs have a high antitumor potential. A common feature of many RIPs is their extraordinarily high level of potency... However, this is a double-edged sword as toxicity is achieved in both healthy and malignant cells, meaning that these toxins must be efficiently targeted to cancer cells to convey specific anticancer activity. Although they are characterized by high cytotoxicity, RIPs lack the selectivity necessary for a therapeutic use because they can act in both healthy and malignant cells [14]. Increased specificity and cytotoxic efficacy can be achieved by conjugation of RIPs to monoclonal antibodies (mAbs) or other carriers to form the so-called immunotoxins (ITs) [15, 16]. Most RIPs have been studied, in various fields,

also as antiviral, antifungal, insecticidal and abortifacient agents [17]. In Chinese medicine, RIPs have been exploited to induce abortion and to treat hydatidiform moles [18]. In medicine, in addition to ITs, plant toxins have been also investigated for their ability to inhibit proliferation of viruses (HIV, HBV, HSV), with a major focus on HIV. Unfortunately, clinical trials performed on HIV+ patients did not lead to successful results [19, 20]. In agriculture, DNA recombinant biotechnology have been used to manage the levels of plant endogenous RIPs or introducing a RIP gene derived from another plant, in order to significantly increase plant resistance to different biotic or abiotic agents [21].

1.1.2 Classification

According to their physical characteristic and the presence or absence of a lectin-like chain, RIPs are divided into three groups: type 1, 2 and 3. The first group comprehends toxins consisting of an enzymatically active single polypeptide chain of about 30 kDa. Type 2 RIPs include proteins with a molecular weight of 60-65 kDa, composed by two polypeptide chains: an A-chain with active enzymatic activity linked by hydrophobic interactions and one disulfide bond to a B-chain, which act as lectin [22]. Differently from type 1 RIPs, the presence of the B-chain facilitates the internalization of toxin inside the cell, by interacting with glycoconjugates on the cell surface [23, 24, 25]. Type 3 RIPs are composed by an enzymatically active polypeptide chain linked to a peptide domain with unknown functions. Although its function is not yet well-characterized, this additional chain needs to be removed to activate RIPs [26]. Type 3 RIPs includes only two proteins: b-32 from *Zea mays* (corn) and JIP60 from *Hordeum vulgare* (barley) [27, 28]. A schematic representation of structural comparison among described groups of RIPs is reported in Figure 1.
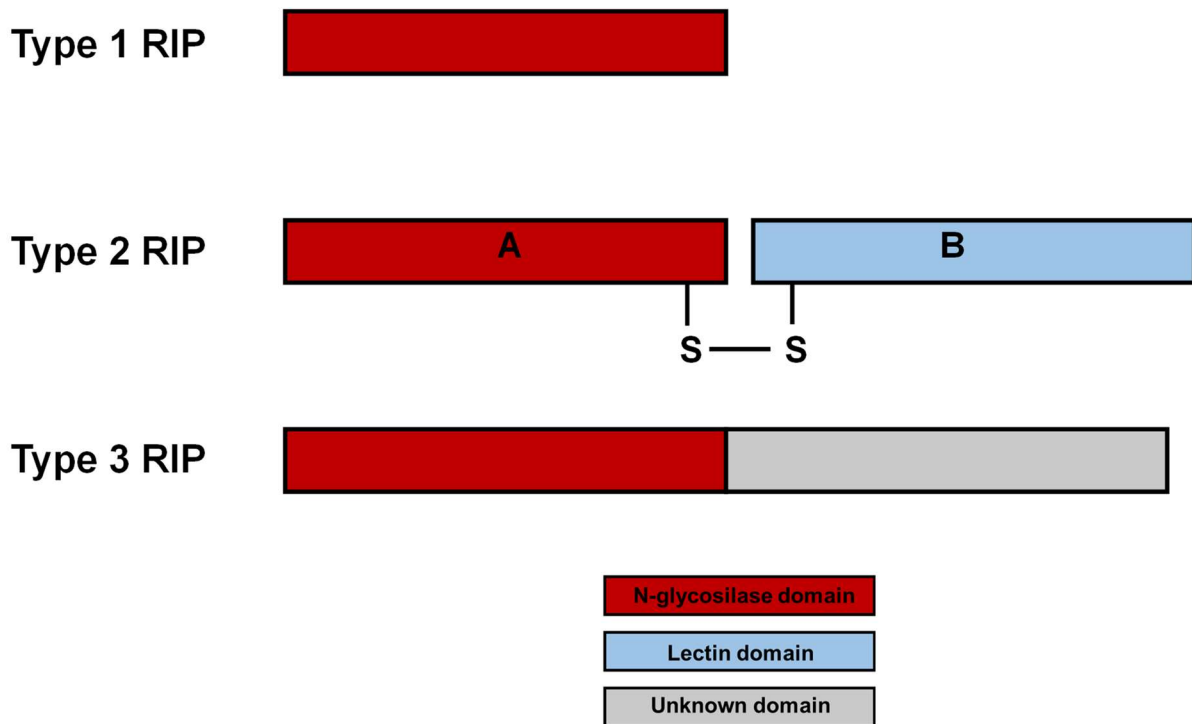
Figure 1. Classification of RIPs. Overview of the structural composition of type 1, 2 and 3 RIPs.

Type 1 RIPs

Type 1 RIPs are widespread in nature and have been purified and characterized from different family plants as *Caryophyllaceae*, *Cucurbitaceae*, *Euphorbiaceae*, *Phytolaccaceae* and *Lauraceae* (Table A) [29]. Notable examples of type 1 RIPs are saporin (from *Saponaria officinalis* L.), pokeweed antiviral protein (PAP, from *Phytolacca Americana*), ocymoidine (from *Saponaria ocymoides*), dianthin (from *Dianthus caryophyllus*), momordin (from *Momordica charantia*) and gelonin (from *Gelonium multifluorum*). RIPs belonging to the first group are single-chain enzymes with a pI≥9.5. Except for those from *Poaceae*, the majority of them are synthesized, starting from intron-less genes, as pre-proteins composed by a signal peptide, the mature toxin and a C-terminal extension [30]. After the process of synthesis, RIPs leave the endoplasmic reticulum (ER) and are secreted from cells following the secretory pathway or addressed and segregated into vacuoles [31]. Localization studies have been performed only for a few type 1 RIPs; for example, in *Saponaria officinalis* seeds, the well-known saporin is located in the intercellular spaces, between the primary cell wall and the plasmalemma and the vacuole of the periplasmic cells [32]. The protocol of purification of

type 1 RIPs, exploiting their p*I* in the alkaline region, is generally made by cation-exchange chromatography on carboxymethyl or sulfopropyl-derivatized matrices [33].

Table A. Type 1 RIPs from different family plant. The table has been modified from Schrot et al., 2015.

Caryophyllaceae		
Agrostemma githago	Agrostin 2,5 e 6	seeds
Dianthus barbathus	Dianthin 29	leaves
Dianthus caryophyllus	Dianthin 30 e 32	leaves
Dianthus sinensis	RIP 1,2,3	leaves
Lychnis chalcedonica	Lychnin	seeds
Saponaria ocymoides	Ocymoidine	seeds
Saponaria officinalis	Saporin S5, S6, S8, S9	seeds
	Saporin L1, L2	leaves
	Saporin R1, R2, R3	roots
Vaccaria pyramidata	Pyramidatine	seeds
Cucurbitaceae		
Benincasa hispida var. chieh-qua	Hyspidin	seeds
Bryonia dioica	Bryodin-L	leaves
	Bryodin 1 e 2	roots
Luffa acutangula	Luffaculin	seeds
Luffa aegyptiaca	LRIP (Luffin c)	seeds
Luffa cykubdruca	Luffin a e b	seeds
Luffa cylindrica	Luffin S	seeds
	Luffacilina	seeds
Momordica balsamina	Momordin II	
Momordica charantia	Momordin I	seeds
	α, β MMC	seeds
	Charantin	seeds
Momordica cochinchinensis	Momorcochin S	seeds
	Momorcochin R	roots
Trichosanthes cucumerina	Trichoanguin	seeds
Trichosanthes cucumeroides	B trichosanthin	roots
Trichosanthes kirilowii	S-Trichokirin	seeds
	Trichosanthin TAP29	roots
	TCS α, β, γ	
Euphorbiaceae		
Croton tiglium	Crotin I e II (2, 3)	seeds
Gelonium multiflorum	Gelonin (GAP)	
Jatropha curcas	Curcin 2	seeds
Manihot palmat	Mapalmin	seeds
Manihot utulissima	Manutin 1 e 2	seeds
Phytolaccaceae		
Phytolacca americana	PAP I, PAP II	leaves
	PAP-S1 e S2	seeds
	PAP-R	roots
Phytolacca dioica	PD-S1, S2, S3	seeds
	PD-L1, L2, L3, L4	leaves
Phytolacca dodecera	Dodecandrin	leaves
Phytolacca acinosa	PAP	
Phytolacca insularis	PIP	leaves
	PIP 2	cdna
Lauraceae		
Cinnamomun camphora	Camphorin	seeds

Type 2 RIPs

Type 2 RIPs include toxins composed of two (heterodimeric) or four chain (tetrameric), with a molecular weight of about 60 kDa or 120 kDa, respectively (Table B). The heterodimeric RIPs are composed by an enzymatic active site, named A-chain, linked through a disulphide bond and other non-covalent bonds to a galactose-specific lectin domain, known as B-chain [34]. Abrin, modeccin, ricin, volkensin and stenodactylin belong to this subclass. The tetrameric toxins are the result of the union of two heterodimers by an additional disulfide bond between the two B-chains. This structure has been reported for Ricinus agglutinin (RCA) [35]. Ricin is the most characterized type 2 RIP. Many studies have been conducted to investigate the ricin mechanisms of biosynthesis and it is plausible that this aspect can be translated to all type 2 RIPs. In castor bean seeds, ricin is synthetized as a preprotein, known as preproricin, composed of a signal peptide, the A and the B-chains linked through a 12-residue linker peptide. The preproricin is translocated to the ER lumen thanks to the signal peptide which, after this, is removed and the N-glycosylation of four exposed asparagine residues occurs. Immediately after, the formation of disulfide bridges occurs, to obtaining the proricin. Using the 12-residue linker peptide between A-chain and B-chain as a signal peptide, proricin is translocated into the Golgi to finally reach protein storage vacuoles. Here the proteolytical cleavage of signal peptide occurs to form the mature toxin. Following these steps, the toxin becomes active only when it arrives to the storage compartments, as cells would prevent any activation of RIP in the cytoplasm [36, 37 38]. Type 2 RIPs are generally more cytotoxic than type 1 [39]. This is related to the presence of B-chain which facilitate the translocation of the A chain into the cytosol through the binding to galactose-containing glycoproteins and/or glycolipids present on the cell surface. Interestingly, several non-toxic type 2 RIPs have been described. This subclass is not cytotoxic to cultured cells in vitro, but shows high inhibiting effect on protein synthesis in cell-free systems [40]. This may be related to the low affinity of B-chain for membrane galactosyl residues which compromises their intracellular uptake [41]. The lectin properties of their B-chains are fundamental for the purification of type 2 RIPs. Indeed, it is performed by affinity chromatography on Sepharose, acid-treated Sepharose or other galactose-containing stationary phases. Elution step of bound protein is performed using galactose or lactose.

Table B. Type 2 RIPs from different plant families. The table has been modified from Schrot *et al*., 2015.

Euphorbiaceae		
Ricinus communis	Ricin (D, E) RCA (Ricinus communis agglutinin)	Seeds
Fabaceae		
Abrus precatorius	Abrin a, b, c, d	Seeds
Abrus pulchellus	Pulchellins	Seeds
Iridaceae		
Iris holleica	IRA-b e IRA-r	bulbs
Lauraceae		
Cinnamomum, camphora	cinnamomin	seeds
Cinnamomum porrectum	porrectin	seeds
Liliaceae		
Poligonatum multiflorum	PMRIPm e PMRIPt	leaves
Passifloraceae		
Adenia volkensii	Volkensin	roots
Adenia stenodactyla	Stenodactylin	caudex
Adenia digitata	Modeccin 4B and 6B	roots
Ranunculaceae		
Eranthis hyemalis	EHL, *Eranthis hyemalis lectin*	bulbs
Sambucaceae		
Sambucus ebulus	Ebulin l	leaves
	Ebulin r1 e r2	rizhome
	Ebulin f	fruits
Sambucus nigra	Nigrin f, SNA-If	fruits
	Nigrin b, SNAI, SNAI', Basic Nigrin b, SNLRP1 2	barks
	Nigrin l1 e l2, SNAld	leaves
	Nigrin s, SNAIII	seeds
Sambucus racemosa	Basic racemosin	barks
Sambucus sieboldiana	Sieboldin b and SSA	barks
Viscaceae		
Phoradendron californicum	PCL, *Phoradendron californicum lectin*	leaves
Viscum album	MLI (viscumin), II, III	leaves

Type 3 RIPs

Type 3 RIPs include only two proteins, b-32 and JIP60, purified from maize and barley, respectively [42]. As for type 1 and 2, type 3 RIPs need to undergo proteolytic cleavage after

being synthetized as single-chain inactive precursors. The sequence of type 3 RIPs gene does not contain the signal peptide, indicating that these proteins are synthesized on free-polysomes in the cytoplasm [43]. To date, the function of the extra domains in the type 3 RIPs remains unknown [44].

1.1.3   Mechanism of cell entry

Type 1 RIPs, being devoid of a B chain, enter with difficulty into cells and consequently are less toxic than type 2 RIPs [45]. Differently from type 1, type 2 RIPs are facilitated in the binding of cell surface because of the presence of the lectin B-chain that, interacting with cell surface galactose-containing glycoproteins and glycolipids, promotes toxin entry into the cell [46]. In addition, type 2 RIPs carbohydrate side chains can also bind the mannose cell receptors [47]. These characteristics explain why there are differences in the cytotoxicity toward in vitro and in vivo systems between type 1 and type 2 RIPs [48]. The studies about mechanism of entry have been mostly carried out on ricin. Nevertheless, it is very likely that other type 2 RIPs follow the same process [49]. After binding to cell surface, toxin reaches the endosomal compartment through clathrin-dependent or independent mechanisms [50]. Once inside the cell, RIP has 3 possible faiths: toxin could be recycled to cell surface, eliminated in the lysosomes or translocated to the Golgi [51]. Most of the toxins reach the Golgi apparatus and the endoplasmic reticulum (ER) lumen, where the disulfide bond that links the two chains of the RIP is reduced [52]. From here, some of the toxin reaches the cytosol as final destination while the rest is unfolded and degraded via the ER-associated degradation pathway (ERAD) [53]. The low number of lysines present on RIPs protects them from the degradation activity of the ERAD machinery located on the ER [54]. The mechanism of entry of type 1 RIPs into the cell have been investigated in some studies, reported below, even if the process has not been completely elucidated. Some researcher reported that endocytosis of type 1 RIPs could occur by pinocytosis [55] or, similarly to type 2 RIPs, through the interaction between either galactosyl residues or the mannose receptor on the cell membrane [56, 57]. In a comparison study between the endocytosis mechanism of ricin and saporin, it has been reported that the type 1 RIP follows a Golgi-independent pathway to the cytosol allowing the internalization of the toxin without receptor binding and recently, it has been observed its nuclear localization [58, 59]. Instead, PAP presents a mechanism intracellular routing similar to type 2 RIPs [60].

1.1.4 Biological activity

RIPs can irreversibly inactivate ribosomes through a RNA N-glycosylase enzymatic activity, causing the inhibition of protein synthesis [61]. Although it has long been considered the only mechanism of cell death, several other strategies through which RIPs can induce cell death have been reported; indeed, the majority of them are a consequence of rRNA damage, while others are independent from it [62].

<u>Glycosylase activity</u>

RIPs are officially classified as rRNA N-glycosylases (EC 3.2.2.22) [63]. RIPs exert their activity via a two-step mechanism: RIPs recognize a specific and conserved region present on 28S rRNA, then they cleave a specific *N*-glycosidic bond between one adenine and the ribose on the rRNA. Endo and co-workers first described this activity on rat liver ribosomes treated with ricin, showing that the A_{4324} was specifically removed from a highly conserved sequence of 14 nucleotides, called GAGA loop, present at the top of a stem region of the 28S rRNA in a universally conserved loop (sarcin/ricin loop, SRL) [64]. This region is important for the interaction between ribosome and elongation factors. Indeed, the adenine removal exposes the apurinic site, preventing the GTPase-dependent binding of elongation factor-1 (EF-1) and 2 (EF-2) to the 60S subunit of the ribosome, thus blocking the translation and inhibiting protein synthesis [65]. RIP mechanism of action is schematized in Figure 2. Although all RIPs possess this enzymatic activity, there are differences in the substrate affinity. Indeed, while ricin exterts its activity on mammalian and yeast ribosomes, but not on bacterial or plant ones, PAP can deadenylate ribosomes from bacteria, plant and yeast. This may be due to a different interaction of the toxin with ribosome, limiting accessibility to the GAGA sequence [66, 67]. Interestingly, some RIPs, as saporin and PAP, can remove more than one adenine at the time, inducing multiple depurination [68].
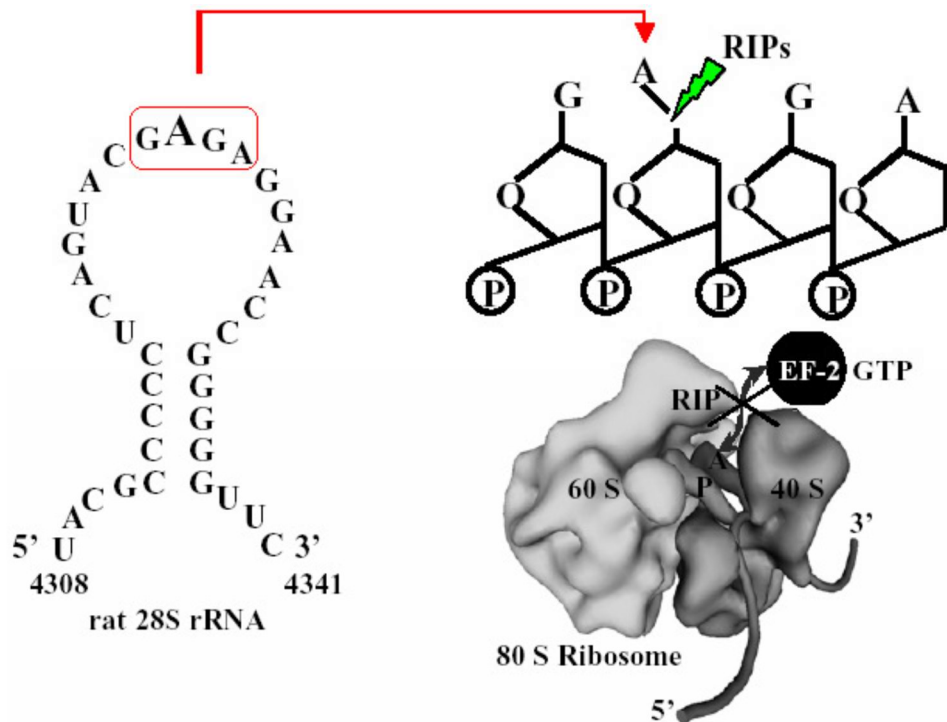
Figure 2. Schematic representation of RIP enzymatic activity (from Girbés *et al*., 2004).

Polynucleotide:adenosine glycosylase activity (PNAG)

In 1997, Barbieri and colleagues demonstrated that RIPs can also act on other polynucleotide substrates such as herring sperm DNA, polyA and RNAs from different sources. Due to this, they proposed the term polynucleotide:adenosine glycosidases (PNAG) [69]. RIPs show significant PNAG activity, even if is not the same among them; the reduction of the disulfide bridge of type 2 RIPs does not induce and increment PNAG activity, which is generally lower compared to type 1 RIPs [70]. In addition, it was reported that RIPs also depurinate poly(ADP-ribosyl)ated poly(ADP-ribose) polymerase, which is part of the DNA repair machinery. [71]. Last, some RIPs possess also a guanosine glycosidase activity, meaning that they are able to remove guanosine either from prokaryotic or eukaryotic rRNA [72, 73].

RIPs and cell death mechanisms

Protein synthesis inhibition that causes necrosis on RIP-treated cells was initially considered the only mechanisms through which RIPs could lead to cell death [74]. However, it was later demonstrated that, in addition to necrosis, RIPs can also induce apoptosis. The ability of RIPs to induce apoptosis was first observed in 1987, when it was shown that ricin and abrin were able to induce apoptosis in rat tissues, as intestine and lymphnodes [75]. Years later, it was

reported that several other RIPs, such as saporin, pokeweed anti-viral protein from seeds (PAP-S) and momordin were able to kill cells through apoptosis [76]. RIP-treated cells undergo apoptosis through different mechanisms, such as the loss of mitochondrial transmembrane electrical potential gradient ($\Delta\psi$m), caspase activation and modulation of regulatory apoptotic proteins [77, 78]. Despite the progress made, the mechanism of RIP-induced apoptosis, as well as the correlation between RIP enzymatic activity and apoptosis, remains an open question. Indeed, some researchers showed that protein synthesis inhibition is necessary to trigger apoptosis, while others indicate that programmed cell death occurs independently from protein synthesis inhibition [79, 80]. To date, it is clear that the N-glycosylase activity is not the only mechanism through which apoptosis can be triggered. Indeed, alternative pathways involved in the induction of apoptosis were proposed: the ribotoxic stress response, the ER-stress with the activation of unfolded protein response (UPR) genes, the interactions with anti-oxidant proteins and the production of reactive oxygen species [81, 82]. Depending on cell type, all these pathways could interact in RIP-induced apoptosis in different ways and moments. Depurinating rRNA, RIPs are able to activate the ribotoxic stress response through activation of mitogen-activated protein kinases (MAPKs), thus inducing apoptosis. Iordanov and colleagues first reported that ricin and α-sarcin had the ability to induce the activation of SAPK/ JNK and p38 MAPK in response to specific damage to 28S rRNA independently from protein synthesis inhibition. Induction of the ribotoxic stress response required actively translating ribosomes at the time of ribosome damage, activation of p38 and extracellular signal-regulated kinases (ERKs) together with JNKs [83]. Moreover, an increased expression of pro-inflammatory proteins, such as IL-8, GRO-α, IL-1β and TNF-α, as well as pro-apoptotic genes, was observed after activation ribotoxic stress response [84]. It is still unclear how cells detect the damage on rRNA and induce signaling activation. A study showed that inhibition of JNK pathway in ricin-treated epithelial cell line reduced caspase activation and poly(ADP-ribose) polymerase cleavage, showing how JNK is crucial for apoptosis induction [85]. Another study indicated that in ricin or modeccin-treated RAW 264.7 cells, inhibition of p38 MAPK strongly prevented the release of TNF-α, thus reducing RIP-induced apoptosis [86]. All together these results indicate that ribotoxic stress response may induce multiple signal transduction pathways through the activation of p38 MAP kinase, which leads to TNF-α release and apoptosis. ER stress and the consequent unfolded protein response (UPR) is another alternative pathway proposed to explain RIP-induced apoptosis. The folding and maturation of newly synthesized secretory

and transmembrane proteins occur in the ER. When the normal activity of ER is perturbed, a process, known as "ER stress" induces UPR, which further determines transitory protein translation arrest and transcription of selected genes in order to preserve ER function. If ER perturbation is acute or prolonged, UPR triggers apoptotic signaling [87]. The presence of a large quantity of misfolded proteins induces the activation of ER transmembrane proteins PERK, IRE1 and ATF6, through the dissociation of Grp78 [88]. The activated PERK phosphorylates the eIF2α (eukaryotic translation initiation factor 2α), inhibiting protein synthesis leading to growth arrest and promoting the transcription of activating transcription factor 4 (ATF4), which further activate UPR genes in the nucleus [89]. Cleaved, activated ATF6 translocates in the nucleus where it activates UPR and ERAD genes, including the transcription factor XBP-1 (X-box binding protein 1), whose mRNA is alternatively spliced by IRE-1 and the resulted product upregulates UPR "stress genes" in the nucleus [90]. MDA-MB-231 and HCT116 cell lines treated with type 2 RIPs showed dose depended enhanced activation of UPR genes as well as apoptosis, suggesting that RIP is involved in ER stress with subsequent induction of apoptotic pathway [91]. RIPs are able to also induce apoptosis by increasing the reactive oxygen species (ROS) and by interacting with anti-oxidant proteins. Trichosanthin-treated choriocarcinoma cells (JAR cells) shows massive ROS production possibly linked to calcium signaling, as ROS and calcium levels increase in a concomitant way [92]. In U937 cells, mistletoe lectin II (MLII) toxin induced high levels of hydrogen peroxide, which activated the intracellular stress signaling and JNK/SAPK pathways, with apoptosis. ROS scavenger treatment resulted in a great reduce of apoptosis [93]. U937 also showed an increase of ROS with the presence of DNA damage after low dose abrin exposure [94]. In addition, it was reported that abrin inhibits the mitochondrial antioxidant protein-1 (AOP-1), leading to increase of intracellular ROS and the release of cytochrome c from the mitochondria to the cytosol, thus activating caspase-9 and -3 [95].

Antiviral activity

Type 1 and some type 2 RIPS have anti-viral activity towards plant, fungal and animal DNA and RNA viruses, but the exact mechanism through which it happens is still unclear [96]. Some of the first studies reported that RIPs were active against viruses as poliovirus, influenza and herpes simplex virus [97]. Initially it was believed that RIPs could act directly on rRNA of infected cells, with consequent cell death and arrest of viral proliferation [98]. It was later discovered that RIP-induced ribosome inactivation is not linked to their antiviral activity [99]. Indeed, two non-toxic recombinant mutants of PAP are able to depurinate HIV-1

RNA in a much better way compared to cellular rRNA [100]. The antiviral activity of RIPs towards cytomegalovirus (CMV)-infected cells was demonstrated using two immunotoxins formed by gelonin or deglycosylated ricin A chain (dgA) linked to immunoglobulins specific for CMV. After conjugation, RIPs showed a selective cytotoxic effect on CMV-infected cells [101, 102]. RIP antiviral efficacy was also tested in phase I/II clinical trials using RIPs and RIP-based immunotoxins, especially to treat HIV patients, without success [103].

1.2 RIP use in experimental and clinical medicine

Due to their ability to induce antitumor activity, RIPs have been investigated for experimental or clinical use in medicine [104, 105]. RIPs have a high antitumor potential for their ability to act on multiple molecular targets [106]. Although they are highly cytotoxic, RIPs lack the selectivity necessary for a therapeutic use which renders the use of these toxin unsafe in clinical practice. The importance of RIPs in medicine is related to the possibility of directing them against a specific population of unwanted cells, as malignant cells, with the aim to selectively eliminate them [107]. Increased specificity and cytotoxic efficacy can be achieved by conjugation of RIP to monoclonal antibodies (mAb) forming the so-called immunotoxins (ITs). ITs have been investigated in disease such as cancer or autoimmune disorders [108, 109]. Other carriers can be used for conjugation as hormones, growth factors, cytokines, interleukins, antigens and vitamin-binding proteins; however, the best results were obtained using monoclonal and polyclonal antibodies [110].

1.2.1   RIP-containing immunotoxins for anti-cancer therapy

The term "immunotoxin" is generally used for a toxin linked to an antibody, while toxins linked to other carriers are commonly known as "chimeric toxins" or "conjugates". IT-efficacy is influenced by cell type, antigen availability, binding affinity and intracellular routing. ITs can be obtained by chemical coupling of native toxins to antibody moieties by the formation of disulphide bonds between the toxin and the carrier [111]. After binding of the antibody to the target cell surface, IT is internalized through receptor-mediated endocytosis. In the endosome, the bond between antibody and toxin is reduced, allowing the free toxin moiety to reach the cytosol and exert its enzymatic activity [112]. Chemically linked ITs are stable but heterogeneous and poorly suitable for clinical practice and commercialization. New generation ITs are synthesized through recombinant DNA techniques, using modified toxins and antibody fragments (as single-chain variable fragments, scFvs) [113]. IT-based therapy was used in the experimental treatment of cancer and autoimmune disorders, with several

preclinical studies and clinical trials showed a great efficacy of IT, but the best results were obtained towards hematological malignancies [114, 115, 116]. Among type 1 and type 2 RIPs, saporin, abrin and ricin are the most used to produce ITs. Type 1 RIPs have the advantage of being less dangerous, more stable and easier to conjugate than type 2 RIPs [117]. Different type 1 RIPs have been employed in the construction of ITs, sometimes resulting more efficient than those containing type 2 RIPs [118, 119]. Saporin-S6 is the most utilized type 1 RIP for the construction of ITs [120]. The efficacy of immunotoxins consisting of monoclonal anti-idiotype conjugated to saporin has been evaluated in the treatment of guinea pig L2C B lymphocytic leukemia [121].Type 2 RIPs are extremely cytotoxic, but the non-specific cell binding of the B-chain represents a problem for clinical use of IT. To face this, different strategies have been suggested, as the use of isolated and/or deglycosylated A chain, modified or blocked B-chain and non-toxic type 2 RIPs as toxic part of IT [122]. Indeed, A-chain ricin (RTA) or blocked RTA were used in patients with T-cell leukemia and lymphomas whereas ITs containing saporin conjugated to an anti-CD30 or anti-CD22 mAbs were investigated for the treatment of patients with Hodgkin's and non-Hodgkin's lymphoma, respectively [123, 124]. Vascular leak syndrome (VLS), hepatotoxicity, immunogenicity as well as the poor penetration of the conjugates into solid tumors represent the major problem observed in patients treated with ITs [125]. VLS is driven by an endothelial damage, which cause an increase of vascular permeability [126]. VLS symptoms are weight gain, edema, hypoalbuminemia, hypotension and sometimes dyspnea [127]. It has been reported that the presence in toxins of short amino acid mofits, which interacting with endothelial-specific integrin, induces the internalization of toxin itself with consequent endothelial cell death [128]. Indeed, when these amino acid motifs are deleted or mutated, toxin-related VLS is reduced [129, 130]. Hepatotoxicity is caused by a multitude of factors and events depending on the type of toxin chosen and uptake process [131]. Another problem of IT patient treatment is related to the onset of an immune response and the impossibility to administrate the conjugate repeatedly, except for patients with an immunodeficient disease. In particular, a patient could either develop antibodies against the mAb portion or the toxic part [132]. The IT-induced immunogenicity can be overcome in different ways; it is possible using ITs with partially or fully humanized antibodies to reduce immune response against mAb portion [133]; immunosuppressive therapies can be infused to reduce IT-associated immune response [134]; in addition, the use of ITs directed against the same antigen but linked to different toxins could reduce immune response against toxin [135]. In some types of solid tumor, the penetration of IT inside tumor mass resulted more difficult [136]. This problem can be

overcome using smaller conjugates where the carrier is an antibody fragments (scFv) or using ITs directed against the endothelial cells of tumor blood vessels, leading to thrombosis and ischemia of the tumor [137]. The use of tenside-like compounds, such as saponins, in combination with ITs, as well as photochemical internalization (PCI) technology are among the other strategies proposed to enhance IT toxicity [138, 139]. Several clinical trials have been conduced to investigate the efficacy of RIP-containing ITs. Anti-CD19 and anti-CD22 conjugated to deglycosylated ricin A-chain (dgA) were evaluated in patients with refractory or relapsed B-cell acute lymphoblastic leukemia (phase I, NCT00450944; NCT01408160) [140]. The anti-CD22 IgG-RFB4-SMPT-dgA immunotoxin was used to treat refractory CD22 positive B-cell lymphoma (phase I, NCT00001271) [141]. An anti-CD33 IT, composed by humanized monoclonal antibody M195 conjugated to recombinant type 1 RIP gelonin (HUM-195/rGEL) completed a phase I clinical trial for the treatment of patients with advanced myeloid malignancies (NCT00038051). Anti-CD25 RFT5-dgA was evaluated in patients with lymphoma/leukemia and metastatic melanoma (phase I, NCT00586547; phase II, NCT00667017; phase II, NCT00314093) [142]. Anti-CD25 RFT5-SMPT-dgA (NCT00025662) was tested to reduce GvHD in patients with myelodysplastic syndromes, leukemia and lymphoma [143].

1.2.2 Immunotoxins in autoimmune disorders

ITs have been also investigated for the treatment of autoimmune disorders [144]. The anti-CD5/RTA was the first IT evaluated in clinical trials for the treatment of rheumatoid arthritis, systemic lupus erythematosus and insulin-dependent diabetes mellitus [145, 146, 147]. Many studies have been conducted by conjugating RIP with antigens that cause autoimmune disease in order to directly interact with the immunocompetent cells [148]. Ricin A-chain was conjugated to the autoantigen thyroglobulin and tested for the treatment of patients with Hashimoto thyroiditis, showing a suppression of thyroglobulin autoantibody response of lymphocytes [149]. Two PAP-containing ITs were tested for the treatment of HIV infection: the first one recognizes viral markers expressed on the surface of infected cells while the second is directed against antigens present on CD4+ lymphocytes, where the virus replicates itself [150]. Gelonin-containing IT directed against the nicotinic acetylcholine receptor 1 was used in the experimental treatment of myasthenia gravis [151]. RIPs-based ITs, such as ATG-saporin-S6 and CTLA-4-saporin-S6, have been also evaluated for the prevention and treatment of graft-versus host disease (GVHD), showing interesting results in pre-clinical models [152, 153].

1.3 Immunoconjugates for sarcoma therapy: preclinical and clinical studies

General characteristics of sarcoma and immunoconjugate (IC)-based therapy for sarcoma treatment, including antibody-drug conjugates (ADCs), immunotoxins (ITs) and radioimmunoconjugates (RICs), have been deeply discussed in the review entitled "Antibody conjugates for sarcoma therapy: how far along are we?", of which I am co-first author [154]. The review aimed to provide a comprehensive overview of the latest advances in IC-based sarcoma immunotherapy and their impact on clinical oncology, showing their anti-tumor efficacy and clinical potential. To date, seven antibody-drug conjugates and two radioimmunoconjugates are under phase 1–2 clinical trials for sarcoma therapy and many other ICs have been evaluated in preclinical studies.

Antibody Conjugates for Sarcoma Therapy: How Far along Are We?

Letizia Polito *,†, Giulia Calafato †, Massimo Bortolotti, Cecilia Chiarelli Olivari, Stefania Maiello and Andrea Bolognesi

Department of Experimental Diagnostic and Specialty Medicine-DIMES, General Pathology Section, Alma Mater Studiorum—University of Bologna, 40126 Bologna, Italy; giulia.calafato2@unibo.it (G.C.); massimo.bortolotti2@unibo.it (M.B.); cecilia.chiarelli@studio.unibo.it (C.C.O.); stefania.maiello2@unibo.it (S.M.); andrea.bolognesi@unibo.it (A.B.)
* Correspondence: letizia.polito@unibo.it
† These authors equally contributed to this work.

Abstract: Sarcomas are one of the most difficult type of cancer to manage and treat because of their extremely heterogeneous molecular and morphological features. Despite the progress made over the years in the establishment of standard protocols for high and low grading/staging sarcoma patients, mostly with chemotherapy and/or radiotherapy, 50% of treated patients experience relapse episodes. Because of this, in the last 20 years, new therapeutic approaches for sarcoma treatment have been evaluated in preclinical and clinical studies. Among them, antibody-based therapies have been the most studied. Immunoconjugates consist of a carrier portion, frequently represented by an antibody, linked to a toxic moiety, i.e., a drug, toxin, or radionuclide. While the efficacy of immunoconjugates is well demonstrated in the therapy of hematological tumors and more recently also of epithelial ones, their potential as therapeutic agents against sarcomas is still not completely explored. In this paper, we summarize the results obtained with immunoconjugates targeting sarcoma surface antigens, considering both preclinical and clinical studies. To date, the encouraging results obtained in preclinical studies allowed nine immunoconjugates to enter clinical trials, demonstrating the validity of immunotherapy as a promising pharmacological tool also for sarcoma therapy.

Keywords: sarcoma; cancer therapy; immunoconjugates; immunotherapy; antibody; drug delivery; ribosome-inactivating proteins; bacterial toxins; radionuclides

1. Introduction

Sarcomas are a heterogeneous-low-incidence group of malignancies that arise from mesenchymal tissue. They comprehend more than 50 histotypes with different molecular biology, epigenetic landscape, and variable response to treatments. Although sarcomas can develop anywhere in the body, they are found mostly in the arms, legs, chest, and abdomen. According to their tissue-origin, sarcomas are classified in two major groups: soft tissue sarcoma (STS) and bone sarcoma (BS).

In 2021, American Cancer Society's estimates show that about 3610 new cases of BS and 13,460 of STS will be diagnosed, with 2060 and 5350 deaths expected, respectively [1]. Epidemiology data indicate that sarcomas have not the same incidence in all age groups, but it is possible to identify two peaks in people <20 years and 65–74 years. For younger people, the percentage of incidence, compared to total sarcoma cases, is 25.1% (BS) and 7.5% (STS). For elder people, this percentage decreases to 13.2% for BS while increases up to 20.3% for STS [2].

The main therapy for sarcoma treatment is surgery accompanied by neoadjuvant or adjuvant chemotherapy/radiotherapy. Standard sarcoma drugs mostly include doxorubicin and ifosfamide, but according to the histological type, cancer staging and grading several other drugs can be used [3].

Over the years, many progresses have been made on STS patients with localized disease at diagnosis, achieving a 5-year relative survival rate of 81.3%. Unfortunately, this rate dramatically drops to 16% in patients with metastasized STS at diagnosis. The 5-year relative survival of patients diagnosed with bone and joint cancer is 66.8% [2]. Approximately 50% of patients with high-grade STS experienced relapse, progression and metastasis after the first-line standard treatment [4]. These data and the heterogeneous nature of sarcomas support the idea that using a personalized therapy instead of a standardized protocol could be a valid strategy to improve the patient's outcome.

Immunotherapy is one of the most promising individualized therapeutic approaches for the treatment of cancer that uses immune system components to fight the disease. Over the years, many clinical trials have reported the effects of antibody-based therapies on a variety of tumors, including sarcoma, in terms of improved overall survival compared to conventional chemotherapy drugs.

2. Immunoconjugates for Targeted Cancer Therapy

Many studies have been conducted to assess the efficacy of monoclonal antibodies (mAbs) in targeted cancer therapy. The specificity of immunotherapy depends on the surface antigen expression of target cells and its cytotoxicity is independent from the parameters that determine the toxicity of chemotherapy and radiotherapy. The selected antigens should have precise characteristics: easy accessibility, high expression on targeted malignant cells, and low or no expression on non-target healthy cells. The main cytotoxic pathways that can be activated after mAbs-antigen binding are: complement-dependent cytotoxicity (CDC) and antibody-dependent cellular cytotoxicity (ADCC), mediated by the Fcγ receptors on effector cells, such as granulocytes, macrophages, and natural killers. Moreover, some antibodies can directly kill the target cell by triggering the apoptotic pathway. However, the antibody cytotoxicity is often limited because of phenomena of CDC and ADCC resistance or selection of apoptosis resistant tumor clones. Two main strategies can be adopted to overcome these obstacles, thus enhancing mAbs efficacy. First, mAbs can be used in combination with standard chemotherapy or administered to patients with highly responding cancer subtypes [5,6]. Second, antibodies can be linked to pharmacologically active molecules, combining the antibody specificity to the therapeutic effects of such molecules. This concept paved the way for the development of immunoconjugates (ICs), which contain anticancer drugs, toxins (from plants or bacteria), or radionuclides. ICs have been evaluated in numerous preclinical studies and in various clinical trials, either administered individually or in combination with conventional chemotherapy [7–9]. ICs are composed of three elements: a carrier molecule (i.e., an antibody or its fragment), a toxic payload, and a linker. After binding to the targeted antigen, the IC is internalized and the toxic payload can exert its pharmacological effect [10]. Choosing an antigen and an antibody should satisfy certain rules. The targeted antigen must be extracellularly exposed and expressed higher on cancer cells rather than healthy ones. The antibody should have high affinity and avidity toward antigen and efficient internalization after binding [11,12].

Various anticancer molecules have been considered for antibody–drug conjugate (ADC) production. The most used agents are distinguished into: (i) DNA-targeting drugs, which lead to DNA alkylation or double-strand break (i.e., duocarmycins, calicheamicins, pyrrolobenzodiazepines, anthracycline, and camptothecin derivatives) and (ii) tubulin-targeting drugs, which block tubulin depolymerization, thus determining cell-cycle arrest into G2/M phase (i.e., monomethyl auristatin E and F, MMAE and MMAF, respectively) [13,14]. Four requirements are essential in addressing the drug choice: potency, stability, water solubility, and easy conjugation. It is crucial to find a balance between drug toxicity, generally with effective concentrations in the nM range, and in vivo systemic tolerability. Moreover, the stability in blood circulation and water solubility of the molecule are necessary to guarantee a proper distribution in body fluids. Lastly, the molecular and chemical structure of the drug should allow the conjugation with the linker, thereby facilitating drug-linker binding to the antibody [15].

In addition to common anticancer drugs, plant or bacteria toxins can be used in IC construction. Ribosome-inactivating proteins (RIPs) are plant toxins able to deadenylate rRNA, thus irreversibly blocking protein synthesis and inducing cell death. Beside ribosomes, RIPs can act on other substrates such as DNA, mRNA, tRNA, and poly(A), whose damage causes the activation of multiple cell death pathways (i.e., apoptosis, necroptosis) and oxidative stress [16,17]. Bacterial toxins are other powerful tools that can be used as payload in IC construction. The most used ones are *Pseudomonas aeruginosa* exotoxin A (PE) and diphtheria toxin, and their truncated forms, which arrest protein synthesis by inactivating the elongation factor 2 through ADP-ribosylation. RIPs or bacterial toxins can be conjugated to an antibody (or its fragment), constituting the so-called immunotoxins (ITs). Over the years, many ITs have been constructed and tested in preclinical and clinical studies in different cancer models, showing promising results both in hematological and solid tumors [18,19]. The use of toxins rather than anticancer drugs in the construction of an IC has some advantages. Being enzymes, toxins act in a catalytic and not in a stoichiometric way as drugs do. Moreover, toxins do not induce drug resistance, a phenomenon that is often observed in patients treated with chemotherapeutics [20]. Lastly, toxins can act on both dividing and non-dividing cells, while most chemotherapeutic drugs only act on proliferating cells [21].

Radionuclides represent another type of payload type used in targeted therapy. In this case, the antibody is (radio)labeled with a radioisotope that emits ionizing particles to obtain a radioimmunoconjugate (RIC). Each particle (α and β^- particles and Auger electrons) is characterized by a specific linear energy transfer, physical half-life, and penetration depth in tumor tissue, thus offering different possibilities of use according to the physical characteristic of the tumor (large tumors, micro-metastasis, single cancer cells) [22,23]. Radioimmunotherapy (RIT) advantages in cancer therapy are represented by the stability and low dimension of (radio)labeled conjugates. RICs can easily reach cancer sites and kill target cells without the typical chemotherapy side effects [24,25]. RICs can act not only on target cells but also on the surrounding ones. This characteristic represents an advantage because also tumor stromal cells and cancer cells with low antigen expression, or expressing mutated antigens, will be eliminated. At the same time, this RIC property is also potentially dangerous because of its aspecific toxicity to normal tissues. Other difficulties are related to RIC manipulation and stability as well as radionuclide half-life. For this reason, it is essential in clinical practice to manage properly radiation intensity, time of exposure, and administration protocol, in order to maximize efficacy and reduce possible damages on radio-sensitive organs such as bone marrow.

The main mechanisms by which drugs, toxins, and radionuclides can damage cancer cells are schematized in Figure 1.

To date, many clinical trials have been conducted to investigate the efficacy and safety of ICs in patients with hematological and solid cancers, administered alone or in combination with other therapeutic agents. In the last 20 years, Food and Drug Administration approved 10 ADCs, 1 IT and 2 RICs for targeted cancer therapy [26–29].
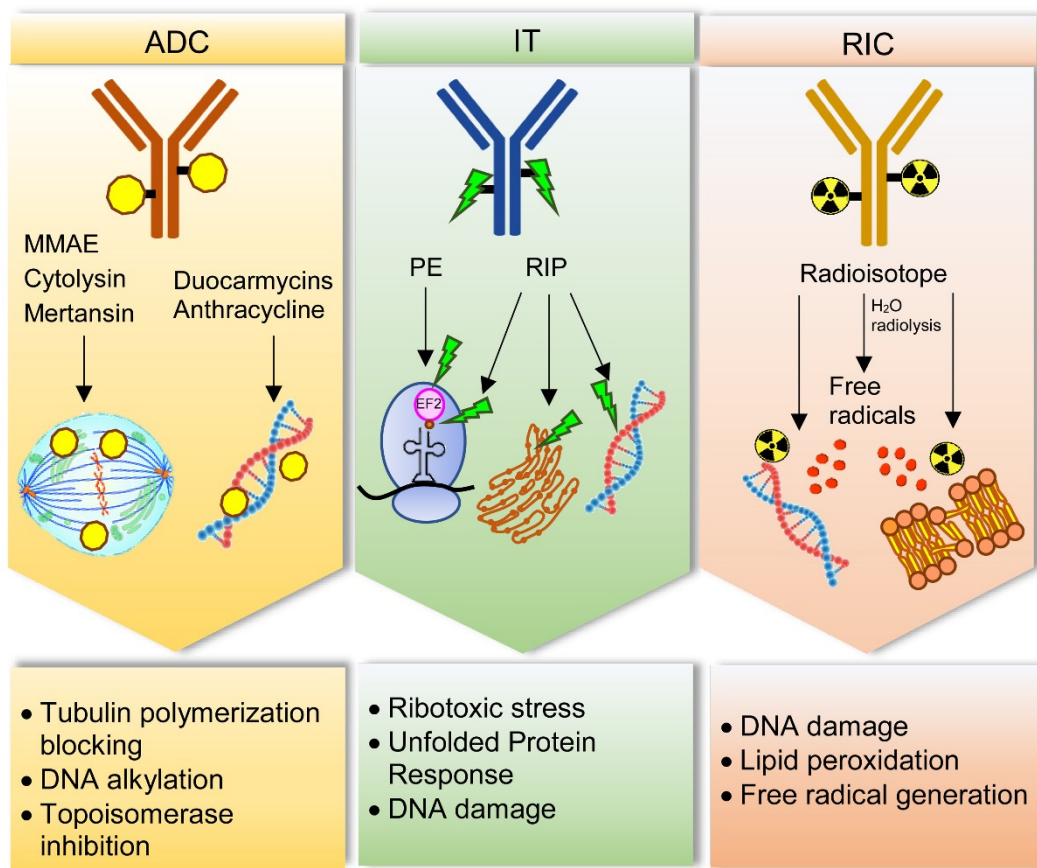
Figure 1. Main cell damage mechanisms induced by immunoconjugates for sarcoma treatment. Antibody–drug conjugates (ADC) can contain drugs acting with different mechanisms. Monomethyl auristatin E (MMAE), cytolysin and mertansin block tubulin polymerization, thus hampering cell cycle. Duocarmycins and anthracycline target DNA, inducing alkylation and topoisomerase inhibition, respectively. Immunotoxins (IT) can be constructed with Pseudomonas exotoxin (PE) or ribosome-inactivating proteins (RIPs). PE inhibits elongation factor-2 (EF2) through its ADP-ribosylation, thus inducing ribotoxic stress and protein synthesis blocking. RIPs can inhibit protein synthesis through rRNA-N-glycosylase activity removing a specific adenine in a stem–loop region of the main ribosomal RNA. In addition, RIPs can act on different substrates such as endoplasmic reticulum, through unfolded protein response, and DNA, by directly damage. Radioimmunoconjugates (RIC) contain radioisotopes, which can damage DNA and cause lipid peroxidation in cell membranes. This effect can occur directly or indirectly through free radicals produced by water radiolysis.

3. Immunoconjugates for Sarcoma Therapy

Although ICs have showed relevant effects mainly on hematological malignancies, numerous studies have paved the way to their application for solid tumors, including sarcomas. Unlike hematological tumors, sarcomas as well as all solid cancers have some molecular and morphological characteristics that make them more difficult to treat with IC-based therapy [30]. In particular, the difficulty of penetration inside tumor mass is related to the abundant extracellular matrix, disorganized vasculature and absence of functional lymphatic vessels that causes increased interstitial fluid pressure [31]. However, protocol optimization, progressive reduction of IC size and implementation of penetration efficacy are expected to significantly improve targeted therapy of solid tumors [32,33].

3.1. Antibody–Drug Conjugates for Sarcoma

Many studies have reported the efficacy of ADCs towards specific antigens expressed in different types of sarcoma.

The endosialin/CD248/TEM1 receptor is a transmembrane glycoprotein expressed on pericytes and fibroblasts during embryogenesis. In adults, its presence dramatically drops in normal tissues while it is expressed in mesenchymal tumors, such as sarcoma,

neuroblastoma, as well as in perivascular and tumor-associated stroma [34]. Moreover, it is associated with tumor angiogenesis and inflammation [35,36]. In sarcomas, this antigen is highly expressed on the surface of malignant, perivascular, and stromal cells, even on high grade and advanced sarcoma [37,38]. Two anti-endosialin ADCs were tested in preclinical models of sarcoma. The antitumor efficacy of the anti-endosialin-MC-VC-PABC-MMAE was tested on two endosialin-positive human cell lines and one sarcoma xenograft model. Inhibiting concentration 50 (IC_{50}) values were 0.5 μg/mL for the Ewing sarcoma (ES) cell line A-673 and 1.5 μg/mL for the osteosarcoma (OS) cells SJSA-1, without any correlation between the extent of cell growth inhibition and endosialin expression levels. The antitumor activity of this ADC was also tested in nude mice bearing A-673 cells xenografts. The dose of 15 mg/kg of anti-endosialin-MC-VC-PABC-MMAE determined a marked and durable inhibition of tumor growth leading to mice survival of 80% after day 150, thus demonstrating the antitumor efficacy of this ADC [39]. The anti-endosialin ENDOS/ADC was tested in sarcoma preclinical models. This IC is composed of a humanized anti-endosialin mAb hMP-E-8.3 linked to a duocarmycin derivative alkylating agent. In this case, SJSA-1 cells resulted more sensitive to ENDOS/ADC than A-673 cells, displaying IC_{50} values of 0.8 nM and 8.6 nM, respectively. Moreover, in a SJSA-1 derived xenograft model, mice treated with ENDOS/ADC showed a strong reduction of tumor volume [40].

Glycoprotein non-metastatic b (GPNMB) is a transmembrane protein involved in bone differentiation and remodeling [41,42]. Different cancer cell types are characterized by high levels of this glycoprotein, among them OS cells [43,44]. In addition, GPNMB is involved in cancer migration, invasion, progression, and metastasis, as well as poor patient prognosis [45,46]. The fully human IgG2 mAb CR011, which recognizes GPNMB extracellular domain, was linked to MMAE in the Glembatumumab vedotin ADC. This IC was tested in preclinical models of OS: 10 short-term cell cultures from patient-derived OS, 5 standard OS cell lines and 4 xenograft cell lines. Glembatumumab vedotin had a significant cytotoxic activity, displaying IC_{50} values lower than 55 μg/mL in most of the treated cells. Moreover, ADC effect correlates with GPNMB expression levels [47]. Glembatumumab vedotin entered phase 2 clinical trial involving 22 patients (ranging 12–50 years) with recurrent or refractory OS. This ADC was administered intravenously at 1.9 mg/kg/dose over 90 min on day 1; the treatment was repeated every 21 days for up to 18 courses. The results showed a limited efficacy. In fact, only one patient had a partial response and two maintained a stable tumor disease. No correlation was observed between GPNMB expression and clinical response (NCT02487979).

Leucine-rich repeat containing 15 (LRRC15), a member of the Leucine-Rich Repeat superfamily, is another target evaluated for ADC-based sarcoma therapy. LRRC15 is overexpressed in cancer-associated fibroblasts and cancer cells from many epithelial and mesenchymal solid tumors. In particular, it was reported that OS tissue samples had high LRRC15 expression both on cancer and stroma cells [48]. ABBV-085 ADC is composed of the anti-LRRC15 humanized IgG1 kappa antibody Ab1 conjugated to the antimitotic drug MMAE. The antitumor efficacy of ABBV-085 was evaluated in a cancer+/stromal+ patient-derived xenograft (PDX) of OS. Results showed that ABBV-085 was extremely effective in terms of tumor growth inhibition, in comparison to other standard OS therapies (doxorubicin, ifosfamide, gemcitabine, cisplatin) [49,50]. A multicenter phase 1 dose-escalation clinical trial of ABBV-085 is currently under investigation in patients with advanced solid tumors, including undifferentiated pleomorphic sarcoma (NCT02565758).

CD56, also called Neural Cell Adhesion Molecule (NCAM), is a homophilic binding glycoprotein present on the surface of neurons and glia where it has a prominent role in neuronal adhesion and migration ability, neurite outgrowth, synapse formation and synaptic plasticity [51,52]. CD56 can also be found in hematopoietic cells, above all in natural killer cells, where it acts as an adhesion molecule [53]. CD56 is over-expressed in different cancer types, like neuroblastoma, rhabdomyosarcoma (RMS) and most of the STS, Wilms tumor, acute myeloid leukemia, glioma, and astrocytoma, as well as in several carcinomas [54–56]. Lorvotuzumab mertansine (IMGN901) is an ADC composed of an anti-

CD56 humanized N901 mAb conjugated to the maytansinoid DM1, via a stable disulfide linker. IMGN901 was tested in vitro on two RMS and two ES cell lines showing a great sensitivity, which is not always correlated to CD56 expression intensity. In vivo studies were conducted in tumor xenograft models; stable complete responses were observed in two out of seven RMS xenografts; even in this case there was not a strong correlation between CD56 expression levels and treatment response. The response variability might be due to factors other than CD56 expression, such as mitotic rate, chemoresistance to tubulin targeting agents and/or intracellular processing of IMGN901 [57]. This conjugate in a phase 1 trial on myeloma patients had demonstrated ample evidence of safety and signals of clinical activity [58]. These results paved the way for a phase 2 clinical trial where IMGN901 was evaluated in patients with relapsed or refractory Wilms tumor, RMS, neuroblastoma, pleuropulmonary blastoma, malignant peripheral nerve sheath tumor, or synovial sarcoma (SS). Patients received lorvotuzumab mertansine intravenously at 110 mg/m^2 over 1–1.5 h on days 1 and 8; the treatment was repeated every 21 days for up to 17 courses in the absence of disease progression or unacceptable toxicity. Despite the high level of CD56 found in all treated pediatric tumors, only few patients had a relevant clinical response. This might be due to many factors: limited penetration of the conjugate/payload into solid tumor cancer cells, presence of unrecognized CD56 isoforms that could interfere with the binding/internalization process and tumor resistance to DM1 (NCT02452554).

Endoglin (ENG or CD105) is a homodimeric glycoprotein, expressed in endothelial cells, bone marrow cells, and macrophages, and involved in embryogenesis, angiogenesis, and vascular establishment as well as homeostasis [59,60]. In tumors its presence is associated with neo-angiogenesis, which represents a key feature of malignant cancer. ENG can be both a transmembrane protein acting as a co-receptor for transforming growth factor-β, and a soluble extracellular matrix protein after cleavage by metalloproteinase 14 occurs. In sarcomas ENG is associated with poor outcome in ES patients, being a key point in tumor cell plasticity, tumor progression and invasiveness [61]. OMTX703 is an ADC composed of the anti-ENG mAb OMTX003, which recognize ENG extracellular domain, linked to cytolysin. The antitumor efficacy of this ADC was evaluated in cell lines, cell line-derived xenografts, and PDX of ES. After OMTX703 treatment, a potent anti-proliferative effect was reported in the ES8 cell line with an IC$_{50}$ value of 260.6 nM. In the same cell line, it was observed a correlation between ENG expression level, which was extremely high, and ADC internalization ability and cytotoxic effect. OMTX703 efficacy was assessed in a ES8 xenograft model (immunocompromised NOD-SCID-IL-2Rg$^{null/null}$ mice), where tumor growth was strikingly reduced with a 60 mg/kg dose of ADC. Interestingly, immunohistochemistry studies confirmed that ENG expression levels in xenograft tumors were quite similar to those found in parental cell lines in vitro. Lastly, OMTX703 antineoplastic effect was evaluated in PDX models, which display the highest ENG expression and better represent the typical heterogeneity of these tumors. It was observed that OMTX703 (30 and 60 mg/kg) was able to produce a dose-dependent antitumor response. A complete response rate of 60% was achieved at the end of the treatment with the highest dose (60 mg/kg) [62].

The urokinase plasminogen activator receptor–associated protein uPARAP/Endo180 plays a crucial role in the process of collagen turnover. The receptor acts through the endocytosis of extracellular matrix collagen, which is further addressed to lysosomal degradation [63,64]. In normal tissues, this receptor is expressed in a limited range of cell types involved in tissue development, such as fibroblasts and osteogenesis-associated mesenchymal cells [65,66]. In cancer cells its expression was found to be high, especially in OS and STS. In a preclinical study the antitumor efficacy of 2h9-vc-MMAE, an ADC composed of an anti-uPARAP mAb linked to MMAE was evaluated in fibrosarcoma (FS) and RMS cell lines (HT1080 and RD, respectively), expressing high levels of uPARAP. The ADC cytotoxic mechanism is related to the binding and internalization properties as well as to ADC lysosomal cleavage. The ADC was able to significantly reduce cell viability on sarcoma cell lines even if to a lesser extent than on hematological cell lines. In addition,

ADC efficacy was evaluated in mice xenografted with human leukemic cells. Complete rescue of all treated animals was observed with no sign of adverse effects [67].

Receptor tyrosine kinase-like orphan receptors (ROR) are a family of transmembrane tyrosine kinases. ROR1 is a Wnt5a receptor expressed during embryonic development and in several hematologic and solid malignancies [68]. NBE-002 is an ADC consisting of a humanized anti-ROR1 mAb conjugated to a derivative of the potent anthracycline PNU-159682 [69]. NBE-002 is currently under evaluation in a phase 1/2 clinical trial in patients (age ≥ 18 years) with advanced solid tumors, including sarcoma; NBE-002 has been given intravenously on day 1 of repeated 21-day courses (NCT04441099).

ROR2 is one of the non-canonical Wnt receptors, which plays significant roles during early embryonic development in several tissue types [70]. The protein may be involved in the early formation of chondrocytes and in osteoblastogenesis [71]. ROR2 is overexpressed during embryonic development and in several important cancer types, including sarcoma, where its levels are strongly correlated with worst prognosis of patient [70]. CAB-ROR2-ADC or BA3021 is a ROR2-targeting ADC composed of a conditionally active biologic (CAB) anti-ROR2 antibody conjugated to an undisclosed payload [72]. This ADC is currently being evaluated in a phase 1/2 clinical trial in patients (age ≥ 18 years) with locally advanced unresectable or metastatic solid tumors, including STS (NCT03504488—recruiting status).

AXL is a member of receptor tyrosine kinases TAM family. AXL is widely expressed in healthy cells and tissues, where it is involved in cell survival, phagocytic clearance of dying cells, natural killer cell differentiation, and cell aggregation [73]. AXL is also highly expressed on a variety of cancer types, OS included, where it plays a central role in tumor proliferation, survival, stem cell phenotype, metastasis, and resistance to cancer therapy [74,75]. CAB-AXL-ADC or BA3011 is composed of a CAB anti-AXL antibody conjugated to an undisclosed payload [76]. This ADC is currently under investigation in a phase 1/2 clinical trial in patients (age ≥ 18 years in phase 1; age ≥ 12 years in phase 2) with advanced solid tumors including different types of sarcoma. In phase 1 trial all patients will receive BA3011, while in phase 2 trial all patients will receive either BA3011 alone or in combination with nivolumab (NCT03425279—recruiting status). Enapotamab Vedotin or HuMax-AXL-ADC is another anti-AXL ADC, firstly tested in vitro and in vivo in preclinical models of non-small cell lung cancer [77]. It consists of a human AXL-specific IgG1 conjugated to the cytotoxic agent MMAE. Enapotamab Vedotin is now being evaluated in a phase 1/2 clinical trial in patients (age ≥ 18 years) with selected, relapsed and advanced or metastatic solid tumors, sarcoma included, which no longer respond to standard therapy (NCT02988817).

CD70 is a transmembrane antigen belonging to the tumor necrosis factor (TNF) ligand super family. Its interaction with CD27 receptor enhances cellular proliferation and induces anti-apoptotic proteins playing a major role in T-cell costimulation. CD70 is often upregulated in T- and B- cell lymphomas and in various solid tumors even if its exact role during the disease onset and progression remains unknown [78]. CD70 was identified as a specific and highly expressed surface protein in uterine leiomyosarcoma cell lines and in clinical samples of this rare and aggressive gynecologic malignancy. The antihuman-CD70 mAb vorsetuzumab was conjugated to MMAF towards uterine leiomyosarcoma cell line and its antitumor effects were evaluated in vitro and in vivo. This anti-CD70 ADC showed a significant cytotoxicity on SK-LMS-1 cells, displaying IC_{50} equal to 0.120 nM and it strongly inhibited tumor growth in SK-LMS-1 xenograft mouse models and in uterine leiomyosarcoma PDX mouse models with a relative tumor reduction of 54.5% and 84.7%, respectively [79].

ADCs tested in preclinical studies and in clinical trials are reported in Table 1.

Table 1. Antibody–drug conjugates tested for sarcoma therapy.

ADC	Target	Antibody	Drug	Tumor	In Vitro	In Vivo	Clinical Trial	Ref.
anti-endosialin-MC-VC-PABC-MMAE	Endosialin	Fully human mAb	MMAE	ES, OS	√	√	-	[39]
ENDOS/ADC	Endosialin	hMP-E-8.3	Duocarmycin derivative	ES, OS	√	√	-	[40]
Glemtumumab vedotin	GPNMB	CR011	MMAE	OS	√	√	NCT02487979 Phase 2	[47]
ABBV-085	LRRC15	LRRC15 Ab1	MMAE	OS	√	√	NCT02565758 Phase 1	[49,50]
IMGN901	NCAM	N901	DM1	RMS, ES	√	√	NCT02452554 Phase 2	[57]
OMTX703	Endoglin	OMTX003	Cytolysin	ES	√	√	-	[62]
2h9-vc-MMAE	uPARAP	2h9	MMAE	FS, RMS	√	-	-	[67]
NBE-002	ROR1	humanized mAb	PNU-159682	S	-	√	NCT04441099 Phase 1/2	[69]
BA3021	ROR2	CAB	undisclosed	STS	√	√	NCT03504488 Phase 1/2	[72]
BA3011	AXL	CAB	undisclosed	S	√	√	NCT03425279 Phase 1/2	[76]
Enapotamab vedotin	AXL	human IgG1-κ	MMAE	S	√	√	NCT02988817 Phase 1/2	[77]
CD70-ADC	CD70	vorsetuzumab	MMAF	uLMS	√	√	-	[79]

The symbols √ and - mean tested and not tested, respectively, in vitro, in vivo or in a clinical trial. Abbreviations: ES, Ewing sarcoma; FS, fibrosarcoma; GPNMB, glycoprotein non-metastatic b; LRRC15, leucine-rich repeat containing 15; MMAE, monomethyl auristatin E; MMAF, monomethyl auristatin F; NCAM, neural cell adhesion molecule; OS, osteosarcoma; RMS, rhabdomyosarcoma; ROR, receptor tyrosine kinase-like orphan receptor; S, sarcoma (unspecified type); STS, soft tissue sarcoma; uLMS, uterine leiomyosarcoma; uPARAP, urokinase plasminogen activator receptor–associated protein.

3.2. Immunotoxins for Sarcoma

Various ITs have been tested for sarcoma therapy, evaluating their binding, internalization ability, and anti-tumor effect.

Chondroitin sulfate proteoglycan 4 (CSPG4) is a tumor-associated surface antigen, firstly found on human melanoma cells [80]. It is used as a marker of proliferation and metastasis in poor prognosis tumor types such as breast cancer and STS, whilst its expression is very low in healthy tissues [81]. The CSPG4-specific PE-based IT, αMCSP-ETA′, was tested for RMS adjuvant therapy. Multiple parameters were evaluated in vitro on three embryonal RMS cell lines (RD, FL-OH1 and TE-671) and one alveolar RMS cell line (Rh30). IT binding was specific on CSPG4$^+$ cells and IT internalization was rapid; αMCSP-ETA′ inhibited RMS cell proliferation with IC$_{50}$ values ranging from 0.02 to 50 nM and induced apoptosis. The binding was also evaluated ex vivo on three patient-derived paraffin-embedded RMS tumor sections, exhibiting good specificity. Although preliminary, these results highlighted the therapeutic potential of this IT (alone or combined with standard drugs) for RMS treatments [82].

The well-known epidermal growth factor receptor (EGFR) is a member of the ErbB tyrosine kinase receptor family. It is involved in routine cellular processes such as proliferation, differentiation, and cellular development [83]. EGFR is highly expressed in several solid cancers [84]. EGFR is overexpressed in up to 76% of embryonal RMS cases, so it is considered a suitable target for RMS immunotherapy [85]. The EGFR-specific recombinant IT 425(scFv)-ETA′ was tested in vitro on three different embryonal RMS cell lines RD, FL-OH1 and TE-671. Experiments demonstrated binding specificity and valuable internalization. Moreover, 425(scFv)-ETA′ was able to reduce cell viability (IC$_{50}$ values

in picomolar range) and to strongly activate apoptotic pathway. The EGFR[+] cell binding activity of the IT 425(scFv)-ETA′ was also demonstrated ex vivo on two patient-derived formalin-fixed paraffin-embedded RMS specimens [86]. EGFR was also used as target of an indirect IT, consisting of a primary EGFR specific mAb followed by a secondary F(ab′)$_2$ anti-mouse Ig linked to saporin-S6. The indirect IT caused a significant inhibition of cell growth and protein synthesis (IC$_{50}$ 0.95 nM) and a strong increase in apoptosis in RD/18 RMS cell line. The toxic activity of the anti-EGFR IT was also observed on RMS cell lines expressing low levels of EGFR [87].

The glycoprotein gp72 is a tumor-associated cell surface antigen present in melanoma, bladder and breast carcinoma and osteogenic sarcoma [88]. 791T/36-RTA derives from the conjugation of the murine anti-gp72 mAb 791T/36 with ricin A chain (RTA) and it specifically inhibited tumor cell growth in vitro in the OS cell line 791T. The cytotoxicity of this IT depended primarily on its very rapid cell surface binding, endocytosis and intracellular processing leading to the release of the toxic payload in the cytoplasm to inhibit protein synthesis [89].

B7H3 is a cell surface glycoprotein expressed on cancer cells and not found on normal tissues [90]. It is involved in natural killer and T cell inhibition, as well as in tumor cell migration and invasion [91]. The recombinant IT 8H9(scFv)-PE38 was constructed with the truncated form of PE (PE38) conjugated to the single-chain fragment variable (scFv) of the anti-B7H3 mAb 8H9. The IT had a cytotoxic effect in vitro on three B7H3[+] human OS cell lines (U2OS, CRL1427, and OHS-M1), with IC$_{50}$ values of 0.03, 0.05, and 0.02 μg/mL, respectively. 8H9(scFv)-PE38 was also tested in vivo in xenograft SCID mice bearing OHS-M1 cells. The results indicated that tumor regression was achievable using 0.15 mg/kg IT without significant systemic toxicity for animals [92].

Another sarcoma-associated antigen is an 80 kDa surface glycoprotein recognized by TP-3, a mAb that particularly reacts with OS. This antigen was found to be highly expressed on OS and in some hemangiopericytoma, chondrosarcoma, malignant fibrous histiocytoma, and synovial sarcoma. Healthy tissues exhibited a very low expression of this antigen [93]. TP-3 mAb was conjugated to pokeweed antiviral protein (PAP) and the cytotoxic effect of this IT was tested in vitro on the human OS cell line OHS. TP-3-PAP was able to kill TP-3^{+} cells in a specific and efficient manner, with IC$_{50}$ values in the picomolar range. Furthermore, the antitumor activity of this IT was assayed in vivo in a TP-3^{+} mouse model bearing human sarcoma lung metastases with good results in terms of number and size reduction of the metastases in a dose dependent manner [94]. Two recombinant TP-3 based ITs were produced combining the toxin PE38 with the monovalent and bivalent disulfide-stabilized Fv of the antibody, TP-3(dsFv)-PE38 and TP-3(dsFv)$_2$-PE38, respectively. These ITs were tested in vitro on three human OS cell lines (OHS-M1, OHS, and SaOS). Results indicated a specific effect for TP-3^{+} cells, with a great binding affinity. Bivalent IT was more cytotoxic than monovalent IT, with IC$_{50}$ of 4–42 ng/mL and 30–235 ng/mL, respectively. The antitumor activity was tested in vivo in SCID mice bearing human OHS-M1 cells; TP-3(dsFv)$_2$-PE38 showed a twofold increased effect compared to monovalent IT [95].

CD133 is a transmembrane glycoprotein, also known as AC133 or prominin-1, which is used as a cellular marker of cancer stem cells (CSCs) in many different malignancies, including sarcomas [96]. CSCs are usually a small subpopulation of cancer cells that are responsible for chemoresistance, relapsed disease and metastasis [97]. Unfortunately, normal stem cells, including hematopoietic, endothelial, and neuronal stem cells are CD133^{+} too. For this reason, new biotechnological strategies are fundamental to selectively kill CSCs, rescuing other CD133^{+} cells. Photochemical internalization is a site-specific and light-dependent drug delivery method that relies on the activation of a molecule, called photosensitizer, which co-localizes with the therapeutic agent of interest in endo-lysosomal compartments of the cells. The photosensitizer meso-tetraphenyl chlorin disulfonate (TPCS2a) was used to perform photochemical internalization of two anti-CD133 ITs. These ITs were obtained conjugating the biotinylated anti-CD133/1 (AC133) and anti-CD133/2 (293C) mAbs to streptavidin–saporin. The efficacy of this method was assessed on the

undifferentiated human sarcoma cell line SW872, on the human FS cell line HT-1080 and on SW872-derived mouse xenografts cells, obtaining specific cytotoxic effects. Moreover, in vitro and in vivo experiments revealed a strong decrease in colony forming ability and a great tumor initiation inhibition of the surviving cells after photochemical internalization of the anti-CD133-saporin [98].

As discussed above, TEM1/endosialin/CD248 is a cell surface receptor highly expressed on human sarcomas that is considered a valid target for immunotherapeutic treatments. The human scFv-Fc fusion protein (78Fc) specifically bound TEM1$^+$ sarcoma cell lines in vitro (SJSA-1, A673, MES-SA, and HOS) and sarcoma cells in xenografted nude mice. The 78Fc was chemically conjugated to the plant toxin saporin to augment its cytotoxicity. In vitro experiments revealed that 78Fc-Sap was able to specifically kill TEM$^+$ sarcoma cells with a significantly higher effect in comparison with saporin alone. In vivo antitumor activity of 78Fc-Sap was assessed on SJSA-1 and A673 derived xenografts showing a high and specific tumor growth inhibition with no systemic toxicity even at the highest dose (0.2 mg/kg) [99].

As previously reported, the anti-endoglin mAb OMTX003 is a valid carrier to construct therapeutic ICs against ES. OMTX003 was also conjugated to nigrin b A chain. OMTX503 IT was highly stable, its cell surface binding ability was specific for endoglin$^+$ cells and the cellular internalization was efficient. It showed an antiproliferative activity in vitro on three ES cell lines with different level of endoglin expression (RM82, TC71 and CADO) with IC$_{50}$ values of 0.118 nM, 9.155 nM, and 17.38 nM, respectively. Thus, the cytotoxic effect was related to the endoglin expression level. OMTX503 was also tested in vivo on RM82-derived mouse xenografts at 0.5 mg/kg, obtaining good and significant results in terms of tumor growth inhibition and cell viability reduction [62].

ITs tested in preclinical studies are reported in Table 2.

Table 2. Immunotoxins tested for sarcoma therapy.

Target	Antibody	Toxin	Tumor	In Vitro	In Vivo	Clinical Trial	Ref.
CSPG4	αMCSP	ETA'	RMS	√	-	-	[82]
EGFR	425 (scFv)	ETA'	RMS	√	-	-	[86]
	murine mAb (clone 528)	Saporin	RMS	√	-	-	[87]
gp72	791T/36	RTA	OS	√	-	-	[89]
B7H3	8H9 (scFv)	PE38	OS	√	√	-	[92]
80 kDa sarcoma associated antigen	TP-3	PAP	OS	√	√	-	[94]
80 kDa sarcoma associated antigen	TP-3 (dsFv) TP-3 (dsFv)$_2$	PE38	OS	√	√	-	[95]
CD133	AC133 293C	Saporin	S	√	√	-	[98]
TEM1	78Fc	Saporin	S	√	√	-	[99]
Endoglin	OMTX003	Nigrin-b A chain	ES	√	√	-	[62]

The symbols √ and - mean tested and not tested, respectively, in vitro, in vivo or in a clinical trial. Abbreviations: CSPG4, chondroitin sulfate proteoglycan 4; dsFv, disulfide-linked fragment variable; EGFR, epidermal growth factor receptor; ES, Ewing sarcoma; ETA', truncated version of *Pseudomonas* exotoxin A; OS, osteosarcoma; PE, *Pseudomonas* exotoxin; RMS, rhabdomyosarcoma; RTA, ricin toxin A-chain; S, sarcoma (unspecified type); scFv, single-chain fragment variable.

3.3. Radioimmunoconjugates for Sarcoma

The first RIC approved in clinical practice was ibritumomab tiuxetan, in which the anti-CD20 mAb rituximab is (radio)labeled with Yttrium-90 for the treatment of non-Hodgkin's lymphoma [100].

Despite most studies reported in literature describe the use of RICs for diagnostic purposes, some works depict the attempts to apply RIT to the treatment of sarcomas.

CD146 is a cancer associated cell adhesion molecule (CAM) overexpressed in several cancer types, including OS; it is associated with tumor progression, neoangiogenesis, and vascular development [101]. Anti-CD146 murine mAb OI-3 was (radio)labeled with Lutetium-177 or Iodine-125 and was tested in biodistribution/dosimetry experiments. Results showed promising data in terms of RIC tumor uptake in nude mice bearing OHS xenografts [102].

Insulin-like growth factor 2 receptor (IGF2R) is another valid target for OS treatment, because it is overexpressed in several cell lines and patient-derived OS cells [103]. A novel murine anti-IGF2R mAb, named 2G11, was (radio)labeled with Indium-111 to determine biodistribution and tumor uptake in OS tumor bearing SCID mice. Successively, 2G11 was (radio)labeled with both Lutetium-177 and Bismuth-213, obtaining good results in vivo in terms of slowing down tumor growth, without local or systemic toxicity referred [104].

Frizzled homologue 10 (FZD10) is the main target used for synovial sarcoma (SS) RIT. FZD10 is a transmembrane receptor of the Wnt signaling pathway whose gene is upregulated specifically in SS, but not expressed in any normal human tissue except for placenta [105]. The murine mAb 92–13 (radio)labeled with Yttrium-90 showed specific binding ability to FZD10 in vitro and in vivo, good internalization into FZD10$^+$ cells and strong antitumor activity in SS mouse xenografts [106,107]. The humanized chimeric anti-FZD10 mAb OTSA101 was (radio)labeled with Indium-111 or Yttrium-90. In a phase 1 clinical trial, 20 patients with advanced/recurrent SS received an injection of the Indium-111-OTSA101 RIC to determine tumor uptake and biodistribution. Successively, only those patients ($n = 10$) that showed a significant tumor uptake, were treated with Yttrium-90-OTSA10. Unfortunately, no patients showed an objective tumor regression. In fact, best overall response was a stable disease in 3 patients [108]. Adsorbed dose simulations can explain tumor response on treated patients. The estimated biodistribution and dosimetry of (radio)labeled anti-FZD10, in normal tissue and tumor, was evaluated through Monte Carlo-based 3D simulations [109]. In a comparative preclinical study, OTSA101 was (radio)labeled with both Yttrium-90 and Astatine-211. Astatine-211-OTSA101, an α-emitting anti-FZD10 RIC, suppressed tumor growth of SS mouse xenografts more efficiently than the same dose of the Yttrium-90-OTSA101, a β-emitting anti FZD10 RIC, without remarkable toxic side effects [110]. This confirmed that α-RIT is superior to β-RIT in treating solid tumors because α-particles, with higher linear energy transfer, may have more advantages in terms of cytotoxicity compared to β-particles, with lower linear energy transfer [111].

The glycoprotein B7H3 is expressed on desmoplastic small round tumor cells (DSRCT), a rare sarcoma that affects adolescents and young adults involving the peritoneum. RIT treatment against DSRCT was tested in a phase 1 clinical trial (NCT01099644) on 52 patients. Murine anti-B7H3 mAb omburtamab (8H9) linked to Iodine-131 was administrated with an intraperitoneal injection. Related toxicity was mild and transient in almost all patients and adsorbed dose was low in normal tissues [112]. To date, Iodine-131-omburtamab is on a phase 2 clinical trial to improve patient survival (NCT04022213—recruiting status).

RICs tested in preclinical studies and clinical trials are reported in Table 3.

Table 3. Radioimmunoconjugates tested for sarcoma therapy.

Target	Antibody	Radionuclide	Half-life	Emission	Tumor	In Vitro	In Vivo	Clinical Trial	Ref.
CD146	OI-3 CHOI-3.1 CHOI-3.3	^{125}I ^{177}Lu	59.5 days 6.7 days	Auger β⁻, Auger	OS	√	√	-	[102]
IGF2R	2G11	^{111}In ^{177}Lu ^{213}Bi	67.4 h 6.7 days 46 min	γ β⁻, Auger α	OS	√	√	-	[104]
FZD10	92–13	^{90}Y	64.1 h	β⁻	SS	√	√	-	[106,107]
FZD10	OTSA101	^{111}In ^{90}Y	67.4 h 64.1 h	γ β⁻	SS	-	√	Phase 1	[108,109]
FZD10	OTSA101	^{90}Y ^{211}At	64.1 h 7.2 h	β⁻ α, Auger	SS	-	√	-	[110]
B7H3	8H9	^{131}I	8.0 days	β⁻	DSRCT	-	√	Phase 2	[112]

The symbols √ and - mean tested and not tested, respectively, in vitro, in vivo or in a clinical trial. Abbreviations: DSRCT, desmoplastic small round cell tumor; FZD10, frizzled homologue 10; IGF2R, insulin-like growth factor 2 receptor; OS, osteosarcoma; SS, synovial sarcoma.

4. Conclusions

This review aims to provide a comprehensive overview of the latest advances in sarcoma immunotherapy and their impact on clinical oncology. The IC studies reported in this review show efficacy and clinical potential in sarcoma therapy. Although rare in adults, sarcomas are more frequent among pediatric tumors. Sarcomas are characterized by molecular and morphological complexity; the rarity and heterogeneity of sarcomas induce clinicians and researchers to seek and validate personalized therapeutic approaches. IC-based immunotherapy has been showing increasingly interesting results in terms of anti-tumor efficacy beside to a reduction of side effects. These positive results depend mainly on the possibility to select new engineered carrier moieties characterized by stability, binding specificity and reduced immunogenicity. The results obtained in preclinical studies with ICs in sarcoma models encouraged the translation from bench to bed.

The clinical studies over the last 20 years allowed nine ADCs to be approved by the FDA and many others are in phase 3 clinical trial [113] in different neoplastic diseases. Currently, seven ADCs and two RICs are under phase 1–2 clinical trials for sarcoma therapy and many other ICs have been evaluated in preclinical studies.

We believe that, in the near future, antibody-based therapeutic approaches could improve sarcoma patient outcome by overcoming some difficulties associated to standard therapy, such as the tumor resistance to the anticancer drugs, leading to patient relapse, and the onset of secondary malignancies [114,115].

Author Contributions: All the authors wrote the paper and collected the literature. All authors have read and agreed to the published version of the manuscript.

Institutional Review Board Statement: Not applicable.

Informed Consent Statement: Not applicable.

Data Availability Statement: Not applicable.

Conflicts of Interest: The authors declare no conflict of interest.

References

1. American Cancer Society–Cancer Statistics Center. Available online: https://cancerstatisticscenter.cancer.org/#!/ (accessed on 29 June 2021).
2. NCI—The Surveillance, Epidemiology, and End Results (SEER) Program. Available online: https://seer.cancer.gov/ (accessed on 29 June 2021).
3. Meyer, M.; Seetharam, M. First-Line Therapy for Metastatic Soft Tissue Sarcoma. *Curr. Treat. Options Oncol.* **2019**, *20*, 6. [CrossRef]
4. In, G.K.; Hu, J.S.; Tseng, W.W. Treatment of advanced, metastatic soft tissue sarcoma: Latest evidence and clinical considerations. *Ther. Adv. Med. Oncol.* **2017**, *9*, 533–550. [CrossRef]
5. Van Cutsem, E.; Köhne, C.H.; Hitre, E.; Zaluski, J.; Chang Chien, C.R.; Makhson, A.; D'Haens, G.; Pintér, T.; Lim, R.; Bodoky, G.; et al. Cetuximab and chemotherapy as initial treatment for metastatic colorectal cancer. *N. Engl. J. Med.* **2009**, *360*, 1408–1417. [CrossRef] [PubMed]
6. Hochster, H.S.; Hart, L.L.; Ramanathan, R.K.; Childs, B.H.; Hainsworth, J.D.; Cohn, A.L.; Wong, L.; Fehrenbacher, L.; Abubakr, Y.; Saif, M.W.; et al. Safety and efficacy of oxaliplatin and fluoropyrimidine regimens with or without bevacizumab as first-line treatment of metastatic colorectal cancer: Results of the TREE Study. *J. Clin. Oncol.* **2008**, *26*, 3523–3529, Erratum in: *J. Clin. Oncol.* **2008**, *26*, 4697. [CrossRef]
7. Bolognesi, A.; Polito, L. Immunotoxins and other conjugates: Pre-clinical studies. *Mini Rev. Med. Chem.* **2004**, *4*, 563–583. [CrossRef]
8. Polito, L.; Bortolotti, M.; Pedrazzi, M.; Bolognesi, A. Immunotoxins and other conjugates containing saporin-s6 for cancer therapy. *Toxins* **2011**, *3*, 697–720. [CrossRef]
9. Bolognesi, A.; Bortolotti, M.; Maiello, S.; Battelli, M.G.; Polito, L. Ribosome-Inactivating Proteins from Plants: A Historical Overview. *Molecules* **2016**, *21*, 1627. [CrossRef] [PubMed]
10. Khongorzul, P.; Ling, C.J.; Khan, F.U.; Ihsan, A.U.; Zhang, J. Antibody-Drug Conjugates: A Comprehensive Review. *Mol. Cancer Res.* **2020**, *18*, 3–19. [CrossRef] [PubMed]
11. Thomas, A.; Teicher, B.A.; Hassan, R. Antibody-drug conjugates for cancer therapy. *Lancet Oncol.* **2016**, *17*, 254–262. [CrossRef]
12. Sievers, E.L.; Senter, P.D. Antibody-drug conjugates in cancer therapy. *Annu. Rev. Med.* **2013**, *64*, 15–29. [CrossRef] [PubMed]
13. Nepali, K.; Ojha, R.; Lee, H.Y.; Liou, J.P. Early investigational tubulin inhibitors as novel cancer therapeutics. *Expert Opin. Investig. Drugs* **2016**, *25*, 917–936. [CrossRef]
14. Hoffmann, R.M.; Coumbe, B.G.T.; Josephs, D.H.; Mele, S.; Ilieva, K.M.; Cheung, A.; Tutt, A.N.; Spicer, J.F.; Thurston, D.E.; Crescioli, S.; et al. Antibody structure and engineering considerations for the design and function of Antibody Drug Conjugates (ADCs). *Oncoimmunology* **2017**, *7*, 1395127. [CrossRef] [PubMed]
15. Chau, C.H.; Steeg, P.S.; Figg, W.D. Antibody-drug conjugates for cancer. *Lancet* **2019**, *394*, 793–804. [CrossRef]
16. Polito, L.; Bortolotti, M.; Farini, V.; Battelli, M.G.; Barbieri, L.; Bolognesi, A. Saporin induces multiple death pathways in lymphoma cells with different intensity and timing as compared to ricin. *Int. J. Biochem. Cell Biol.* **2009**, *41*, 1055–1061. [CrossRef] [PubMed]
17. Polito, L.; Bortolotti, M.; Pedrazzi, M.; Mercatelli, D.; Battelli, M.G.; Bolognesi, A. Apoptosis and necroptosis induced by stenodactylin in neuroblastoma cells can be completely prevented through caspase inhibition plus catalase or necrostatin-1. *Phytomedicine* **2016**, *23*, 32–41. [CrossRef]
18. Weidle, U.H.; Tiefenthaler, G.; Schiller, C.; Weiss, E.H.; Georges, G.; Brinkmann, U. Prospects of bacterial and plant protein-based immunotoxins for treatment of cancer. *Cancer Genom. Proteom.* **2014**, *11*, 25–38.
19. Gilabert-Oriol, R.; Weng, A.; von Mallinckrodt, B.; Melzig, M.F.; Fuchs, H.; Thakur, M. Immunotoxins constructed with ribosome-inactivating proteins and their enhancers: A lethal cocktail with tumor specific efficacy. *Curr. Pharm. Des.* **2014**, *20*, 6584–6643. [CrossRef]
20. Mansoori, B.; Mohammadi, A.; Davudian, S.; Shirjang, S.; Baradaran, B. The Different Mechanisms of Cancer Drug Resistance: A Brief Review. *Adv. Pharm. Bull.* **2017**, *7*, 339–348. [CrossRef]
21. Polito, L.; Djemil, A.; Bortolotti, M. Plant Toxin-Based Immunotoxins for Cancer Therapy: A Short Overview. *Biomedicines* **2016**, *4*, 12. [CrossRef]
22. Gill, M.R.; Falzone, N.; Du, Y.; Vallis, K.A. Targeted radionuclide therapy in combined-modality regimens. *Lancet Oncol.* **2017**, *18*, 414–423. [CrossRef]
23. Steiner, M.; Neri, D. Antibody-radionuclide conjugates for cancer therapy: Historical considerations and new trends. *Clin. Cancer Res.* **2011**, *17*, 6406–6416. [CrossRef]
24. Pandit-Taskar, N. Targeted Radioimmunotherapy and Theranostics with Alpha Emitters. *J. Med. Imaging Radiat. Sci.* **2019**, *50*, S41–S44. [CrossRef]
25. Gopal, A.K.; Gooley, T.A.; Maloney, D.G.; Petersdorf, S.H.; Eary, J.F.; Rajendran, J.G.; Bush, S.A.; Durack, L.D.; Golden, J.; Martin, P.J.; et al. High-dose radioimmunotherapy versus conventional high-dose therapy and autologous hematopoietic stem cell transplantation for relapsed follicular non-Hodgkin lymphoma: A multivariable cohort analysis. *Blood* **2003**, *102*, 2351–2357. [CrossRef]
26. Biochempeg. Available online: https://www.biochempeg.com/article/74.html (accessed on 29 June 2021).
27. ClinicalTrials.gov. Available online: https://clinicaltrials.gov/ct2/results?cond=&term=immunoconjugate&cntry=&state=&city=&dist= (accessed on 29 June 2021).

28. Drugbank. Available online: https://go.drugbank.com/unearth/q?utf8=%E2%9C%93&query=immunoconjugate&searcher= drugs (accessed on 29 June 2021).
29. Kim, E.G.; Kim, K.M. Strategies and Advancement in Antibody-Drug Conjugate Optimization for Targeted Cancer Therapeutics. *Biomol. Ther. (Seoul)* **2015**, *23*, 493–509. [CrossRef] [PubMed]
30. Govindan, S.V.; Sharkey, R.M.; Goldenberg, D.M. Prospects and progress of antibody-drug conjugates in solid tumor therapies. *Expert Opin. Biol. Ther.* **2016**, *16*, 883–893. [CrossRef] [PubMed]
31. Minchinton, A.I.; Tannock, I.F. Drug penetration in solid tumours. *Nat. Rev. Cancer* **2006**, *6*, 583–592. [CrossRef] [PubMed]
32. Trédan, O.; Galmarini, C.M.; Patel, K.; Tannock, I.F. Drug resistance and the solid tumor microenvironment. *J. Natl. Cancer Inst.* **2007**, *99*, 1441–1454. [CrossRef]
33. Tiller, K.E.; Tessier, P.M. Advances in Antibody Design. *Annu. Rev. Biomed. Eng.* **2015**, *17*, 191–216. [CrossRef]
34. Thway, K.; Robertson, D.; Jones, R.L.; Selfe, J.; Shipley, J.; Fisher, C.; Isacke, C.M. Endosialin expression in soft tissue sarcoma as a potential marker of undifferentiated mesenchymal cells. *Br. J. Cancer* **2016**, *115*, 473–479. [CrossRef]
35. Naylor, A.J.; Azzam, E.; Smith, S.; Croft, A.; Poyser, C.; Duffield, J.S.; Huso, D.L.; Gay, S.; Ospelt, C.; Cooper, M.S.; et al. The mesenchymal stem cell marker CD248 (Endosialin) is a negative regulator of bone formation in mice. *Arthritis Rheum.* **2012**, *64*, 3334–3343. [CrossRef]
36. Simonavicius, N.; Ashenden, M.; van Weverwijk, A.; Lax, S.; Husoi, D.L.; Buckley, C.D.; Huijbers, I.J.; Yarwood, H.; Isacke, C.M. Pericytes promote selective vessel regression to regulate vascular patterning. *Blood* **2012**, *120*, 1516–1527. [CrossRef]
37. Rouleau, C.; Curiel, M.; Weber, W.; Smale, R.; Kurtzberg, L.; Mascarello, J.; Berger, C.; Wallar, G.; Bagley, R.; Honma, N.; et al. Endosialin protein expression and therapeutic target potential in human solid tumors: Sarcoma versus carcinoma. *Clin. Cancer Res.* **2008**, *14*, 7223–7236. [CrossRef]
38. Rouleau, C.; Smale, R.; Fu, Y.S.; Hui, G.; Wang, F.; Hutto, E.; Fogle, R.; Jones, C.M.; Krumbholz, R.; Roth, S.; et al. Endosialin is expressed in high grade and advanced sarcomas: Evidence from clinical specimens and preclinical modeling. *Int. J. Oncol.* **2011**, *39*, 73–89. [CrossRef] [PubMed]
39. Rouleau, C.; Gianolio, D.A.; Smale, R.; Roth, S.D.; Krumbholz, R.; Harper, J.; Munroe, K.J.; Green, T.L.; Horten, B.C.; Schmid, S.M.; et al. Anti-Endosialin Antibody-Drug Conjugate: Potential in Sarcoma and Other Malignancies. *Mol. Cancer Ther.* **2015**, *14*, 2081–2089. [CrossRef] [PubMed]
40. Capone, E.; Piccolo, E.; Fichera, I.; Ciufici, P.; Barcaroli, D.; Sala, A.; De Laurenzi, V.; Iacobelli, V.; Iacobelli, S.; Sala, G. Generation of a novel Antibody-Drug Conjugate targeting endosialin: Potent and durable antitumor response in sarcoma. *Oncotarget* **2017**, *8*, 60368–60377. [CrossRef]
41. Selim, A.A.; Abdelmagid, S.M.; Kanaan, R.A.; Smock, S.L.; Owen, T.A.; Popoff, S.N.; Safadi, F.F. Anti-osteoactivin antibody inhibits osteoblast differentiation and function in vitro. *Crit. Rev. Eukaryot. Gene Expr.* **2003**, *13*, 265–275. [CrossRef]
42. Sheng, M.H.; Wergedal, J.E.; Mohan, S.; Lau, K.H. Osteoactivin is a novel osteoclastic protein and plays a key role in osteoclast differentiation and activity. *FEBS Lett.* **2008**, *582*, 1451–1458. [CrossRef] [PubMed]
43. Kubista, B.; Klinglmueller, F.; Bilban, M.; Pfeiffer, M.; Lass, R.; Giurea, A.; Funovics, P.T.; Toma, C.; Dominkus, M.; Kotz, R.; et al. Microarray analysis identifies distinct gene expression profiles associated with histological subtype in human osteosarcoma. *Int. Orthop.* **2011**, *35*, 401–411. [CrossRef]
44. Taya, M.; Hammes, S.R. Glycoprotein Non-Metastatic Melanoma Protein B (GPNMB) and Cancer: A Novel Potential Therapeutic Target. *Steroids* **2018**, *133*, 102–107. [CrossRef]
45. Rich, J.N.; Shi, Q.; Hjelmeland, M.; Cummings, T.J.; Kuan, C.T.; Bigner, D.D.; Counter, C.M.; Wang, X.F. Bone-related genes expressed in advanced malignancies induce invasion and metastasis in a genetically defined human cancer model. *J. Biol. Chem.* **2003**, *278*, 15951–15957. [CrossRef]
46. Zhou, L.T.; Liu, F.Y.; Li, Y.; Peng, Y.M.; Liu, Y.H.; Li, J. Gpnmb/osteoactivin, an attractive target in cancer immunotherapy. *Neoplasma* **2012**, *59*, 1–5. [CrossRef]
47. Roth, M.; Barris, D.M.; Piperdi, S.; Kuo, V.; Everts, S.; Geller, D.; Houghton, P.; Kolb, E.A.; Hawthorne, T.; Gill, J.; et al. Targeting Glycoprotein NMB With Antibody-Drug Conjugate, Glembatumumab Vedotin, for the Treatment of Osteosarcoma. *Pediatr. Blood Cancer* **2016**, *63*, 32–38. [CrossRef] [PubMed]
48. Cui, J.; Dean, D.; Wei, R.; Hornicek, F.J.; Ulmert, D.; Duan, Z. Expression and clinical implications of leucine-rich repeat containing 15 (LRRC15) in osteosarcoma. *J. Orthop. Res.* **2020**, *38*, 2362–2372. [CrossRef] [PubMed]
49. Purcell, J.W.; Tanlimco, S.G.; Hickson, J.; Fox, M.; Sho, M.; Durkin, L.; Uziel, T.; Powers, R.; Foster, K.; McGonigal, T.; et al. LRRC15 Is a Novel Mesenchymal Protein and Stromal Target for Antibody-Drug Conjugates. *Cancer Res.* **2018**, *78*, 4059–4072. [CrossRef] [PubMed]
50. Ben-Ami, E.; Perret, R.; Huang, Y.; Courgeon, F.; Gokhale, P.C.; Laroche-Clary, A.; Eschle, B.K.; Velasco, V.; Le Loarer, F.; Algeo, M.P.; et al. LRRC15 Targeting in Soft-Tissue Sarcomas: Biological and Clinical Implications. *Cancers* **2020**, *12*, 757. [CrossRef] [PubMed]
51. Thiery, J.P.; Duband, J.L.; Rutishauser, U.; Edelman, G.M. Cell adhesion molecules in early chicken embryogenesis. *Proc. Natl. Acad. Sci. USA* **1982**, *79*, 6737–6741. [CrossRef]
52. Huang, R.; Yuan, D.J.; Li, S.; Liang, X.S.; Gao, Y.; Lan, X.Y.; Qin, H.M.; Ma, Y.F.; Xu, G.Y.; Schachner, M.; et al. NCAM regulates temporal specification of neural progenitor cells via profilin2 during corticogenesis. *J. Cell Biol.* **2020**, *219*, e201902164. [CrossRef]

53. Oboshi, W.; Aki, K.; Tada, T.; Watanabe, T.; Yukimasa, N.; Ueno, I.; Saito, K.; Hosoi, E. Flow Cytometric Evaluation of Surface CD56 Expression on Activated Natural Killer Cells as Functional Marker. *J. Med. Investig.* **2016**, *63*, 199–203. [CrossRef]

54. Mechtersheimer, G.; Staudter, M.; Möller, P. Expression of the natural killer cell-associated antigens CD56 and CD57 in human neural and striated muscle cells and in their tumors. *Cancer Res.* **1991**, *51*, 1300–1307.

55. Molenaar, W.M.; Muntinghe, F.L. Expression of neural cell adhesion molecules and neurofilament protein isoforms in Ewing's sarcoma of bone and soft tissue sarcomas other than rhabdomyosarcoma. *Hum. Pathol.* **1999**, *30*, 1207–1212. [CrossRef]

56. Ikushima, S.; Yoshihara, T.; Matsumura, T.; Misawa, S.; Morioka, Y.; Hibi, S.; Imashuku, S. Expression of CD56/NCAM on hematopoietic malignant cells. A useful marker for acute monocytic and megakaryocytic leukemias. *Int. J. Hematol.* **1991**, *54*, 395–403.

57. Wood, A.C.; Maris, J.M.; Gorlick, R.; Kolb, E.A.; Keir, S.T.; Reynolds, C.P.; Kang, M.H.; Wu, J.; Kurmasheva, R.T.; Whiteman, K.; et al. Initial testing (Stage 1) of the antibody-maytansinoid conjugate, IMGN901 (Lorvotuzumab mertansine), by the pediatric preclinical testing program. *Pediatr. Blood Cancer* **2013**, *60*, 1860–1867. [CrossRef]

58. Ailawadhi, S.; Kelly, K.R.; Vescio, R.A.; Jagannath, S.; Wolf, J.; Gharibo, M.; Sher, T.; Bojanini, L.; Kirby, M.; Chanan-Khan, A. A Phase I Study to Assess the Safety and Pharmacokinetics of Single-agent Lorvotuzumab Mertansine (IMGN901) in Patients with Relapsed and/or Refractory CD-56-positive Multiple Myeloma. *Clin. Lymphoma Myeloma Leuk.* **2019**, *19*, 29–34. [CrossRef]

59. López-Novoa, J.M.; Bernabeu, C. The physiological role of endoglin in the cardiovascular system. *Am. J. Physiol. Heart Circ. Physiol.* **2010**, *299*, H959–H974. [CrossRef]

60. Arthur, H.M.; Ure, J.; Smith, A.J.; Renforth, G.; Wilson, D.I.; Torsney, E.; Charlton, R.; Parums, D.V.; Jowett, T.; Marchuk, D.A.; et al. Endoglin, an ancillary TGFbeta receptor, is required for extraembryonic angiogenesis and plays a key role in heart development. *Dev. Biol.* **2000**, *217*, 42–53. [CrossRef] [PubMed]

61. Pardali, E.; van der Schaft, D.W.; Wiercinska, E.; Gorter, A.; Hogendoorn, P.C.; Griffioen, A.W.; ten Dijke, P. Critical role of endoglin in tumor cell plasticity of Ewing sarcoma and melanoma. *Oncogene* **2011**, *30*, 334–345. [CrossRef]

62. Puerto-Camacho, P.; Amaral, A.T.; Lamhamedi-Cherradi, S.E.; Menegaz, B.A.; Castillo-Ecija, H.; Ordóñez, J.L.; Domínguez, S.; Jordan-Perez, C.; Diaz-Martin, J.; Romero-Pérez, L.; et al. Preclinical Efficacy of Endoglin-Targeting Antibody-Drug Conjugates for the Treatment of Ewing Sarcoma. *Clin. Cancer Res.* **2019**, *25*, 2228–2240. [CrossRef] [PubMed]

63. Wienke, D.; MacFadyen, J.R.; Isacke, C.M. Identification and characterization of the endocytic transmembrane glycoprotein Endo180 as a novel collagen receptor. *Mol. Biol. Cell* **2003**, *14*, 3592–3604. [CrossRef] [PubMed]

64. Kjøller, L.; Engelholm, L.H.; Høyer-Hansen, M.; Danø, K.; Bugge, T.H.; Behrendt, N. uPARAP/endo180 directs lysosomal delivery and degradation of collagen IV. *Exp. Cell Res.* **2004**, *293*, 106–116. [CrossRef] [PubMed]

65. Engelholm, L.H.; Nielsen, B.S.; Netzel-Arnett, S.; Solberg, H.; Chen, X.D.; Lopez Garcia, J.M.; Lopez-Otin, C.; Young, M.F.; Birkedal-Hansen, H.; Danø, K.; et al. The urokinase plasminogen activator receptor-associated protein/endo180 is coexpressed with its interaction partners urokinase plasminogen activator receptor and matrix metalloprotease-13 during osteogenesis. *Lab. Investig.* **2001**, *81*, 1403–1414. [CrossRef]

66. Isacke, C.M.; van der Geer, P.; Hunter, T.; Trowbridge, I.S. p180, a novel recycling transmembrane glycoprotein with restricted cell type expression. *Mol. Cell Biol.* **1990**, *10*, 2606–2618. [CrossRef] [PubMed]

67. Nielsen, C.F.; van Putten, S.M.; Lund, I.K.; Melander, M.C.; Nørregaard, K.S.; Jürgensen, H.J.; Reckzeh, K.; Christensen, K.R.; Ingvarsen, S.Z.; Gårdsvoll, H.; et al. The collagen receptor uPARAP/Endo180 as a novel target for antibody-drug conjugate mediated treatment of mesenchymal and leukemic cancers. *Oncotarget* **2017**, *8*, 44605–44624. [CrossRef]

68. Borcherding, N.; Kusner, D.; Liu, G.H.; Zhang, W. ROR1, an embryonic protein with an emerging role in cancer biology. *Protein Cell* **2014**, *5*, 496–502. [CrossRef] [PubMed]

69. Beerli, R.R.; Waldmeier, L.; Gébleux, R.; Pretto, F.; Grawunder, U. NBE-002, an anthracycline-based immune-stimulatory antibody drug conjugate (iADC) targeting ROR1 for the treatment of triple-negative breast cancer. In Proceedings of the American Association for Cancer Research Annual Meeting 2019, Atlanta, GA, USA, 29 March–3 April 2019.

70. Debebe, Z.; Rathmell, W.K. Ror2 as a therapeutic target in cancer. *Pharmacol. Ther.* **2015**, *150*, 143–148. [CrossRef]

71. Liu, Y.; Bhat, R.A.; Seestaller-Wehr, L.M.; Fukayama, S.; Mangine, A.; Moran, R.A.; Komm, B.S.; Bodine, P.V.; Billiard, J. The orphan receptor tyrosine kinase Ror2 promotes osteoblast differentiation and enhances ex vivo bone formation. *Mol. Endocrinol.* **2007**, *21*, 376–387. [CrossRef] [PubMed]

72. Sharp, L.L.; Chang, C.; Frey, G.; Wang, J.; Liu, H.; Xing, C.; Yalcin, S.; Walls, M.; Ben, Y.; Boyle, W.J.; et al. Anti-tumor efficacy of BA3021, a novel Conditionally Active Biologic (CAB) anti-ROR2 ADC. In Proceedings of the American Association for Cancer Research Annual Meeting 2018, Chicago, IL, USA, 14–18 April 2018.

73. Zhu, C.; Wei, Y.; Wei, X. AXL receptor tyrosine kinase as a promising anti-cancer approach: Functions, molecular mechanisms and clinical applications. *Mol. Cancer* **2019**, *18*, 153. [CrossRef] [PubMed]

74. Rankin, E.B.; Giaccia, A.J. The Receptor Tyrosine Kinase AXL in Cancer Progression. *Cancers* **2016**, *8*, 103. [CrossRef]

75. Han, J.; Tian, R.; Yong, B.; Luo, C.; Tan, P.; Shen, J.; Peng, T. Gas6/Axl mediates tumor cell apoptosis, migration and invasion and predicts the clinical outcome of osteosarcoma patients. *Biochem. Biophys. Res. Commun.* **2013**, *435*, 493–500. [CrossRef]

76. Sharp, L.L.; Chang, C.; Frey, G.; Wang, J.; Liu, H.; Xing, C.; Yalcin, S.; Walls, M.; Ben, Y.; Boyle, W.J.; et al. Anti-tumor efficacy of BA3011, a novel Conditionally Active Biologic (CAB) anti-AXL-ADC. In Proceedings of the American Association for Cancer Research Annual Meeting 2018, Chicago, IL, USA, 14–18 April 2018.

77. Koopman, L.A.; Terp, M.G.; Zom, G.G.; Janmaat, M.L.; Jacobsen, K.; Gresnigt-van den Heuvel, E.; Brandhorst, M.; Forssmann, U.; de Bree, F.; Pencheva, N.; et al. Enapotamab vedotin, an AXL-specific antibody-drug conjugate, shows preclinical antitumor activity in non-small cell lung cancer. *JCI Insight* **2019**, *4*, e128199. [CrossRef]
78. Wajant, H. Therapeutic targeting of CD70 and CD27. *Expert Opin. Ther. Targets.* **2016**, *20*, 959–973. [CrossRef]
79. Nakae, R.; Matsuzaki, S.; Serada, S.; Matsuo, K.; Shiomi, M.; Sato, K.; Nagase, Y.; Matsuzaki, S.; Nakagawa, S.; Hiramatsu, K.; et al. CD70 antibody-drug conjugate as a potential therapeutic agent for uterine leiomyosarcoma. *Am. J. Obstet Gynecol.* **2021**, *224*, 197.e1–197.e23. [CrossRef] [PubMed]
80. Pluschke, G.; Vanek, M.; Evans, A.; Dittmar, T.; Schmid, P.; Itin, P.; Filardo, E.J.; Reisfeld, R.A. Molecular cloning of a human melanoma-associated chondroitin sulfate proteoglycan. *Proc. Natl. Acad. Sci. USA* **1996**, *93*, 9710–9715. [CrossRef]
81. Rolih, V.; Barutello, G.; Iussich, S.; De Maria, R.; Quaglino, E.; Buracco, P.; Cavallo, F.; Riccardo, F. CSPG4: A prototype oncoantigen for translational immunotherapy studies. *J. Transl. Med.* **2017**, *15*, 151. [CrossRef]
82. Brehm, H.; Niesen, J.; Mladenov, R.; Stein, C.; Pardo, A.; Fey, G.; Helfrich, W.; Fischer, R.; Gattenlöhner, S.; Barth, S. A CSPG4-specific immunotoxin kills rhabdomyosarcoma cells and binds to primary tumor tissues. *Cancer Lett.* **2014**, *352*, 228–235. [CrossRef]
83. Murphrey, M.B.; Quaim, L.; Varacallo, M. Biochemistry, Epidermal Growth Factor Receptor. [Updated 12 September 2020]. In StatPearls [Internet]. Treasure Island (FL): StatPearls Publishing, 2021. Available online: https://www.ncbi.nlm.nih.gov/books/NBK482459/ (accessed on 2 July 2021).
84. Kersting, N.; Kunzler Souza, B.; Araujo Vieira, I.; Pereira Dos Santos, R.; Brufatto Olguins, D.; José Gregianin, L.; Tesainer Brunetto, A.; Lunardi Brunetto, A.; Roesler, R.; Brunetto de Farias, C.; et al. Epidermal Growth Factor Receptor Regulation of Ewing Sarcoma Cell Function. *Oncology* **2018**, *94*, 383–393. [CrossRef]
85. Ganti, R.; Skapek, S.X.; Zhang, J.; Fuller, C.E.; Wu, J.; Billups, C.A.; Breitfeld, P.P.; Dalton, J.D.; Meyer, W.H.; Khoury, J.D. Expression and genomic status of EGFR and ErbB-2 in alveolar and embryonal rhabdomyosarcoma. *Mod. Pathol.* **2006**, *19*, 1213–1220. [CrossRef]
86. Niesen, J.; Brehm, H.; Stein, C.; Berges, N.; Pardo, A.; Fischer, R.; Ten Haaf, A.; Gattenlöhner, S.; Tur, M.K.; Barth, S. In vitro effects and ex vivo binding of an EGFR-specific immunotoxin on rhabdomyosarcoma cells. *J. Cancer Res. Clin. Oncol.* **2015**, *141*, 1049–1061. [CrossRef] [PubMed]
87. Ricci, C.; Polito, L.; Nanni, P.; Landuzzi, L.; Astolfi, A.; Nicoletti, G.; Rossi, I.; De Giovanni, C.; Bolognesi, A.; Lollini, P.L. HER/erbB receptors as therapeutic targets of immunotoxins in human rhabdomyosarcoma cells. *J. Immunother.* **2002**, *25*, 314–323. [CrossRef] [PubMed]
88. Embleton, M.J.; Byers, V.S.; Lee, H.M.; Scannon, P.; Blackhall, N.W.; Baldwin, R.W. Sensitivity and selectivity of ricin toxin A chain-monoclonal antibody 791T/36 conjugates against human tumor cell lines. *Cancer Res.* **1986**, *46*, 5524–5528.
89. Byers, V.S.; Pawluczyk, I.Z.; Hooi, D.S.; Price, M.R.; Carroll, S.; Embleton, M.J.; Garnett, M.C.; Berry, N.; Robins, R.A.; Baldwin, R.W. Endocytosis of immunotoxin-791T/36-RTA by tumor cells in relation to its cytotoxic action. *Cancer Res.* **1991**, *51*, 1990–1995. [PubMed]
90. Modak, S.; Kramer, K.; Gultekin, S.H.; Guo, H.F.; Cheung, N.K. Monoclonal antibody 8H9 targets a novel cell surface antigen expressed by a wide spectrum of human solid tumors. *Cancer Res.* **2001**, *61*, 4048–4054.
91. Dong, P.; Xiong, Y.; Yue, J.; Hanley, S.J.B.; Watari, H. B7H3 As a Promoter of Metastasis and Promising Therapeutic Target. *Front. Oncol.* **2018**, *8*, 264. [CrossRef]
92. Onda, M.; Wang, Q.C.; Guo, H.F.; Cheung, N.K.; Pastan, I. In vitro and in vivo cytotoxic activities of recombinant immunotoxin 8H9(Fv)-PE38 against breast cancer, osteosarcoma, and neuroblastoma. *Cancer Res.* **2004**, *64*, 1419–1424. [CrossRef] [PubMed]
93. Bruland, O.S.; Fodstad, O.; Stenwig, A.E.; Pihl, A. Expression and characteristics of a novel human osteosarcoma-associated cell surface antigen. *Cancer Res.* **1988**, *48*, 5302–5309.
94. Anderson, P.M.; Meyers, D.E.; Hasz, D.E.; Covalcuic, K.; Saltzman, D.; Khanna, C.; Uckun, F.M. In vitro and in vivo cytotoxicity of an anti-osteosarcoma immunotoxin containing pokeweed antiviral protein. *Cancer Res.* **1995**, *55*, 1321–1327.
95. Onda, M.; Bruland, Ø.S.; Pastan, I. TP-3 immunotoxins improve antitumor activity in mice with osteosarcoma. *Clin. Orthop. Relat. Res.* **2005**, *430*, 142–148. [CrossRef]
96. Barzegar Behrooz, A.; Syahir, A.; Ahmad, S. CD133: Beyond a cancer stem cell biomarker. *J. Drug Target.* **2019**, *27*, 257–269. [CrossRef] [PubMed]
97. Liu, B.; Ma, W.; Jha, R.K.; Gurung, K. Cancer stem cells in osteosarcoma: Recent progress and perspective. *Acta Oncol.* **2011**, *50*, 1142–1150. [CrossRef] [PubMed]
98. Stratford, E.W.; Bostad, M.; Castro, R.; Skarpen, E.; Berg, K.; Høgset, A.; Myklebost, O.; Selbo, P.K. Photochemical internalization of CD133-targeting immunotoxins efficiently depletes sarcoma cells with stem-like properties and reduces tumorigenicity. *Biochim. Biophys. Acta* **2013**, *1830*, 4235–4243. [CrossRef]
99. Guo, Y.; Hu, J.; Wang, Y.; Peng, X.; Min, J.; Wang, J.; Matthaiou, E.; Cheng, Y.; Sun, K.; Tong, X.; et al. Tumour endothelial marker 1/endosialin-mediated targeting of human sarcoma. *Eur. J. Cancer.* **2018**, *90*, 111–121. [CrossRef]
100. Rizzieri, D. Zevalin® (ibritumomab tiuxetan): After more than a decade of treatment experience, what have we learned? *Crit. Rev. Oncol. Hematol.* **2016**, *105*, 5–17. [CrossRef]
101. Wang, Z.; Yan, X. CD146, a multi-functional molecule beyond adhesion. *Cancer Lett.* **2013**, *330*, 150–162. [CrossRef] [PubMed]

102. Westrøm, S.; Bønsdorff, T.B.; Abbas, N.; Bruland, Ø.S.; Jonasdottir, T.J.; Mælandsmo, G.M.; Larsen, R.H. Evaluation of CD146 as Target for Radioimmunotherapy against Osteosarcoma. *PLoS ONE* **2016**, *11*, e0165382. [CrossRef] [PubMed]

103. Hassan, S.E.; Bekarev, M.; Kim, M.Y.; Lin, J.; Piperdi, S.; Gorlick, R.; Geller, D.S. Cell surface receptor expression patterns in osteosarcoma. *Cancer* **2012**, *118*, 740–749. [CrossRef] [PubMed]

104. Karkare, S.; Allen, K.J.H.; Jiao, R.; Malo, M.E.; Dawicki, W.; Helal, M.; Godson, D.L.; Dickinson, R.; MacDonald-Dickinson, V.; Yang, R.; et al. Detection and targeting insulin growth factor receptor type 2 (IGF2R) in osteosarcoma PDX in mouse models and in canine osteosarcoma tumors. *Sci. Rep.* **2019**, *9*, 11476. [CrossRef] [PubMed]

105. Nagayama, S.; Katagiri, T.; Tsunoda, T.; Hosaka, T.; Nakashima, Y.; Araki, N.; Kusuzaki, K.; Nakayama, T.; Tsuboyama, T.; Nakamura, T.; et al. Genome-wide analysis of gene expression in synovial sarcomas using a cDNA microarray. *Cancer Res.* **2002**, *62*, 5859–5866.

106. Fukukawa, C.; Hanaoka, H.; Nagayama, S.; Tsunoda, T.; Toguchida, J.; Endo, K.; Nakamura, Y.; Katagiri, T. Radioimmunotherapy of human synovial sarcoma using a monoclonal antibody against FZD10. *Cancer Sci.* **2008**, *99*, 432–440. [CrossRef]

107. Hanaoka, H.; Katagiri, T.; Fukukawa, C.; Yoshioka, H.; Yamamoto, S.; Iida, Y.; Higuchi, T.; Oriuchi, N.; Paudyal, B.; Paudyal, P.; et al. Radioimmunotherapy of solid tumors targeting a cell-surface protein, FZD10: Therapeutic efficacy largely depends on radiosensitivity. *Ann. Nucl. Med.* **2009**, *23*, 479–485. [CrossRef]

108. Giraudet, A.L.; Cassier, P.A.; Iwao-Fukukawa, C.; Garin, G.; Badel, J.N.; Kryza, D.; Chabaud, S.; Gilles-Afchain, L.; Clapisson, G.; Desuzinges, C.; et al. A first-in-human study investigating biodistribution, safety and recommended dose of a new radiolabeled MAb targeting FZD10 in metastatic synovial sarcoma patients. *BMC Cancer* **2018**, *18*, 646. [CrossRef]

109. Sarrut, D.; Badel, J.N.; Halty, A.; Garin, G.; Perol, D.; Cassier, P.; Blay, J.Y.; Kryza, D.; Giraudet, A.L. 3D absorbed dose distribution estimated by Monte Carlo simulation in radionuclide therapy with a monoclonal antibody targeting synovial sarcoma. *EJNMMI Phys.* **2017**, *4*, 6. [CrossRef]

110. Li, H.K.; Sugyo, A.; Tsuji, A.B.; Morokoshi, Y.; Minegishi, K.; Nagatsu, K.; Kanda, H.; Harada, Y.; Nagayama, S.; Katagiri, T.; et al. α-particle therapy for synovial sarcoma in the mouse using an astatine-211-labeled antibody against frizzled homolog 10. *Cancer Sci.* **2018**, *109*, 2302–2309. [CrossRef]

111. Hull, A.; Li, Y.; Bartholomeusz, D.; Hsieh, W.; Allen, B.; Bezak, E. Radioimmunotherapy of Pancreatic Ductal Adenocarcinoma: A Review of the Current Status of Literature. *Cancers* **2020**, *12*, 481. [CrossRef] [PubMed]

112. Modak, S.; Zanzonico, P.; Grkovski, M.; Slotkin, E.K.; Carrasquillo, J.A.; Lyashchenko, S.K.; Lewis, J.S.; Cheung, I.Y.; Heaton, T.; LaQuaglia, M.P.; et al. B7H3-Directed Intraperitoneal Radioimmunotherapy With Radioiodinated Omburtamab for Desmoplastic Small Round Cell Tumor and Other Peritoneal Tumors: Results of a Phase I Study. *J. Clin. Oncol.* **2020**, *38*, 4283–4291. [CrossRef] [PubMed]

113. Joubert, N.; Beck, A.; Dumontet, C.; Denevault-Sabourin, C. Antibody-Drug Conjugates: The Last Decade. *Pharmaceuticals* **2020**, *13*, 245. [CrossRef] [PubMed]

114. Hatina, J.; Kripnerova, M.; Houfkova, K.; Pesta, M.; Kuncova, J.; Sana, J.; Slaby, O.; Rodríguez, R. Sarcoma Stem Cell Heterogeneity. *Adv. Exp. Med. Biol.* **2019**, *1123*, 95–118. [CrossRef]

115. Abarrategi, A.; Tornin, J.; Martinez-Cruzado, L.; Hamilton, A.; Martinez-Campos, E.; Rodrigo, J.P.; González, M.V.; Baldini, N.; Garcia-Castro, J.; Rodriguez, R. Osteosarcoma: Cells-of-Origin, Cancer Stem Cells, and Targeted Therapies. *Stem Cells Int.* **2016**, *2016*, 3631764. [CrossRef] [PubMed]

1.4 Preclinical bi-dimensional and tridimensional models for cancer therapy

Cell cultures have been proven to be indispensable for a variety of applications, from research to industrial perspectives. Cell culture techniques have come a long way since the first cell line, HeLa, was established. Established cell lines can be cultured as monolayer adherent cells or in suspension. Bi-dimensional cultures are inexpensive, easy to grow and manipulate; in addition, many different types of cancer cell lines can be easily purchased, allowing researches on almost any type of tumor. However, it is important underlying that 2D models cannot simulate the microenvironment and the architecture of the original tumors. Moreover, 2D-cultured cells are stretched and undergo cytoskeletal rearrangements acquiring artificial polarity, which in turn causes aberrant gene and protein expression [155]. For many years, 2D cultured cancer cells have been used for anticancer drug screening and discovery. However, different studies reported that many high cytotoxic drugs tested in 2D models were actually ineffective or less cytotoxic in clinical practice [156]. The advancements in cell imaging and analytical systems, as well as the applications of new scaffolds and matrices, have paved the way to the establishment of tridimensional cell models. 3D-cultured systems are receiving more and more attention because they can recapitulate tumor histology and structural complexity, interaction with tumor microenvironment, gene expression and signaling pathway profiles, present on "in vivo" tumor, thus proving to be a useful tool for cancer research and many other applications [157, 158, 159]. Spheroids and organoids are the most promising 3D models developed since they can better mimic the pathophysiology of human cancers, filling the gap between traditional 2D cultures and animal models. Different methods to "assemble" in vitro 3D-cultured models have been developed to recapitulate in vivo suboptimal growth conditions and to study the features of tumor microenvironment. These methods are usually categorized into two main types: scaffold-based and scaffold-free systems. The use of 3D models could potentially improve the robustness and reliability of preclinical research outcomes, reducing animal testing and favoring their transition to clinical practice. Specific features of spheroids and organoids will be discussed in the following paragraphs.

1.4.1   Single spheroids

3D single spheroid models are largely used in biology to evaluate cell death, proliferation, differentiation, and metabolism of tumor cells as well as preclinical outcome of tumor cells treated with standard chemotherapy drugs or radiotherapy [160]. Single spheroids maintain cell-cell interaction and enrichment in cancer stem cells, showing some similarity even if not

completely to what happen in "in vivo" tumors [161]. Spheroids can be obtained starting from a single-cell suspension that is self-assembling or forced to aggregate [162]. Tumor spheroids ($>500\,\mu m$ in diameter) are formed by many layers where cells have different phenotypic, functional, and metabolic status. In particular, spheroids present an external proliferative layer, an intermediate zone composed of quiescent and senescent cells and an inner apoptotic and necrotic core deriving from the reduced presence of nutrients and oxygen in these areas [163]. Under hypoxic conditions, cancer cells switch from oxidative phosphorylation to anaerobic glycolysis, producing lactate that cause the acidification of the inner areas of spheroids. Low pH and hypoxia induce cancer cells belonging to this region to undergo in a quiescent/senescent state as occurs in "in vivo" tumors [164]. Cell-containing spheroids are mostly spatially close but unable to form specialized cell connections; in few cases, spheroids present a strong cell-cell interaction that is enforced by desmosomes and cell junction through E-cadherins and the secretion of ECM proteins (collagens, fibronectin, laminin, elastin tenascin) [165, 166]. These characteristics cause the increase of spheroid density, which further limit the penetration and transport of drugs into spheroids. In addition, many studies reported that spheroids are enriched in cancer stem cells (CSC), a subpopulation of cell with stem-like properties, present in the mass of different types of tumors, characterized by unlimited self-renewal capacity and differentiation potential [167, 168]. CSC are characterized by increased activity of aldehyde dehydrogenase (ALDH) as well as overexpression of CD133 and CD44 [169, 170]. In tumors, poor intracellular uptake of drugs, oxygen, nutrients and metabolites gradients and CSC are strongly connected to phenomenon of chemotherapy resistance and influence the therapeutic effects of various anticancer drugs [171, 172, 173]. Overcoming the limitations of traditional monolayer cell culture and resembling many of the characteristics of the original tumor, spheroids are a promising tool in cancer research, drug screening and preclinical studies. There are four major techniques to promote spheroids formation, avoiding cells adhesion to the surfaces and favoring cell–cell interactions and self-aggregation: agitation-based techniques, hanging-drop procedures, liquid overlay methods, and microfluidics [174]. Among them, the use of liquid overlay method allows the creation of single spheroids in 96-well ultra-low attachment plate for high-throughput cell functional and toxicity analysis [175]. However, spheroid culture system has many limitations: i.) obtaining spheroids of uniform size and shape need optimization; ii.) spheroid formation may requires specialized culture plates and equipment; iii.) spheroids are difficult to manipulate before to proceed with downstream experiments [176].

1.4.2 Organoids

The recent development of in vitro culture techniques for growing tissue as 3D cultures have paved the way for the establishment of 3D organoids. 3D organoids are self-organized formation resembling the phenotypic, structural and genetic features of the tissue from which they are derived from [177]. Organoids can be generated from healthy or diseased tissue, such as patient-derived tumor specimens, making these models increasingly used in different range of studies such as disease modeling, drug discovery, personalized treatment and screening, and regenerative medicine [178, 179]. To date, 3D organoid cultures have been established starting from a multitude of healthy and cancer tissues including colon, breast, liver, lung, pancreas, endometrium, stomach, prostate, ovary, bladder, kidney, brain, bone, and esophagus [180]. Tumor-derived organoids are characterized by gene expression and signaling pathway profiles, heterogeneity, cell-matrix interactions and structural complexity that recapitulate the tumor from which they are derived [181, 182]. Personalized medicine and drug screening represent one of the main fields in which organoids can be applied [183]. Considering that organoids maintain the genetic heterogeneity of the primary tumor, patient-derived organoids can be used to identify the ideal treatment for a specific patient, allowing the selection of the compound (or a combination of payloads) that induce the best response [184, 185]. After the establishment of patient-derived organoids, a rapid viability functional assay can be used to determine drug sensitivities of primary specimens and offer information to help adapting therapy to individual cancer patients [186]. Moreover, considering the possibility to obtain healthy and tumor specimen from the same patient, patient-derived organoids enable to identify drugs that selectively target cancer cells rather than healthy ones, decreasing the risk of side effects [187]. Organoids from primary human pancreatic ductal adenocarcinoma (PDAC) have been established to identify specific effective drugs [188]; Phan and coworkers used patient-derived tumor organoids to identify actionable drug sensitivities of three ovarian cancer samples and one high-grade serous peritoneal cancer specimen [189]. To do that, authors used a "mini-ring approach, a simple high-throughput strategy that entails, generating mini-rings around the rim of the wells, which allows to perform assays in high throughput with minimal manipulation [190, 191]. Organoids have been also used to assess the involvement of mutational processes in tumorigenesis. In this context, the use of CRISPR-Cas9 technology on organoids had led to remarkable improvements [192,193]. Tumor organoids have been also utilized to evaluate the role of tumor microenvironment in cancer progression. Allowing the presence of native immune and stromal cells, this model has led to a better understanding of

cell–cell interactions, immune checkpoint blockade modelling and CAR-T cell-mediated cytotoxicity testing [194, 195, 196].

Chapter 2 – Aim of the project

Ribosome-Inactivating Proteins (RIPs) are plant toxins with N-glycosylase rRNA activity, which prevents the binding between the elongation factor EF-2 and the major subunit of ribosomes, thus causing irreversible blockade of protein synthesis [197]. RIPs can also act on other substrates (DNA, tRNA, mRNA, polyA and PARP), inducing cell death through multiple pathways such as apoptosis, necroptosis and autophagy [198]. Due to their activity on multiple molecular targets, RIPs have high antitumor potential. However, they lack the selectivity necessary for their therapeutic use. The increase in specificity and cytotoxic efficacy can be achieved by conjugating RIPs to monoclonal antibodies (mAbs) to form the so-called immunotoxins (ITs) [199].

Although rare, sarcomas are one of the most common types of cancer in children and include more than 50 highly heterogeneous tumor histotypes originating from mesenchymal tissue. Among the most widespread types of childhood sarcomas we find: embryonic rhabdomyosarcoma, osteosarcoma and Ewing's sarcoma [200]. The standard treatment regimen for these cancers consists of a multimodal approach combining surgery, chemotherapy and radiotherapy [201, 202]. However, this strategy does not often prove to be conclusive, given that many patients with localized primary sarcoma can undergo relapse, progression and metastasis following standard treatment. Furthermore, the situation remains critical in metastatic patients, where the 5-year survival rate is 15%, unlike what is found in patients with localized disease, where 5-year survival rate is equal to 81% [203]. In order to improve patient outcome, new therapeutic strategies need to be evaluated. Among these, immunotherapy is one of the most promising for the treatment of cancer [204]. Immunotherapy can exploit different therapeutic approaches, including the use of targeting-carriers conjugated to a cytotoxic molecule. This strategy has paved the way for the development of ITs, containing plant or bacterial toxins, used in numerous preclinical studies and in various clinical trials, both administered individually and in combination with conventional chemotherapeutic agents [205, 206]. Moreover, the conjugation of mAb with RIPs enhances the toxic activity of unconjugated mAb which is often limited because of phenomena of complement dependent cytotoxicity (CDC) and antibody dependent cell cytotoxicity (ADCC) resistance or selection of apoptosis resistant tumor clones [207]. In order to evaluate the efficacy of new drugs and develop personalized therapeutic protocols, 3D-culture systems are receiving more and more attention. Indeed, tridimensional models can recapitulate tumor histology and structural complexity, tumor cell differentiation, interaction with tumor microenvironment, gene expression and signaling pathway profiles present on "in vivo" tumor. Considering this, 3D models can overcome the limitation of traditional 2D monolayer

cells, proving to be a useful tool for cancer research and many other applications [208, 209, 210]. Organoids and single spheroids represent the most promising disease 3D models; however, differently from single spheroids, organoids can better mimic the pathophysiology of human cancers [211]. The use of IT-based therapy assumes that target cells overexpress antigens against which ITs are directed. It has been described in literature that the transferrin receptor 1 (TfR1), the epidermal growth factor receptor 1 and 2 (EGFR1, Her2) were overexpressed in stabilized cell lines and in primary cultures of early or advanced sarcoma [212, 213, 214, 215]. In addition, it is well-known the use of these antigens in targeted-cancer therapy, such as the targeting therapy against EGFR in breast cancer [216, 217, 218, 219]. Considering this, the research project, carried out during my PhD period, aims to evaluate and compare the cytotoxic effect of specific ITs directed against TfR1, EGFR1 and Her2, in RD18 and U2OS-derived 2D (adherent cells) and 3D models (spheroids and organoids) of sarcoma. To do that, we first established RD18 and U2OS-derived adherent monolayer cells, single spheroids and organoids. Then, we analyzed the expression of TfR1, EGFR1 and Her2, comparing the results between 2D and 3D models. We proceed by choosing the immunoconjugates directed against the selected antigens to investigate type 1 RIP-containing IT cytotoxicity (Tf-SO6, αEGFR1-Ocy, αHer2-Ocy) and apoptosis involvement in organoids, spheroids and bi-dimensional cultures. Last, we investigated the specific IT-induced cytotoxic effect on a patient-derived sarcoma organoid model.

Chapter 3 – Materials and Methods

3.1   Materials

RIPs

Saporin (SO6) was purified from *Saponaria officinalis* seeds through ion-exchange chromatography on S-Sepharose and CM-Sepharose columns (Pharmacia, Sweden) as reported by Stirpe et al., 1983 [220]. Ocymoidine (Ocy) was purified from the seeds of *Saponaria ocymoides* as described in Bolognesi et al., 1995 [221] with one more step, which consists of a hydrophobic interaction chromatography on a phenyl-Sepharose column (Pharmacia, Sweden).

Targeting ligand and antibodies for immunotoxin preparation

Murine monoclonal antibody (mAb) anti-EGFR1 (Mint5) clone 528 was purchased from Oncogene Science (Uniondale, NY, U.S.A). Murine mAb anti-Her2 (MGR-3) was kindly provided by Dr. Silvie Ménard and Dr. Serenella Pupa, National Cancer Institute (Milan, Italy).

Immunotoxins

Transferrin-saporin (Tf-SO6) and anti-EGFR1-ocymoidine (αEGFR1-Ocy) were produced as described in Gosselaar et al., 2002 [222] and in Di Massimo et al., 1997 [223], respectively. Anti-Her2-ocymoidine (αHer2-Ocy) was produced following the same method used for anti-EGFR1 conjugate.

Briefly, unconjugated carrier and RIP were dissolved in 50mM sodium borate buffer and derivatized adding 2-iminothiolane (Sigma-Aldrich St. Louis, MO, US). After 18 h (Tf-so6) or 20 h (αEGFR1-ocy, αHer2-ocy) of reaction at room temperature (RT), conjugate was separated from RIP homopolymers and free carrier by gel filtration on a Sephacryl S200 high-resolution column (100 cm × 2.5 cm) (GE-Healthcare, Buckinghamshire, UK). The conjugates obtained where analyzed by sodium dodecyl sulfate-polyacrylamide gel electrophoresis (SDS-PAGE), in non-reducing conditions: samples were incubated in sample buffer (40 mM Tris-HCl, pH 6.8, 2%SDS, 0.005 % bromophenol blue, 1 mg/ml iodoacetamide) for 30 min at RT and loaded in a 4-15 % PhastGel gradient. At the end of electrophoretic run, gel-containing samples was stained with Commassie brilliant blue, according to manufacturer's instructions (Pharmacia Biotech, Uppsala, Sweden). Molecular weight markers were from Sigma Aldrich. Immunotoxins-RIP/carrier ratio was assessed by densitometric analysis. Immunoconjugates final concentration was reported as RIP content.

Table C. Immunotoxins properties: characteristics of derivatization, conjugation and cell-free protein synthesis activity.

DERIVATIZATION			CONJUGATION	CELL-FREE PROTEIN SYNTHESIS INHIBITORY ACTIVITY
N° of SH-group inserted/molecule (mol/mol)			RIP/carrier (mol/mol)	IC_{50} (ng/mL)
	Carrier	RIP	IT	IT
Tf-SO6	1.15	1.60	1.58	5.03
αEGFR1-Ocy	2.09	0.79	1.82	6.9
αHer2-Ocy	1.47	0.94	2.05	5.75

Cell lines and culture plates

Human embryonal rhabdomyosarcoma (RD18) and human osteosarcoma (U2OS) cell lines were kindly provided by Prof. Pier Luigi Lollini. RD18 and U2OS were maintained respectively in DMEM or RPMI 1640 medium (Corning, NY, US) containing 10% heat-inactivated fetal bovine serum (FBS), 2 mM L-glutamine, 100 U/ml penicillin and 100 μg/ml streptomycin (Sigma-Aldrich), therefore called DMEM or RPMI complete medium, respectively. Cells lines were cultured at 37°C with 5% CO_2 in a HeraCell Haereus incubator (Hanau, Germany) and periodically analyzed for detection of mycoplasma infection. Single spheroids were cultured in serum-free DMEM F-12 medium containing 5 μg/mL bovine insulin, 20 ng/mL rEGF, 20 ng/mL bFGF, 1× B27, 0.5 μg/mL cortisone, 1% penicillin/streptomycin (Corning), therefore named DMEM F-12 complete medium. Organoids were cultured in serum-free Mammocult containing Mammocult supplements (1:10), 0.5 μg/mL hydrocortisone and 4 μg/mL heparin, then named Mammocult complete medium (StemCell Technologies, Vancouver, Canada). Matrigel was purchased by Corning. Cell lines were validated each time after P10 passage by Laragen Inc through Promega GenePrint 24 System. Trypan Blue and trypsin/EDTA were obtained from Biowhittaker (Vervies, Belgium). AO/PI Viability Staining Solution was obtained by Nexcelom (Lawrence, MA, US). Flasks, plates and other cell-related plastic were purchased by BD (Franklin Lakes, NJ, US), Corning and Thermofisher (Waltham, MA, US).

Antibodies for flow cytometry and IHC

Anti-ERBb2/Her2 APC-conjugated mAb (Catalog # IC0041A) was purchased by Novus Biologicals (Centennial, CO, US). Anti-EGFR FITC-conjugated mAb (Catalog #ab11400), anti-Transferrin Receptor PE-conjugated mAb (Catalog #ab18242) and anti-CD133 APC-conjugated mAb (Catalog #ab253259) were bought by Abcam (Cambridge, UK). Ki-67/Caspase-3 (Catalog #PPM240DSAA) and secondary combinatorial staining MACH 2 double Stain 2 (Catalog #MRCT525G) were purchased by Biocare Medical (Pacheco, CA, US). Antibodies were diluted following manufacturer's instructions.

Kits

For adherent cells, viability was assessed using the colorimetric kit CellTiter 96® AQueous One Solution Cell Proliferation Assay (Promega Corporation, WI, US) which contains a tetrazolium compound [3-(4,5-dimethylthiazol-2-yl)-5-(3-carboxymethoxyphenyl)-2-(4-sulfophenyl)-2H-tetrazolium, MTS] and an electron coupling reagent (1-methoxy phenazine methosulfate, PMS). For single spheroids and organoids, cell viability was measured using the luminometric kit CellTiter-Glo® 3D Cell Viability Assay (Promega). Organoids morphology was analyzed using Hematoxylin and Eosin Stain Kit (Vector Laboratories, Burlingame, CA, US). For adherent cells, caspase activity was evaluated using the luminescent kit Caspase-Glo® 3/7 Assay (Promega), which includes a proluminescent caspase-3/7 DEVD-aminoluciferin substrate and a thermostable luciferase in a reagent optimized for caspase-3/7 activity, luciferase activity and cell lysis. For single spheroids and organoids, caspase involvement was measured using the luminometric kit Caspase-Glo® 3/7 3D Assay (Promega), which uses the same chemistry as the Caspase-Glo® 3/7 Assay with an improved technology specific for 3D models.

Reagents and other biotechnological material

Dispase and Ammonium Chloride Solution were purchased from Life Technologies (Carlsbad, CA, US). Collagenase VI, HistoGel and PBS were acquired by Thermofisher. 10% Neutral Buffered Formalin was bought from VWR (Radnor, PA, US). Cellometer Disposable Imaging Chambers were purchased from Nexcelom. All buffers and reagents for IHC were acquired by Biocare medical. Water used was prepared with a Milli-Q apparatus (Millipore, Milford, MA, US).

Instruments and software

For adherent cells and organoids, flow cytometry analysis was done using Attune NxT cell analyzer (UCLA - Flow cytometry core). For single spheroids, flow cytometry experiments were performed using Cytoflex analyzer (Beckman Coulter, Brea, CA, US) and data were plotted using CytExpert software. Viability counting was measured by Cellometer Auto 2000 Cell Viability Counter (Nexcelom). Colorimetric absorbance (492 nm) of adherent cells, in viability experiments, was analyzed by the microtiter plate reader Multiscan EX (ThermoLabsystem, Helsinki, Finland). The luminometer Fluoroskan Ascent FL (Labsystem, Finland) was used for the luminescence measures in adherent cells (apoptosis experiments) and single spheroids (viability and apoptosis experiments). For organoids, luminescence of viability and apoptosis experiments was measured with a SpectraMax iD3 (Molecular Devices, San Jose, CA, US). Organoids treatments were made through EpMotion (Eppendorf, Hamburg, Germany). Morphological analysis of adherent cells and single spheroids was performed using a phase-contrast microscope with a digital camera from Nikon Eclipse TS100 (Chiyoda, Tokyo, Japan). Organoids morphological imaging was performed by Celigo S Imaging Cell Cytometer (Nexcelom) in bright-field mode through Celigo S Software. H&E and IHC images were acquired with a Revolve Upright and Inverted Microscope System (Echo Laboratories, San Diego, CA, US).

Statistical analysis

Statistical analysis was performed using Prism 9. Results are plotted as all values obtained in 4, 3 or 2 independent experiments ± SD. Data were analyzed by One-way Anova, followed by multiple comparison using Tukey or Dunnett's test.

3.2   Methods

3.2.1   Cultures of adherent cell lines

RD18 and U2OS adherent cell lines were thawed from nitrogen-frozen stocks and cultured in T25 flasks with complete DMEM or RPMI medium, respectively. Cell were harvested accordingly to scheduled experiments or passed 3 times a week when confluence was around 70%. According to the type of assay, cells were seeded in T25 flasks (flow cytometry) or 94-well transparent or white plates (cell viability and apoptosis). Details will be described in the following paragraphs.

Adherent cells were counted in Neubauer chamber using Trypan Blue or by Cellometer Auto 2000 Cell Viability Counter using AO/PI viability staining in disposable chambers. Cells were used for the establishment of cell line-derived single spheroids and organoids and for flow-cytometry, cell viability or apoptosis assays. After passage 10, adherent cells were validated by Laragen before to be discarded. Number of cells/well for the different assays and seeding methods will be described in the following paragraphs.

3.2.2 Analysis of markers expression by flow cytometry in adherent cells

Expression of selected markers, CD133, TfR1, EGFR1 and Her2, was examined by flow cytometry after staining with conjugated primary antibodies, antiCD133-APC (1:20), antiTfR1-PE (1:50), antiEGFR1-FITC (1:10) and antiHer2-APC (1:10). For adherent RD18 and U2OS cells, 500.000 cells/sample were collected in falcon starting from 70% confluent T25 flask. Samples were centrifuged at 400 g for 5 minutes, washed with 1 ml of cold PBS containing 1% FBS, centrifuged again and incubated in the dark for 30 min on ice in a volume of 100 µl containing the specific dilution of fluorophore-conjugated primary antibody: antiTfR1-PE (1:50), antiEGFR1-FITC (1:10), antiHer2-APC (1:10), antiCD133-APC (1:20). Then samples were washed twice and resuspended in 500 µl of cold PBS containing 1% FBS. Stained- adherent cells were analyzed by flow cytometry Attune NxT cell analyzer (UCLA).

3.2.3 Cell viability in adherent cell lines by MTS assay

Adherent cell viability was assessed by MTS using the CellTiter 96® AQueous One Solution Cell Proliferation Assay, a colorimetric kit designed to determine the metabolic activity and viability of cells. In MTS assay, tetrazolium MTS compound is bio-reduced by metabolically active cells to a red colored formazan product, which is RPMI-soluble. NADPH-dependent dehydrogenases, present in viable cells, are the enzymes responsible for this. The measure of resulting formazan solution absorbance at 492 nm is proportional to the number of metabolically active cells, thus to viable cells. RD18 and U2OS were seeded (5000 cells/well in 100 µl of complete DMEM and RPMI complete medium, respectively) in 96-well transparent microtiter plates. After 24 hours, medium was fully removed and replaced with DMEM or RPMI-containing the indicated scalar dilutions of unconjugated RIP (from 0.01 to 10.000 nM), carrier alone (from 0.01 to 100 nM) or IT (from 0.01 to 100 nM). After 72 h of continuous treatments, payloads-containing medium was removed and CellTiter 96 AQueous One Solution Reagent was added with a 1:6 dilution factor (CellTiter Reagent-RPMI) in a

final volume of 120 µl. Plate were incubated 1 h at 37°C and immediately after, absorbance was measured at 492 nm using the microtiter plate reader Multiscan EX. Data have been normalized to vehicle values and plotted with Prism 9.

3.2.4 Imaging of adherent cells

Morphological analysis of adherent cells was performed using a phase-contrast microscope with a digital camera from Nikon Eclipse TS100. Imaging of 96-well plates, used for MTS or Caspase 3/7 assays, was assessed at each ending time point.

3.2.5 Caspase 3/7 activation assay in adherent cells

In adherent cells, involvement of apoptotic cell death was assessed by measuring effector caspase activation. Caspase 3/7 activation was evaluated by the luminescent assay Caspase-Glo® 3/7, which contains a luminogenic caspase substrate with a tetrapeptide sequence, DEVD-aminoluciferin, recognized by caspase 3/7 and a thermostable luciferase. Once caspases cleave the substrate, it is generated aminoluciferin, which is used by the luciferase, generating a luminescent signal that is proportional to caspase-3/7 activity. RD18 and U2OS were seeded (5000 cells/well in 100 µl of complete DMEM and RPMI complete medium, respectively) in 96-well white plates. 24 hours after seeding, RD18 and U2OS adherent cells were treated with the IC_{50} of the selected ITs, calculated in relative 72 h dose-response curves, and the same concentration was chosen for the unconjugated RIPs (in 100 µl of DMEM or RPMI complete medium). After 8, 16 or 24h, medium was fully removed and 100 µl of Caspase-Glo® 3/7, diluted 1:2 in RPMI complete medium, were added. Plates were shaken for 5 minutes at 420 rpm and incubated for 20 minutes in the dark at RT. Luminescent signal was measured by Fluoroskan Ascent FL (integration time 10 sec). Data have been normalized to vehicle values and plotted with Prism 9.

3.2.6 Establishment of cell line-derived single spheroids

When 70% confluence was achieved, RD18 and U2OS adherent cells were trypsinized and resuspended in DMEM F-12 complete medium reaching a single-cell suspension. Cells were counted in Neubauer chamber using Trypan Blue. RD18 or U2OS adherent cells were seeded, without touching bottom plate, in ultra-low attachment black 96-well U-bottom plate to allow one single-spheroid formation for each well. This surface is composed by a hydrophilic, neutrally charged hydrogel coating, covalently bound to a polystyrene vessel surface.

Hydrogel coating inhibits specific and non-specific cell-surface interaction, thus forcing cells to grow in a suspension state and enabling single spheroids formation. Starting from RD18 and U2OS single cell suspension, we seeded 5000 cells/well in 100 µl of DMEM-F12 complete medium, drop by drop, without touching the bottom of the well. Immediately after seeding, plates were centrifuged at 400 g for 5 minutes to concentrate all cells in the bottom of the well. Single spheroids were monitored every day using a phase-contrast microscope with a digital camera. Single spheroids were used for flow-cytometry, cell viability and apoptosis experiments. Number of cells/well for the different assays and seeding methods will be described in the following paragraphs.

3.2.7 Analysis of markers expression by flow cytometry in single spheroids

Expression of selected markers, CD133, TfR1, EGFR1 and Her2, was examined by flow cytometry after staining with conjugated primary antibodies, antiCD133-APC (1:20), antiTfR1-PE (1:50), antiEGFR1-FITC (1:10) and antiHer2-APC (1:10). Starting from RD18 and U2OS single cell suspension, we seeded 5000 cells/well in ultra-low attachment black 96-well U-bottom plates, as described in "single-spheroid formation assay". After indicated single spheroids formation time, we removed medium and incubated them with 100 µl/well of 1× trypsin/EDTA for 10 minutes at 37°C to allow single spheroids dissociation. We added 100 µl/well of DMEM-F12 complete medium and gently pipetted dissociated single spheroids. We centrifuged plates at 400 g for 5 minutes, removed medium and incubated them in 100 µl/well of fluorophore-conjugated primary antibody for 30 minutes in the dark on ice. After 3 washes, each of them followed by a centrifugation step, samples were resuspended in 100 µl/well of PBS containing 1% FBS. Stained-single spheroids were analyzed by flow cytometry Cytoflex analyzer (CRBA).

3.2.8 Cell viability in single spheroids by ATP assay

Single spheroids viability was measured by ATP assay using the luminometric CellTiter-Glo® 3D Cell Viability kit. The assay is specifically designed for determining amount of intracellular ATP, produced by viable cells, in 3D microtissue. The assay reagent penetrates large single spheroids and has increased lytic capacity, allowing accurate determination of 3D viability compared to other methods. The kit used is based on the luciferin/luciferase reaction that produces the oxyluciferin luminescent product when ATP is present. The luminescent signal is directly proportional to ATP amount produced by cells. Single-suspension RD18 and

U2OS cells (5000 cells/well resuspended in 100 µl of DMEM-F12 complete medium) were seeded drop by drop, without touching well bottom, in ultra-low attachment black 96-well U-bottom plate to allow single spheroids formation. Plates were centrifuged at 400 g for 5 minutes. After the indicated growth time, medium was slowly removed (being careful not to aspirate the spheroid) and replaced by the indicated scalar dilutions (see adherent cells viability section) of payloads for 72 h. Then, treatments were slowly aspirated and 100 µl of CellTiter-Glo 3D reagent, diluted 1:2 in DMEM-F12 complete medium, were added. Plates were shaked at 420 rpm for 5 minutes, to induce cell lysis, and incubated for 25 minutes in the dark at RT to stabilize the luminescent signal. Luminescent signal was measured by Fluoroskan Ascent FL (integration time 1 sec). Data have been normalized to vehicle values and plotted with Prism 9.

3.2.9 Imaging of single spheroids

Morphological analysis of single spheroids was performed using a phase-contrast microscope with a digital camera from Nikon Eclipse TS100. Imaging of 96-well plates, used for ATP or Caspase 3/7 assays, was performed at each ending time point.

3.2.10 Caspase 3/7 activation assay in single spheroids

The involvement of caspases in single spheroids and was evaluated using the Caspase-Glo® 3/7 3D luminometric kit, which, while operating with the same mechanism as Caspase-Glo® 3/7, has a better lithic capacity, essential for 3D models. Single-suspension RD18 and U2OS cells (5000 cells/well resuspended in 100 µl of DMEM-F12 complete medium) were seeded drop by drop, without touching well bottom, in ultra-low attachment black 96-well U-bottom plate to allow single spheroids formation. Seeding method was the same used for viability assays. After appropriate single spheroids growing time, medium was slowly removed and replaced with treatments. Single spheroids were incubated with the IC_{50} of the selected ITs, calculated in relative 72 h dose-response curves, and the same concentration was chosen for the unconjugated RIPs (in 100 µl of DMEM-F12 complete medium). After 8, 16 or 24 h, medium was carefully removed and 100 µl of Caspase-Glo® 3/7 3D, diluted 1:2 in DMEM-F12 complete medium, were added. Plates were shaken for 5 minutes at 420 rpm and incubated for 30 minutes in the dark at RT. Luminescent signal was measured by Fluoroskan Ascent FL (integration time 10 sec). Data have been normalized to vehicle values and plotted with Prism 9.

3.2.11 Establishment of cell line-derived organoids

When 70% confluence was achieved, RD18 and U2OS adherent cells were trypsinized and resuspended in thawed DMEM or RPMI complete medium. After centrifugation (400 g for 5 minutes), pellet was resuspended in cold DMEM or RPMI complete medium, and cell suspension was filtered through 100 μm strainer and placed in ice. Counting was performed by Cellometer Auto 2000 Cell Viability Counter using AO/PI viability staining in disposable chambers. According to the number of cells/well needed, an aliquot of cold cell suspension was centrifuged (400 g for 5 minutes) and resuspended in a 1:1.33 Mammocult-Matrigel mixture. Hereinafter, all steps were performed on ice. Briefly, calculated volume of cold Mammocult complete medium was added to cell pellet and resuspended by pipetting. Then, calculated volume of cold Matrigel was added to Mammocult-cell suspension. Mammocult-Matrigel-cell mixture was resuspended multiple times to ensure homogenous mixing avoiding bubbles formation. Mixture was vortexed 3 times for 5 seconds at low rpm and placed back on ice after each vortexing step, then it was immediately used for seeding in IHC, flow-cytometry or viability/apoptosis experiments. Number of cells/well, specific Mammocult-Matrigel-cell mixure volume used for the different assays and seeding methods will be described in the following paragraphs.

3.2.12 Analysis of markers expression by flow cytometry in cell-derived organoids

Expression of selected markers, CD133, TfR1, EGFR1 and Her2, was examined by flow cytometry after staining with conjugated primary antibodies, antiCD133-APC (1:20), antiTfR1-PE (1:50), antiEGFR1-FITC (1:10) and antiHer2-APC (1:10). For adherent RD18 and U2OS cells, 500.000 cells/sample were collected in falcon starting from 70% confluent T25 flask. For RD18 and U2OS-derived organoids, we seeded 20.000 cells/well in 24-well plates to allow maxi-ring organoids formation in 6 days. Two wells have been seeded for each experimental condition. After 6 days, we aspirated all media in maxi-ring containing wells and we carefully washed them with 1 ml of warm PBS. Then we added 1 ml of Dispase solution per well to allow organoids release from Matrigel and incubated plate for 20 minutes at 37°C. To dislodge them, we gently pipetted and transferred the organoids to falcon tube. Samples were centrifuged at 800 g for 5 minutes, washed with 1 ml of cold PBS containing 1% FBS, centrifuged again and incubated in the dark for 30 min on ice in a volume of 100 μl containing the specific dilution of fluorophore-conjugated primary antibody. Samples were

washed twice and resuspended in 500 µL of cold PBS containing 1% FBS. Stained-organoids were analyzed by flow cytometry Attune NxT cell analyzer (UCLA).

3.2.13 IHC processing of cell line-derived organoids: seeding, fixing, paraffin embedding and cutting

For IHC experiments, maxi-rings organoids were established in 24-well plates starting from cold RD18 or U2OS Mammocult-Matrigel mixture. We used a P200 pipette with a low attachment 300 µL tip to resuspend up and down a few times. We aspirated 70 µL/well of the mixture and, keeping the tip at a 45 degree angle, ejected the mixture slowly while moving the tip in a circular motion around the rim at the bottom of a single well in a 24 well plate. To ensure homogeneity, it is necessary vortex shortly every 3 wells, together with tip change as well as stop pipetting at the first resistance of the pipet dispenser to avoid introducing air bubbles. Once all maxi-rings were plated, we quickly incubated the plate to a humidified 37°C incubator at 5% CO2 for a minimum of 45 minutes. After the rings were visibly solidified, we added 1 ml of the pre-warmed Mammocult drop-by-drop directly to the center of the wells using a P1000. For histology characterization, we seeded 20.000 cells/well and after 2 days, we treated them with the IC_{50} of Saporin for 72 h. For each experimental condition (vehicle or IC_{50} so6), Four wells have been seeded and then collected after incubation time. To verify integrity and homogeneity of maxi-rings, we imagined plates every day using Celigo S Image Cytometer. After 6 days from seeding, we aspirated all media from each well without breaking or touching maxi-rings and washed them with 500 µl of warm PBS. Then, we carefully removed PBS and added 500 µl/well of 10% buffered formalin. We shortly incubated 24-well plate at 37°C for 5 minutes and for another 30 min on ice before to leave the plate at 4°C O.N. The morning after, we transferred all the wells/condition (4 wells/condition) to a falcon tube, taking care to scrape all maxi-ring-containing organoids and washing each well with 1 ml of PBS. Samples were centrifuged for 5 minutes at 2000 g and supernatant was aspirated without disturbing the pellet. 4 µl of melted histogel were added to the pellet followed by a quick vortex and spin and let it solidify for 4 minutes on ice. In the meantime, we labelled a histology cassette with a pencil, and we added 5 µl of histogel to the cassette letting it solidify. Using a spatula, we carefully placed the organoids-histogel pellet on top of the histogel already solidified in the cassette. Then, we added 5 µl of histogel on top of the pellet to stabilize it. We proceeded by closing the cassette, wrapping it in parafilm and leaving it on ice for 2–3 min. We placed the unwrapped cassette in a beaker- containing 70%

EtOH before to proceed with standard paraffin embedding (UCLA - Translational Pathology Core Laboratory - TPCL). Before cutting, blocks of paraffin-embedded samples were cooled down at -20°C for 30 minutes. When ready, blocks were placed on microtome where sections of 4 μm were obtained. After cutting 8-10 slices, we picked them up and then placed them in the water bath (pre-warmed at 37°C). We used microscope slides to collect sample slices that were left to dry for further staining experiments.

3.2.14 Hematoxylin and Eosin staining of cell line-derived organoids

Paraffin-embedded slices of cell line-derived organoids were baked in iQ Kinetic desert bath at 45° for 20 minutes to remove paraffin from samples. Hereinafter, it is necessary blotting off liquid excess after each step. We proceeded with hydration steps as follow: immerse slides in xylene for 5 min, 3 times, then in 100% ethanol for 2 min, 2 times. For H&E staining, we used staining Vector Labs Kit, using an optimized protocol; we incubated slides in Hematoxylin for 1 minute and rinsed them in 2 bakers containing 1L of tap water (15 seconds each). Then we applied to slides Bluing reagent for 5 minutes and rinsed them again in 2 bakers of 1L of tap water (15 seconds each). We quickly immersed slides in 100% ethanol for 10 seconds, blotted off excess and applied Eosin Y to slides for 2 minutes. We immersed again slides in 100% ethanol for 10 seconds and proceeded with dehydration steps as follow: immerse in 100% ethanol for 2 min, 2 times, then quickly in xylene for 5 min, 3 times. Coverslip mounting was performed using Permount. Slides were left to dry under a chemical hood O.N. The day after, images were acquired through a revolve upright and inverted microscope system.

3.2.15 IHC characterization of cell line-derived organoids: ki67/Caspase 3 staining

Paraffin-embedded slices of cell line-derived organoids were de-paraffinized as described above (section 3.2.5). Hereinafter, it is necessary blotting off liquid excess after each step. We proceeded with hydration steps as follow: immerse slides in xylene for 10 minutes, 3 times, in 100% ethanol for 2 min, 2 times, then in first 95% ethanol bath, in second 95% one and in 70%, 50%, 25% ethanol bath for 2 minutes each. We placed slides in glass slide holder contaning diH$_2$O and for 10 minutes on a shaker at low speed. After, slides were completely dried, we performed first blocking with Peroxidaze 1 incubating slides at RT for 4 minutes. Slides were washed in TBS and antigen heat retrieval was made with 2100-Retriever using Diva Decloaker solution. Then, slides were deeply washed in diH$_2$O and were incubated again

with Peroxidaze 1 at RT for 2 minutes. After multiple washing with TBS, we incubated slides with background punisher universal blocker at RT for 5 minutes. Immediately after, we performed primary staining with abI ki67/Caspase 3: ki67 slides were incubated 2h at RT while Caspase 3 ones O.N. at 4°C. After primary antibody staining, slides were deeply washed in TBS, stained with abII MACH 2 Double Stain 2 at RT for 40 minutes and washed again in TBS. Then, we proceed with detection as follow: ki67 slides were incubated with DAB at RT for 1 minute while Caspase 3 slides were incubated with Warp Red at RT for 7 minutes. Counterstain was performed with 10% Hematoxylin at RT for 10 minutes. All detection steps were quenched with diH_2O. Dehydration steps consisted of: immerse in 50% and in 70% ethanol bath for 2 minutes each, then in first and second 95% ethanol bath for 2 minutes each, in 100% ethanol for 2 min, 2 times and in xylene for 10 minutes, 3 times. Coverslip mounting and imaging was performed as described in section 3.2.14.

3.2.16 Cell viability in cell line or patient-derived organoids by ATP assay

Cell line-derived or patients-derived organoids viability was measured by ATP assay using the luminometric CellTiter-Glo® 3D Cell Viability kit. For cell viability experiments, mini-ring organoids were established in white 96-well plates starting from cold RD18, U2OS or processed biopsy patient SARC0116 Mammocult-Matrigel mixture. For organoids viability screening, we seeded 1000 cells/well for cell-derived organoids and 5000 cells/well for patients-derived organoids. We used a P20 pipette with a low attachment 20 μL tip to resuspend up and down a few times. We aspirated 10 μL of the mixture and, keeping the tip at a 45 degree angle, ejected the mixture slowly while moving the tip in a circular motion around the rim at the bottom of a single well of the 96-well plate. To ensure homogeneity, it is necessary vortex shortly every 3 wells, together with tip change as well as stop pipetting at the first resistance of the pipet dispenser to avoid introducing air bubbles. Once all mini-rings were plated, we quickly incubated the plate to a humidified 37°C incubator at 5% CO2 for a30 minutes to allow mini-rings solidification. All steps described below were performed with the robotic system EpMotion. After 30 minutes, we added 100 μL of the pre-warmed Mammocult directly to the center of the wells. To minimize evaporation, we also added pre-warmed PBS to empty wells (100 μL) and to space between wells (50 μL). We incubated in a humidified 37°C incubator at 5% CO2 for 2 days (cell-derived organoids) or 3 days (patients-derived organoids) prior to media removal and payload treatments with indicated scalar dilution of payloads for 72 h. To verify establishment, integrity and homogeneity of mini-

rings, we imagined plates every day using Celigo S Image Cytometer. After 72 h, payload-containing-Mammocult medium was removed and wells were washed with 100 μl of pre-warmed PBS. To release organoids from Matrigel, we incubated them at 37 °C for 25 minutes in 50 μl/well of 5 mg/mL Dispase solution and shaked plate on plate shaker for 5 minutes at 80 rpm. Then we added 30 μl (cell derived-organoids) or 75 μl (patients-derived organoids) to each Dispase-containing well. We shaked plate for additional 5 minutes at 80 rpm and incubated it for 20 minutes at RT in the dark to stabilize the luminescent signal. Luminescent signal was measured by SpectraMax iD3 (integration time 500 ms). Data have been normalized to vehicle values and plotted with Prism 9.

3.2.17 Organoids imaging

Morphological analysis of cell or patients-derived organoids was performed daily by Celigo S Imaging Cell Cytometer, in bright-field mode, through Celigo S Software. Imaging of 96 or 24-well plates, used for ATP or Caspase 3/7 assays or flow-cytometry/IHC experiments, was performed using two focal planes of confluence. The morphological analysis was qualitative; indeed it was evaluated the homogeneity of the organoids and their distribution in space.

3.2.18 Caspase 3/7 activation assay in cell-derived organoids

Involvement of apoptotic cell death was assessed by measuring effector caspase activation. The involvement of caspases in cell-derived organoids was evaluated using the Caspase-Glo® 3/7 3D luminometric kit, which, while operating with the same mechanism as Caspase-Glo® 3/7, has a better lithic capacity, essential for 3D models. RD18 and U2OS organoids (1000/well) were seeded in 96-well white plates. Seeding method was the same used for viability assays. Two days after seeding, RD18 or U2OS derived-organoids were treated with the IC_{50} of the selected ITs, calculated in relative 72 h dose-response curves, and the same concentration was chosen for the unconjugated RIPs (in 100 μl of Mammocult complete medium). After 8, 16, 24, 48 and 72 h, medium was fully removed and wells were washed with 100 μl of pre-warmed PBS. To release organoids from Matrigel, we incubated them at 37 °C for 25 minutes in 50 μl/well of 5 mg/mL Dispase solution and shaked plate on plate shaker for 5 minutes at 80 rpm. Then we added 50 μl of Caspase-Glo® 3/7 3D to each Dispase-containing well. We shaked plate for additional 5 minutes at 80 rpm and incubated it for 30 minutes at RT in the dark to stabilize the luminescent signal. Luminescence was measured by

SpectraMax iD3 (integration time 500 ms). Data have been normalized to vehicle values and plotted with Prism 9.

3.2.19 Establishment of patient-derived organoids

Rhabdomyosarcoma SARC0116 (2) fresh tumor specimens were obtained from a consented UCLA patient (IRB#10-001857; IRB#19-002214). To perform compounds screening, human tumor tissue was processed as described in Nguyen and Soragni 2020 [224]. We minced the tumor sample (1–3 mm^3 fragments) using a bistoury in a sterile petri dish and added 5 ml of collagenase IV (200 U/ml) to start first enzymatic digestion. We collected the fragments in a 50 ml Falcon tube, washed the dish with an additional 5 ml of collagenase and incubated it at 37°C for 2h. After first digestion, we collected the cell suspension-containing supernatant (used for clinical-approved drug screening at Soragni Lab) and incubated undigested large tumor fragments with collagenase IV at 37°C for additional 2h. After second digestion, we collected the cell suspension-containing supernatant (used for clinical-approved drug screening at Soragni Lab) and incubated undigested large tumor fragments with collagenase IV at 37°C O.N. After third digestion, we collected the cell suspension-containing supernatant and centrifuged it at 600 g for 5 minutes. We carefully aspirated supernatant and pellet was resuspended in in 1 ml of cold serum-free RPMI medium plus 9 ml of cold Ammonium Chloride solution to allow red blood cell lysis. We incubated it on ice for 10 minutes, inverting the tube every 2–3 minutes and centrifuged at 600 g for 5 min. To obtain a homogenous cell suspension, we resuspended cell pellet in 1 ml of cold serum-free RPMI medium and filtered it using a 100 μm strainer. We washed the tube with additional 9 mL of cold serum-free RPMI medium, passed it again in the same strainer and maintained cell suspension (10 ml final volume) on ice. Counting was performed by Cellometer Auto 2000 Cell Viability Counter using AO/PI viability staining in disposable chambers. According to the number of cells/well needed, an aliquot of cold cell suspension was centrifuged (400 g for 5 minutes) and resuspended in a 1:1.33 Mammocult-Matrigel mixture. Hereinafter, all the steps were performed on ice. Briefly, calculated volume of cold Mammocult complete medium was added to cell pellet and resuspended by pipetting. Then, calculated volume of cold Matrigel was added to Mammocult-cell suspension. Mammocult-Matrigel-cell mixture was resuspended multiple times to ensure homogenous mixing avoiding bubbles formation. Mixture was vortexed 3 times for 5 s at low rpm and placed back on ice after each vortexing step, then it was immediately plated for viability assay. Number of cells/well, used for

viability assays, and seeding method will be described in the following paragraphs. For SARC0116 we did not proceed with any other types of experiment because of the lack of biological material; indeed, most of it was used for clinical-approved drug screening at Soragni's laboratory.

Chapter 4 – Results

4.1 Establishment of 2D model in culture plates

In order to evaluate the expression of the selected antigen as well as the antitumor effect of immunoconjugates in 2D model, we decided to culture two sarcoma immortalized human cell lines: RD18 (embryonal rhabdomyosarcoma) and U2OS (osteosarcoma). Starting from nitrogen-frozen stock, we thawed and cultured RD18 and U2OS cells in T25 flasks with complete DMEM or RPMI medium, respectively, allowing for the creation of cellular monolayer, a well-known 2D model commonly used in preclinical research.

4.1.1 Flow cytometry analysis of CD133, TfR1, EGFR1 and Her2 expression in adherent sarcoma cells

The selection of tumor markers was made basing on the results found in the literature related to the overexpression of antigens in stabilized cell lines or in primary cultures of early or advanced sarcoma [225, 226, 227, 228]. Therefore, we selected the transferrin receptor 1 (TfR1), the epidermal growth factor receptor 1 and 2 (EGFR1, Her2) as targets. To evaluate the intensity of expression of the selected tumor markers on RD18 and U2OS adherent cell lines, flow cytometry analysis was carried out using fluorophore-conjugated primary antibodies: antiTfR1-PE (1:50), antiEGFR1-FITC (1:10), antiHer2-APC (1:10). Moreover, to verify the possible expression of the CD133 stem cell marker, thus evaluating the presence of staminal properties on cell model, the antiCD133-APC (1:20) antibody was also used [229]. Considering the previous data reported in literature, U937 cells were chosen as non-target cells [230, 231]. For adherent RD18 and U2OS target cells and non-target U937 cells, expression of selected markers, CD133, TfR1, EGFR1 and Her2, was examined by flow cytometry after staining with fluorophore-conjugated primary antibodies. Flow cytometry graphs are reported in Figure 1A (RD18 cell line), 1B (U2OS cell line) and 1C (U937 cell line).
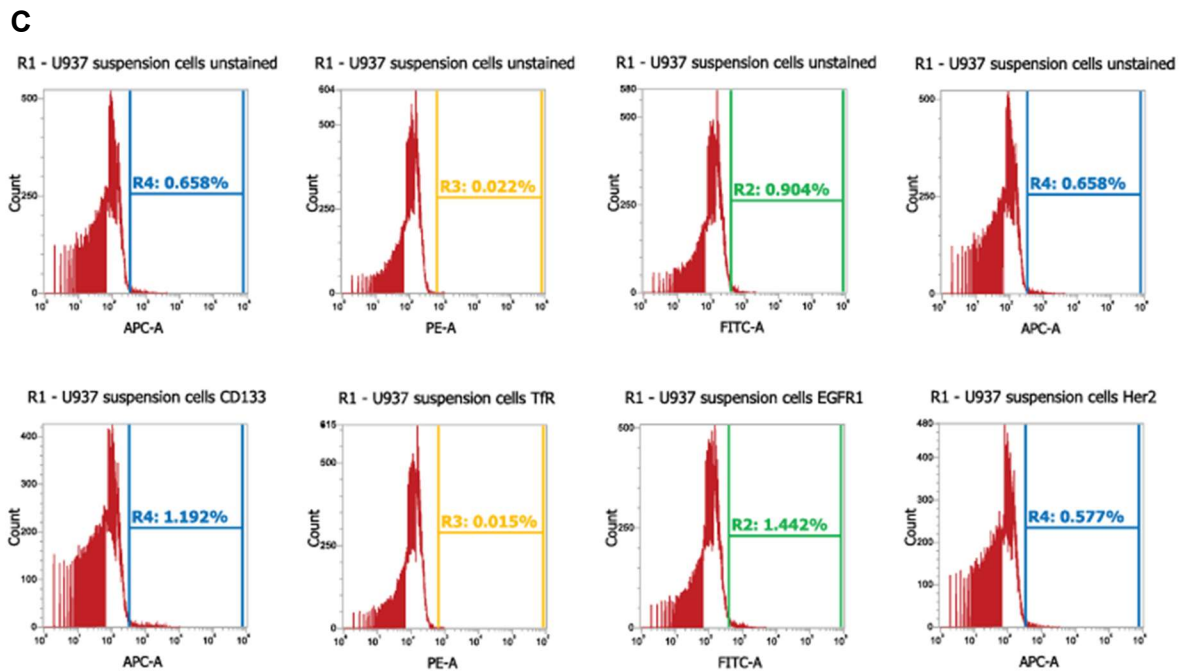
A

B

C
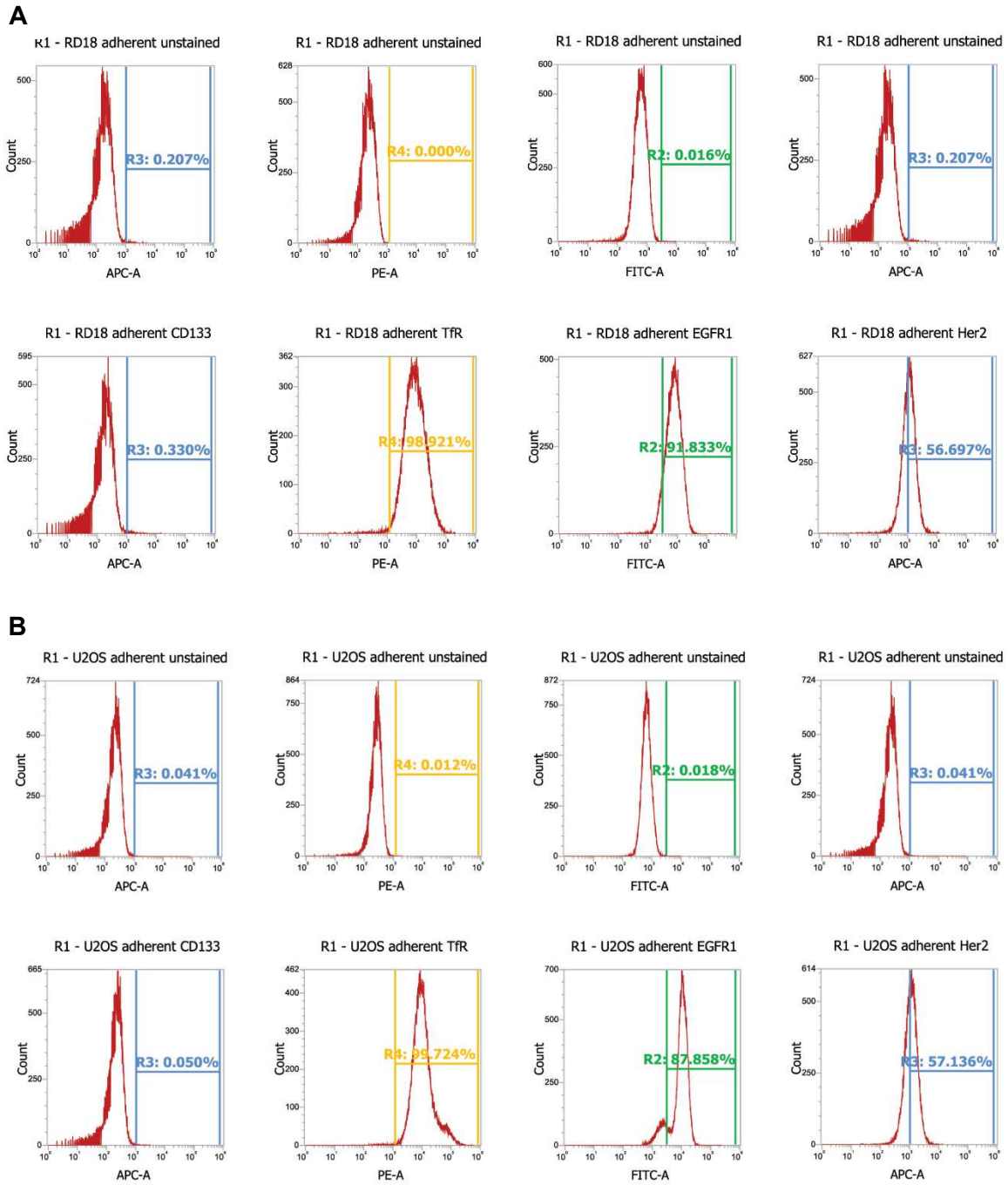
Figure 1. A) Flow cytometry expression of CD133, TfR1, EGFR1 and Her2 on RD18 adherent cells. **B)** Flow cytometry expression of CD133, TfR1, EGFR1 and Her2 on U2OS adherent cells. **C)** Flow cytometry expression of CD133, TfR1, EGFR1 and Her2 on U937 non-target cells. Samples were incubated with antiCD133-APC (1:20), antiTfR1-PE (1:50), antiEGFR1-FITC (1:10) and antiHer2-APC (1:10) in PBS containing 1% FBS. Above, negative control for each fluorophore represented by unstained samples, below stained cells with fluorophore-conjugated antibodies. Results are representative of 3 independent experiments. Adherent cells were analyzed by flow cytometry Attune NxT cell analyzer (UCLA).

Staminal marker CD133 had a low expression on both adherent cell lines; however, we should probably verify the expression of the others staminal markers before to arrive at any conclusion. As reported in table 9, RD18 and U2OS strongly overexpressed TfR1 (98% in RD18, 99% in U2OS) and EGFR1 (91% in RD18, 87% in U2OS), while Her2 was expressed lower that the other two markers (56% in RD18, 57% in U2OS). To verify that the overexpression of markers was selective on target cells, U937 cell line was chosen as non-target cell. As showed in Figure 1C, all the selected antigens, staminal marker included, showed a low or no expression on U937 cell line (Table 9).

4.1.2 Cell viability assays in adherent sarcoma cells

On the basis of flow-cytometry results showing that TfR1, EGFR1 and Her2 were highly expressed on both RD18 and U2OS cell lines, we selected 3 ITs, directed against such antigens to assess their possible antitumor effect and present on ITs biobank of Prof. Andrea Bolognesi's Toxic Enzymes and Immunotargeting Laboratory. These are transferrin-Saporin (Tf-SO6), αEGFR1-Ocymoidine (αEGFR1-Ocy), αHer2-Ocymoidine (αHer2-Ocy). As reported in the "Materials and methods section", conjugation of carrier and toxic payloads

was previously performed via the insertion of artificial disulphide bonds. Transferrin (Tf, ligand carrier) was conjugated to the type 1 RIP saporin (toxic payload), composing the conjugate Tf-SO6 that targets TfR1 as transferrin is the ligand of TfR1. Type I RIP ocymoidine (toxic payload) was conjugated to αEGFR1 (antibody carrier) and αHer2 (antibody carrier), composing immunotoxin αEGFR1-Ocy, directed against EGFR1, and αHer2-Ocy, targeting Her2. Specific cytotoxicity induced by ITs was compared to the corresponding unconjugated RIPs, saporin (SO6) and ocymoidine (Ocy), and to the carrier alone, Tf, αEGFR1 and αHer. IT and RIP concentrations inhibiting cell viability by 50% (IC_{50}) values among cell models are reported in Table 10. To test the cytotoxic effect of ITs on adherent RD18 and U2OS cell lines, cell viability was assayed by MTS assay after 72 h of continuous treatment with ITs, unconjugated RIP or carrier alone (Figure2 and 3). In the RD18 cell line, Tf-SO6 conjugate showed an enhanced targeted efficacy compared to unconjugated RIP saporin or carrier alone transferrin. For example, as showed in Figure 2A, at the concentration of 1 nM, the cytotoxicity of Tf-SO6 was significantly higher compared to unconjugated RIP or carrier. Tf-SO6 had an IC_{50} value of 1.3 nM, while unconjugated SO6 and Tf alone had values of 24.2 nM and >100 nM, respectively (Table 1), meaning that the IT was 18 times more toxic than unconjugated RIP. αEGFR1-Ocy IT was more cytotoxic than unconjugated RIP ocymoidine or carrier alone αEGFR1. At the concentration of 0.01 nM, the cytotoxicity of αEGFR1-Ocy started to be significantly higher compared to unconjugated RIP or carrier (Figure 2B). αEGFR1-Ocy had an IC_{50} value of 0.3 nM, while unconjugated Ocy and αEGFR1 alone had values of 58.9 nM and >100 nM, respectively. Overall, the IT was ≅200 times more cytotoxic than unconjugated RIP (Table 1). Furthermore, αHer2-Ocy also showed a greater cytotoxic effect compared to unconjugated RIP saporin or carrier alone αHer2 (Figure 2C). αHer2-Ocy started to be significantly more toxic at 10 nM compared to unconjugated RIP or carrier (Figure 2C); αHer2-Ocy had an IC_{50} value of 8.8 nM, while unconjugated Ocy and αHer2 alone had values of 58.9 nM and >100 nM, respectively, showing a specific toxicity 6 times greater than unconjugated RIP (Table 1). In the U2OS adherent cell line, Tf-SO6 conjugate showed an enhanced targeted efficacy compared to unconjugated RIP saporin or carrier alone transferrin. Figure 3A clearly shows that, at the concentration of 0.1 nM, the cytotoxicity of Tf-SO6 was significantly higher compared to unconjugated RIP or carrier. Tf-SO6 had an IC_{50} of 0.1 nM, while unconjugated SO6 and Tf alone IC_{50} was 13.1 nM and >100 nM, respectively (Table 2), implying that IT was over 2 order of magnitude more toxic than unconjugated RIP. αEGFR1-Ocy IT was more cytotoxic

than unconjugated RIP ocymoidine or carrier alone αEGFR1. Indeed, as reported in Figure 3B, the cytotoxicity of αEGFR1-Ocy started to be significantly higher compared to unconjugated RIP at 0.01 nM. Moreover, αEGFR1-Ocy had an IC_{50} value of 1.3 nM, while unconjugated Ocy and αEGFR1 alone had values of 73.9 nM and >100 nM, respectively. Thus, the IT was 56 times more cytotoxic than unconjugated RIP (Table 2). Similarly, αHer2-Ocy showed a great cytotoxic effect compared to unconjugated RIP saporin or carrier alone αHer2. In fact, figure 3C shows that cytotoxic effect of αHer2-Ocy was significantly higher rather than RIP alone at 0.01 nM, or carrier alone at 0.1 nM. αHer2-Ocy had an IC_{50} value of 3.7 nM, while unconjugated Ocy and αHer2 alone had values of 73.9 nM and >100 nM, respectively, with a toxicity 19 times greater than unconjugated RIP (Table 2). In order to evaluate the specificity of the ITs, we evaluated IT efficacy on the irrelevant cell line, U937, where it was already observed a low expression of all targets (Figure 4A, 4B and 4C). At the highest dose (100 nM), all conjugates killed around 20-40% of cells with IC_{50} value > 100 nM, meaning that IT-induced cytotoxicity was specific for target-cells since in non-target ones, IC_{50} values of the ITs and the negative ctrl (carrier) were equal (Table 3). Both in RD18 and U2OS adherent cell lines, but not in the control cell line, all tested ITs showed an enhanced efficacy compared to corresponding unconjugated RIP or carrier alone, with αHer2-Ocy showing the lower effect among the 3 ITs tested.
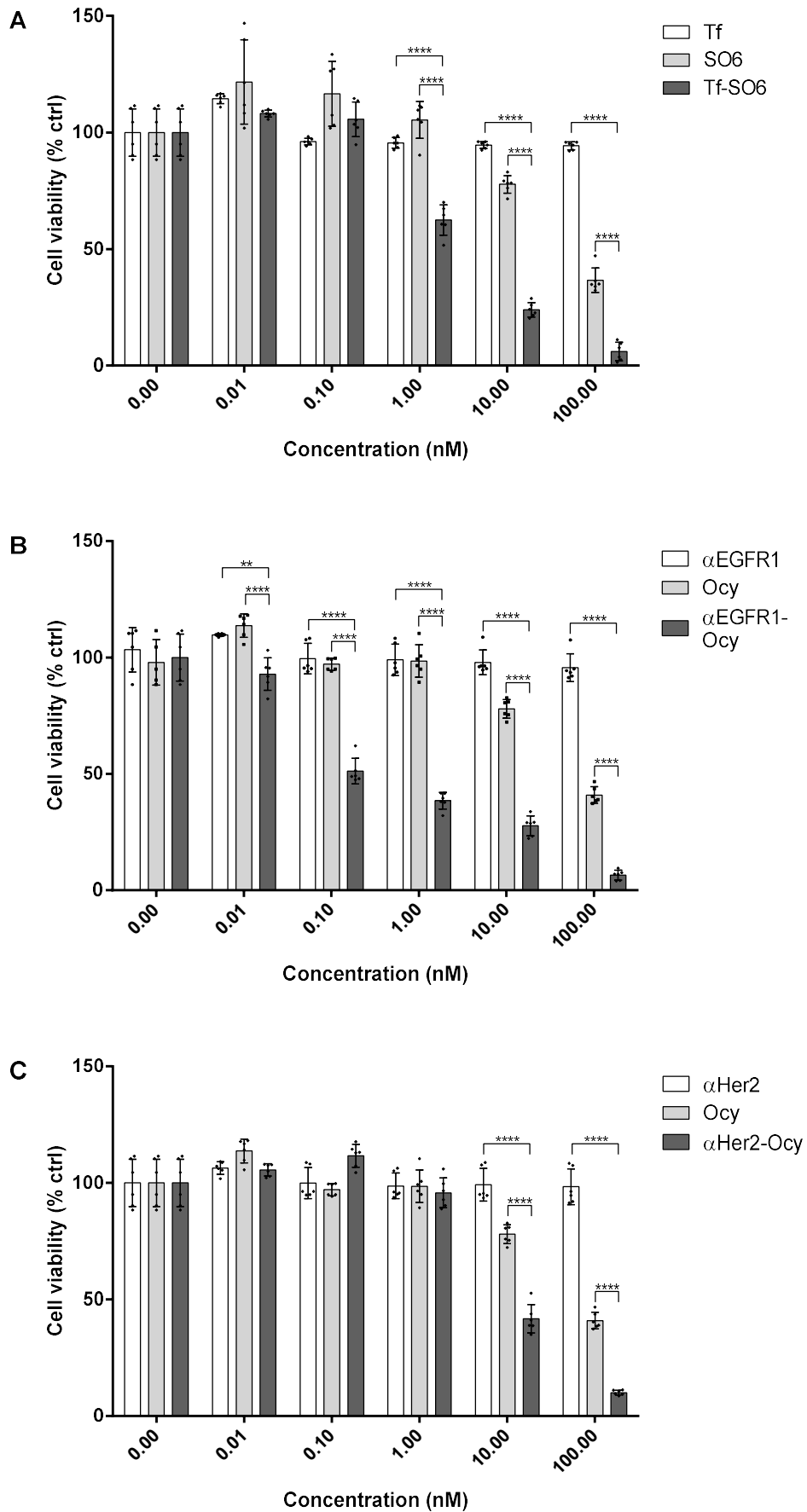
RD18

Figure 2. Dose-response curves on RD18 adherent cells. **A)** Cells were treated for 72 h with Tf-SO6, unconjugated SO6 and Tf. **B)** Cells were treated for 72 h with αEGFR1-Ocy, unconjugated Ocy and αEGFR1. **C)** Cells were treated for 72 h with αHer2-Ocy, unconjugated Ocy and αHer2. Cells (5000/well) were seeded in transparent 96-well plates in a final volume of 100 μl of DMEM complete medium containing appropriate concentration of compounds. Viability was evaluated using a colorimetric assay based on MTS reduction. Results are the means of two independent experiments, each performed in triplicate. Statistical analysis was performed with Prism 9 using ANOVA/Tukey's multiple comparison test (**** $p < 0.0001$). Data have been normalized to vehicle values (PBS) and plotted with Prism 9.

Table 1. IC_{50} values related to RD18 adherent cells treated for 72 h with ITs, unconjugated RIPs and carriers. IC_{50} were calculated using non-linear regression (Prism).

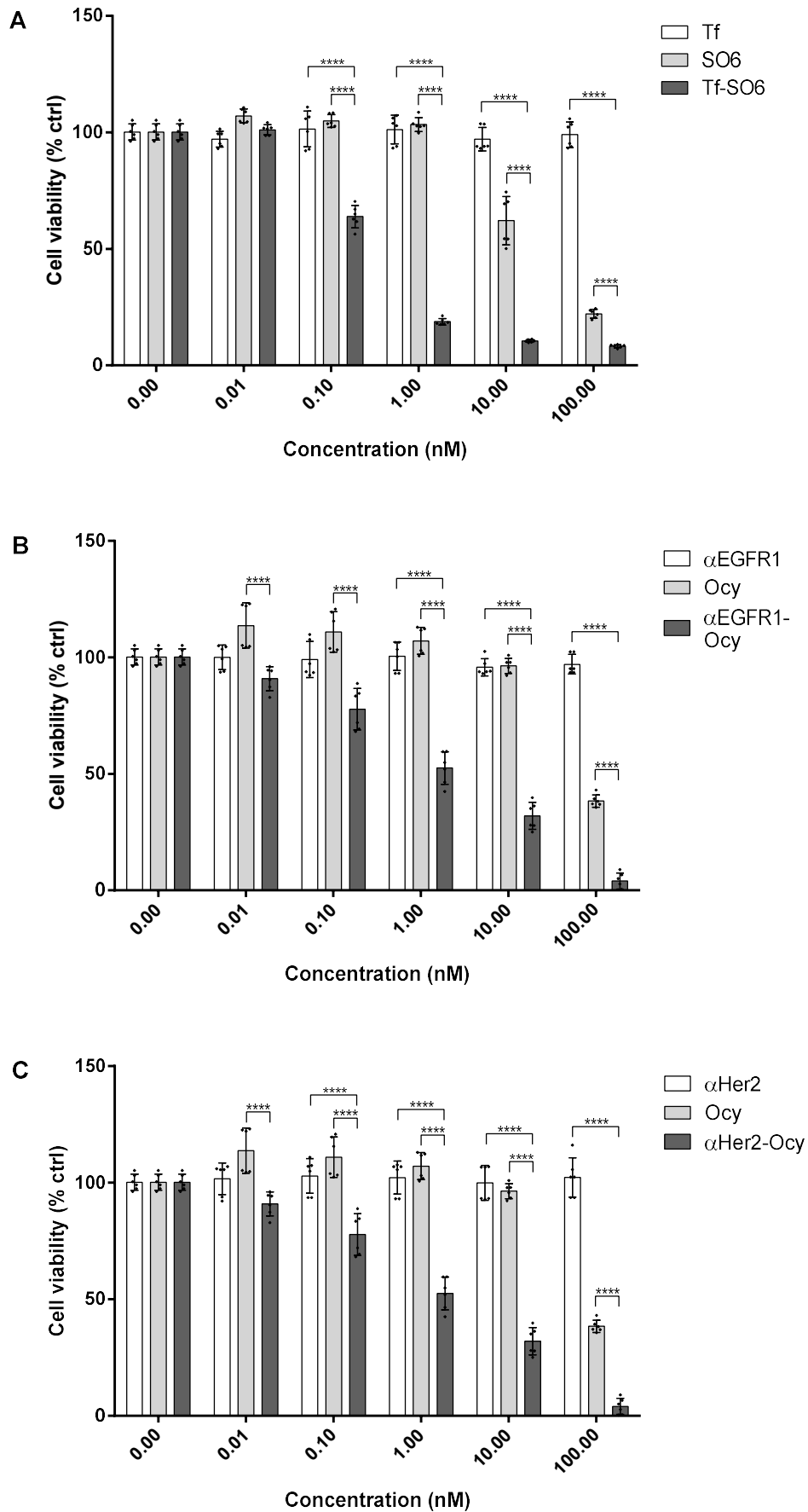|	Tf	SO6	Tf-SO6	αEGFR1	Ocy	αEGFR1-Ocy	αHer2	αHer2-Ocy
IC_{50} (nM)	>100	24.2	1.3	>100	58.9	0.3	>100	8.8

U2OS

Figure 3. Dose-response curves on U2OS adherent cells **A)** Cells were treated for 72 h with Tf-SO6, unconjugated SO6 and Tf. **B)** Cells were treated for 72 h with αEGFR1-Ocy, unconjugated Ocy and αEGFR1. **C)** Cells treated for 72 h with αHer2-Ocy, unconjugated Ocy and αHer2. Cells (5000/well) were seeded in transparent 96-well plates in a final volume of 100 μl of RPMI complete medium containing appropriate concentration of compounds. Viability was evaluated using a colorimetric assay based on MTS reduction. Results are the means of two independent experiments, each performed in triplicate. Statistical analysis was performed with Prism 9 using ANOVA/Tukey's multiple comparison test (**** $p < 0.0001$). Data have been normalized to vehicle values (PBS) and plotted with Prism 9.

Table 2. IC_{50} values related to U2OS adherent cells treated for 72 h with ITs, unconjugated RIPs and carriers. IC_{50} were calculated using non-linear regression (Prism 9).

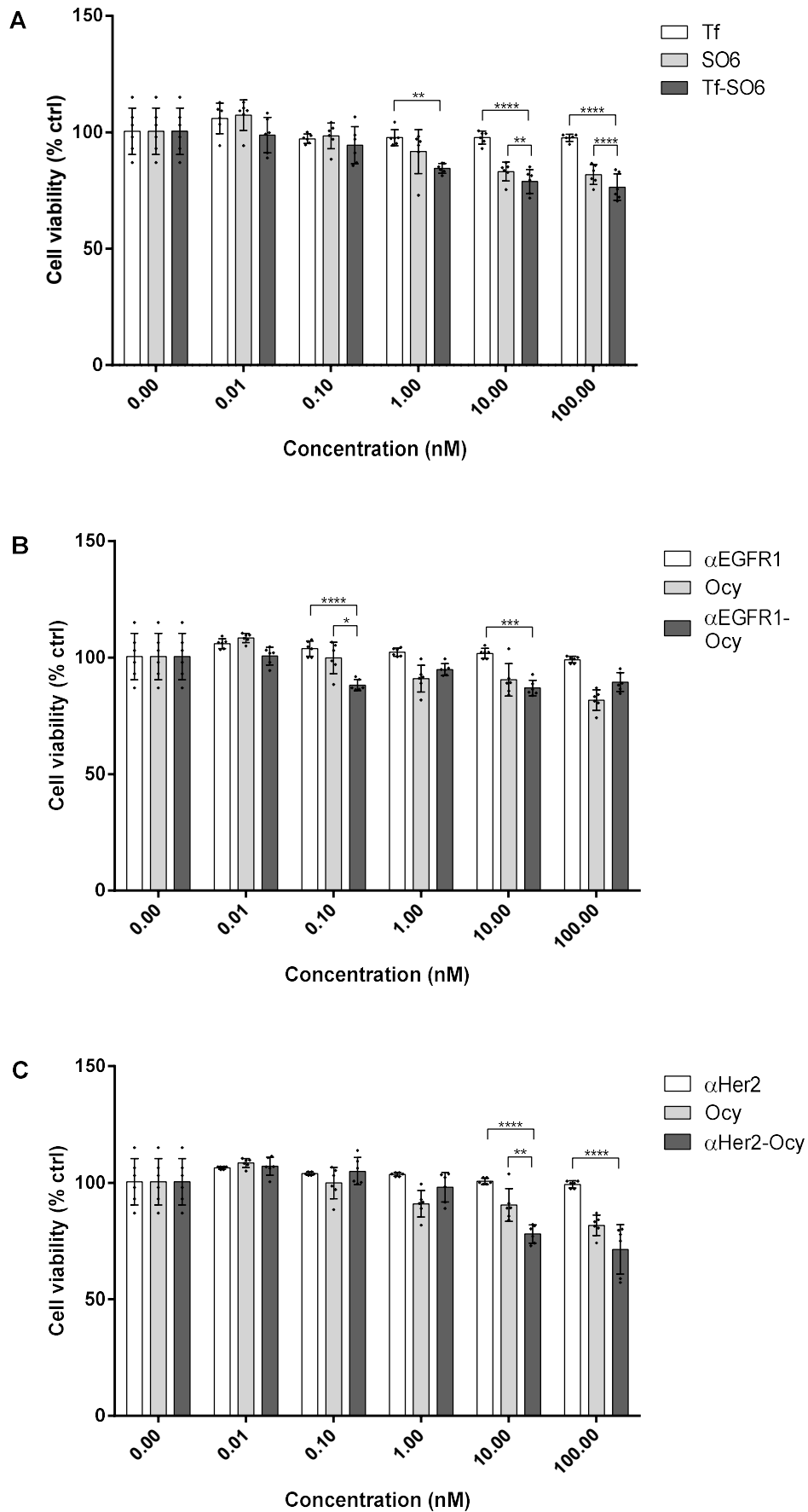|	**Tf**	**SO6**	**Tf-SO6**	**αEGFR1**	**Ocy**	**αEGFR1-Ocy**	**αHer2**	**αHer2-Ocy**
IC_{50} (nM)	>100	13.1	0.1	>100	73.9	1.3	>100	3.7

U937

Figure 4. Dose-response curves on U937 non-target cells **A)** Cells were treated for 72 h with Tf-SO6, unconjugated SO6 and Tf. **B)** Cells were treated for 72 h with αEGFR1-Ocy, unconjugated Ocy and αEGFR1. **C)** Cells were treated for 72 h with αHer2-Ocy, unconjugated Ocy and αHer2. Cells (5000/well) were seeded in transparent 96-well plates in a final volume of 100 μl of RPMI complete medium containing appropriate concentration of compounds. Viability was evaluated using a colorimetric assay based on MTS reduction. Results are the means of two independent experiments, each performed in triplicate. Statistical analysis was performed with Prism 9 using ANOVA/Tukey's multiple comparison test (**** $p < 0.0001$). Data have been normalized to vehicle values (PBS) and plotted with Prism 9.

Table 3. IC_{50} values related to U937 non-target cells treated for 72 h with ITs, unconjugated RIPs and carriers. IC_{50} were calculated using non-linear regression (Prism 9).

	Tf	SO6	Tf-SO6	αEGFR1	Ocy	αEGFR1-Ocy	αHer2	αHer2-Ocy
IC_{50} (nM)	>100	47.7	>100	>100	1076	>100	>100	>100

4.1.3 Representative imaging of viability experiments in RD18 adherent cells

Imaging of RD18 adherent cells MTS viability assay reports the morphological analysis of adherent cells treated with the indicated IT, RIP or carrier for 72 h at the concentration of 100 nM. As clearly reported in Figure 5, representative imaging confirmed the results already obtained in viability assay.
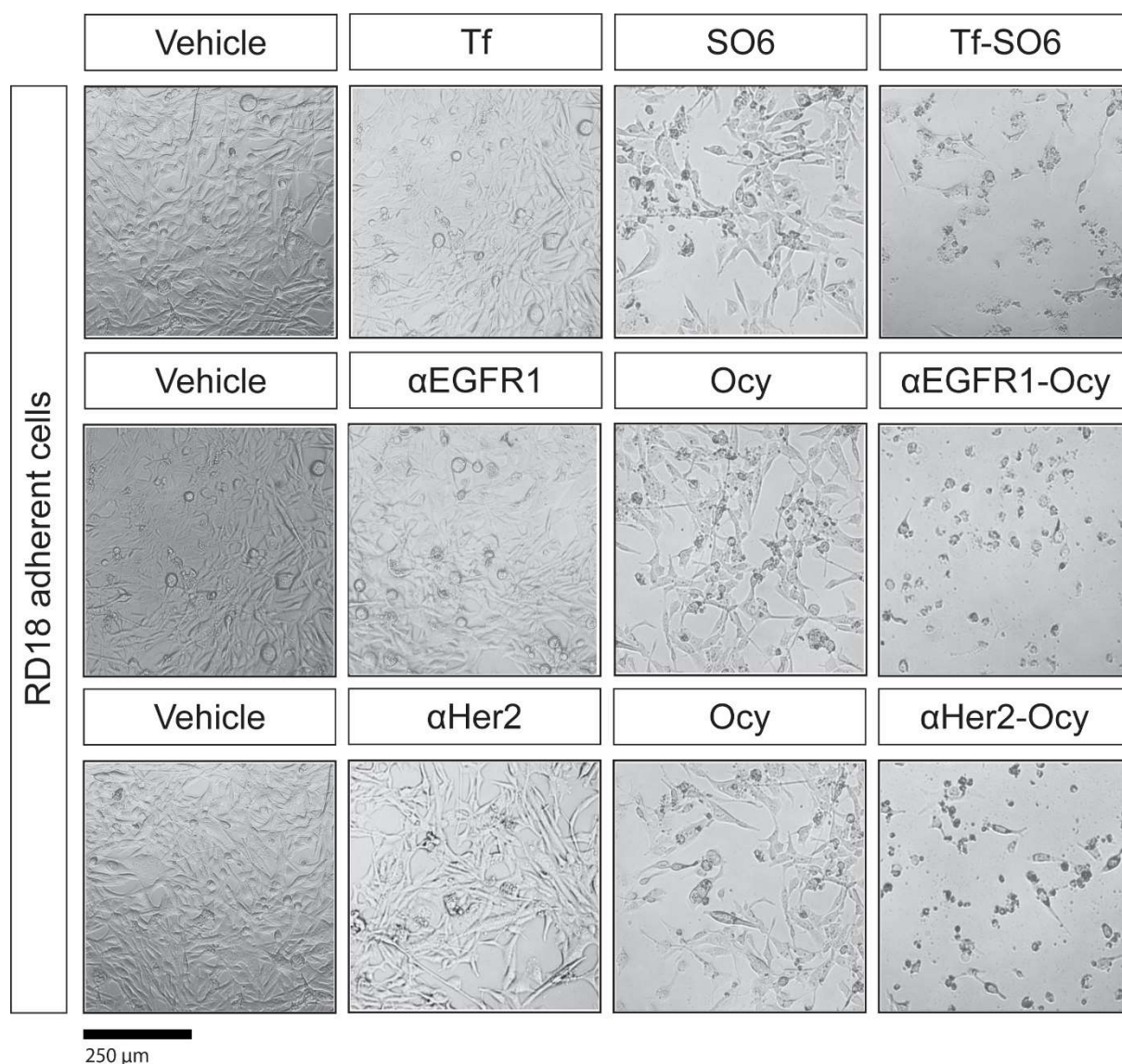
Figure 5. Representative imaging of MTS assay on RD18 adherent cells. Cells were treated with the indicated IT and RIP or carrier alone for 72 h at 100 nM. Vehicle represents control samples (PBS). Imaging was performed using a phase-contrast microscope with a digital camera from Nikon Eclipse TS100 with 100× magnification.

4.1.4 Time-dependent effect of ITs on caspase 3/7 activation in RD18 and U2OS adherent cells

It has been previously reported that type I RIPs and corresponding ITs could induce apoptosis in target cells [232, 233, 234]. Therefore, we decided to evaluate the effector caspase 3/7 activation in RD18 and U2OS cell lines treated with ITs or RIPs. Effector caspases 3/7 activation was measured after 8, 16 and 24 h of treatment. Both cell lines were treated with the IC_{50} concentrations of each IT (previously calculated in adherent cells dose-response curves). For unconjugated RIPs, we used the same concentration of the corresponding IT. To further verify the correlation between caspase activation and viability, we performed in parallel a cell

62

viability assay. All ITs tested induced a significant activation of caspase 3/7 compared to control (PBS) at 16 h and 24 h in both RD18 and U2OS adherent cells ($p < 0.0001$). After 16 h of treatment, all the three ITs induced similar intensity of caspase 3/7, activation reaching values from 200 to 250% compared to control (PBS). After 24 h, caspases 3/7 activation increased, achieving values from 300 to 350% compared to control (PBS). RIPs were not able to activate effector caspases at any time tested respect to control (PBS) (Figure 6 and 7). We compared IT-deriving caspase activation with that one induced by RIPs at 8, 16, and 24 h. Both at 16 h and 24 h, all ITs induced a significantly higher caspase 3/7 activation compared to that one induced by RIP alone at the same times ($p < 0.0001$). Interestingly, in U2OS adherent cells, αHer2-Ocy-induced apoptosis was significantly higher, compared to Ocy alone or control values, also at 8 h ($p < 0.0001$, Figure 7). IT-dependent apoptosis activation proceeded in parallel with the decrease of viability (Figure 6 and 7). Caspase 3/7 activation profile was very similar among ITs tested and between the two target cell lines used, thus supporting the idea that type I RIP-based ITs can induce caspase-dependent apoptosis in target cells.
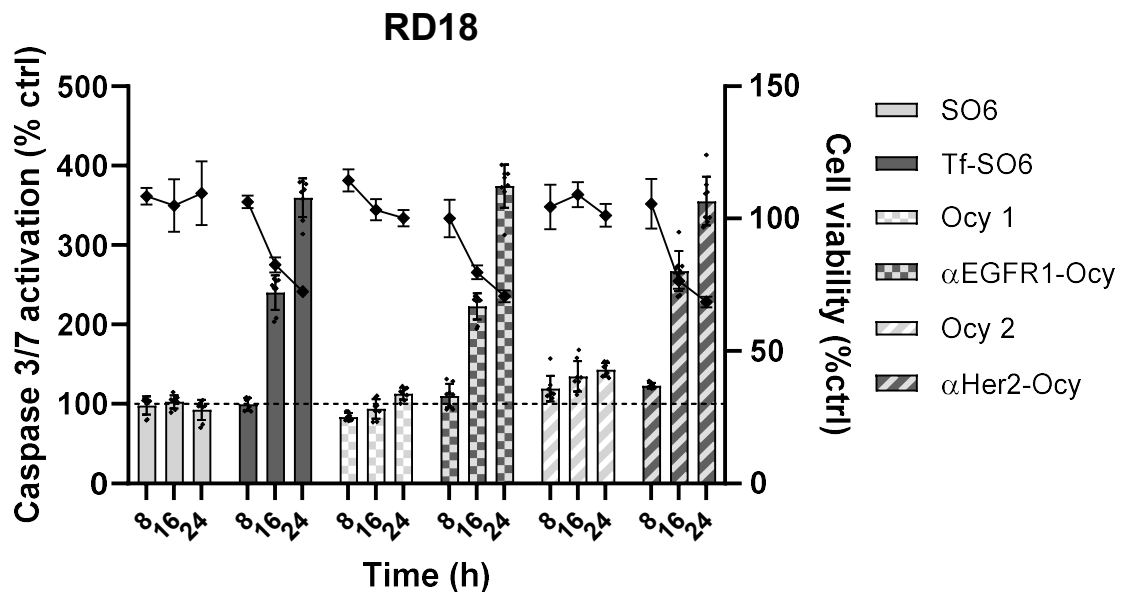

Figure 6. Caspases 3/7 activation in RD18 adherent cells exposed to IC_{50} of Tf-SO6, αEGFR1-Ocy and αHer2-Ocy or corresponding RIPs. Adherent cells (5000/well) were seeded in 96-well white (apoptosis assay) or transparent (viability assay) plates in a final volume of 100 μl of DMEM complete medium containing appropriate concentration of compounds. Caspase activity was compared to viability and expressed as the percentage of control values (PBS). Results of caspase 3/7 activation assay (bars) are the means of four independent experiments, each performed in duplicate. Results of viability assay (lines) are the means of two independent experiments, each performed in triplicate. Statistical analysis was performed with Prism 9 using ANOVA/Tukey's multiple comparison test ($p < 0.0001$). Data have been plotted with Prism 9.

Figure 7. Caspases 3/7 activation in U2OS adherent cells exposed to IC$_{50}$ of Tf-SO6, αEGFR1-Ocy and αHer2-Ocy or corresponding RIPs. Adherent cells (5000/well) were seeded in 96-well white (apoptosis assay) or transparent (viability assay) plates in a final volume of 100 μl of RPMI complete medium containing appropriate concentration of compounds. Caspase activity was compared to viability and expressed as the percentage of control values (PBS). Results of caspase 3/7 activation assay (bars) are the means of four independent experiments, each performed in duplicate. Results of viability assay (lines) are the means of two independent experiments, each performed in triplicate. Statistical analysis was performed with Prism 9 using ANOVA/Tukey's multiple comparison test (p < 0.0001). Data have been plotted with Prism 9.
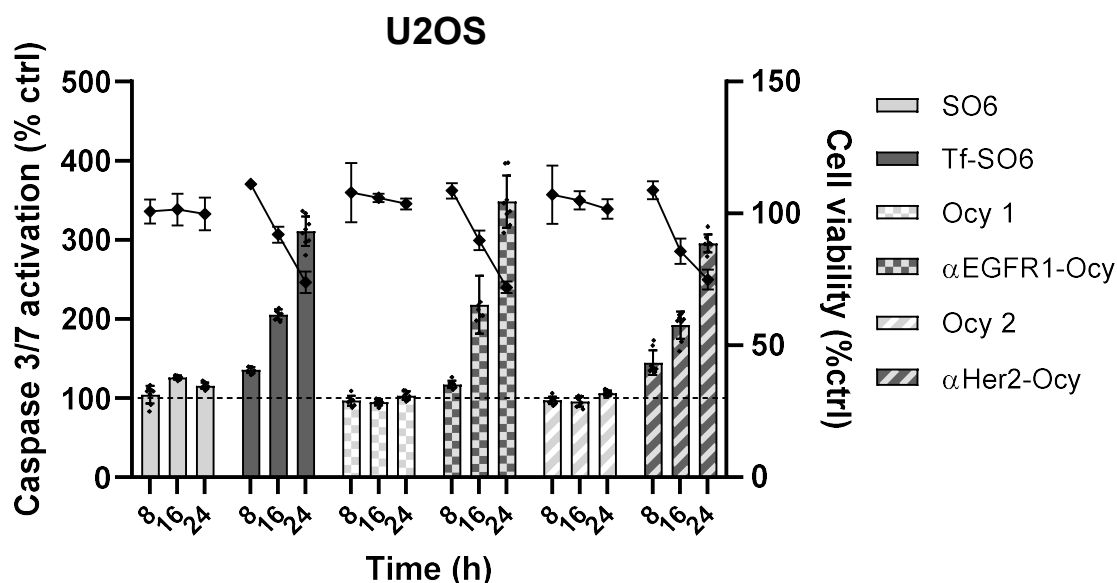
4.2 Establishment of 3D models

Tridimensional models have been used in preclinical cancer research as an intermediate model between in vitro cancer cell line cultures and in vivo tumors. Indeed, 3D models (mostly organoids and only in part spheroids) can better recapitulate characteristics and architecture of original tumor. In order to compare the cytotoxic effect of selected ITs in 2D (adherent cell lines) and 3D models of sarcoma, we established two different types of tridimensional models: single spheroids and organoids.

4.2.1 RD18 and U2OS single spheroid formation assay

In order to verity if the ITs could show an antitumor effect in 3D models and compare these results with those ones already obtained in adherent cells, we generated a single-spheroid in 96-well plates. We used plates containing a specialized ultra-low attachment U-bottom surface. As described in "Materials and methods section", starting from RD18 and U2OS single cell suspension, we seeded 5000 cells/well in 100 μl of DMEM-F12 complete medium,

drop by drop, without touching the bottom of the well. RD18 single spheroids were obtained within a culture time of 72 h, while U2OS single spheroids within 24 h (Figure 8). This procedure allowed for the formation of a single spheroids in each well with homogeneous sizes (≅500 μm), compact morphology and well-circumscribed edges.
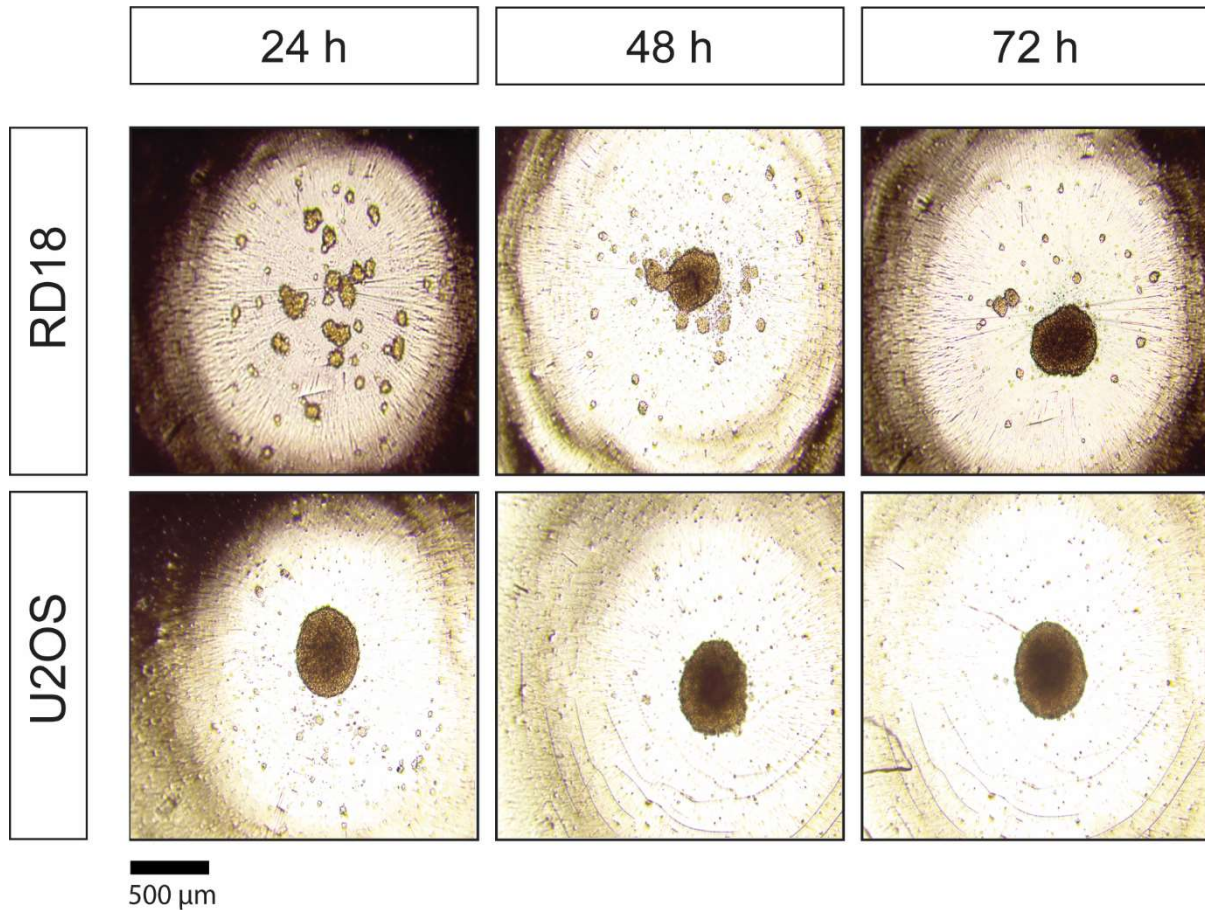

Figure 8. Time-course single spheroid formation assay. 5000 cells/well were seeded in 100 μl of DMEM-F12 complete medium in ultra-low attachment black 96-well U-bottom plates. Single-spheroid formation was monitored daily using a phase contrast microscope with a digital camera (40× magnification).

4.2.2 Flow cytometry analysis of CD133, TfR1, EGFR1 and Her2 expression in 3D single-spheroid sarcoma model

To compare the marker expression level between 2D and 3D models, flow cytometry analysis was performed on RD18 and U2OS-derived single spheroids with the same concentration of fluorophore-conjugated primary antibodies used for adherent cells. Moreover, to evaluate if single spheroids could recapitulate the staminal features present on "in vivo" tumor [235], we evaluated the expression of the CD133 stem cell marker. Overview of the results obtained

among models are reported in Table 9 while single spheroids flow cytometry graphs are reported in Figure 9A (RD18 single spheroids) and 9B (U2OS single spheroids). Staminal marker CD133 was overexpressed only on RD18 single spheroids (77%), while U2OS single spheroids showed low levels of CD133. This not necessarily means that the latter did not have staminal features; we should probably analyze the expression of a panel of several staminal markers before to arrive to any conclusion. RD18 and U2OS strongly overexpressed TfR1 (84% in RD18, 98% in U2OS) and EGFR1 (99% in RD18, 98% in U2OS) while Her2 was expressed at lower levels compared to the other two markers (77% in RD18, 73% in U2OS).
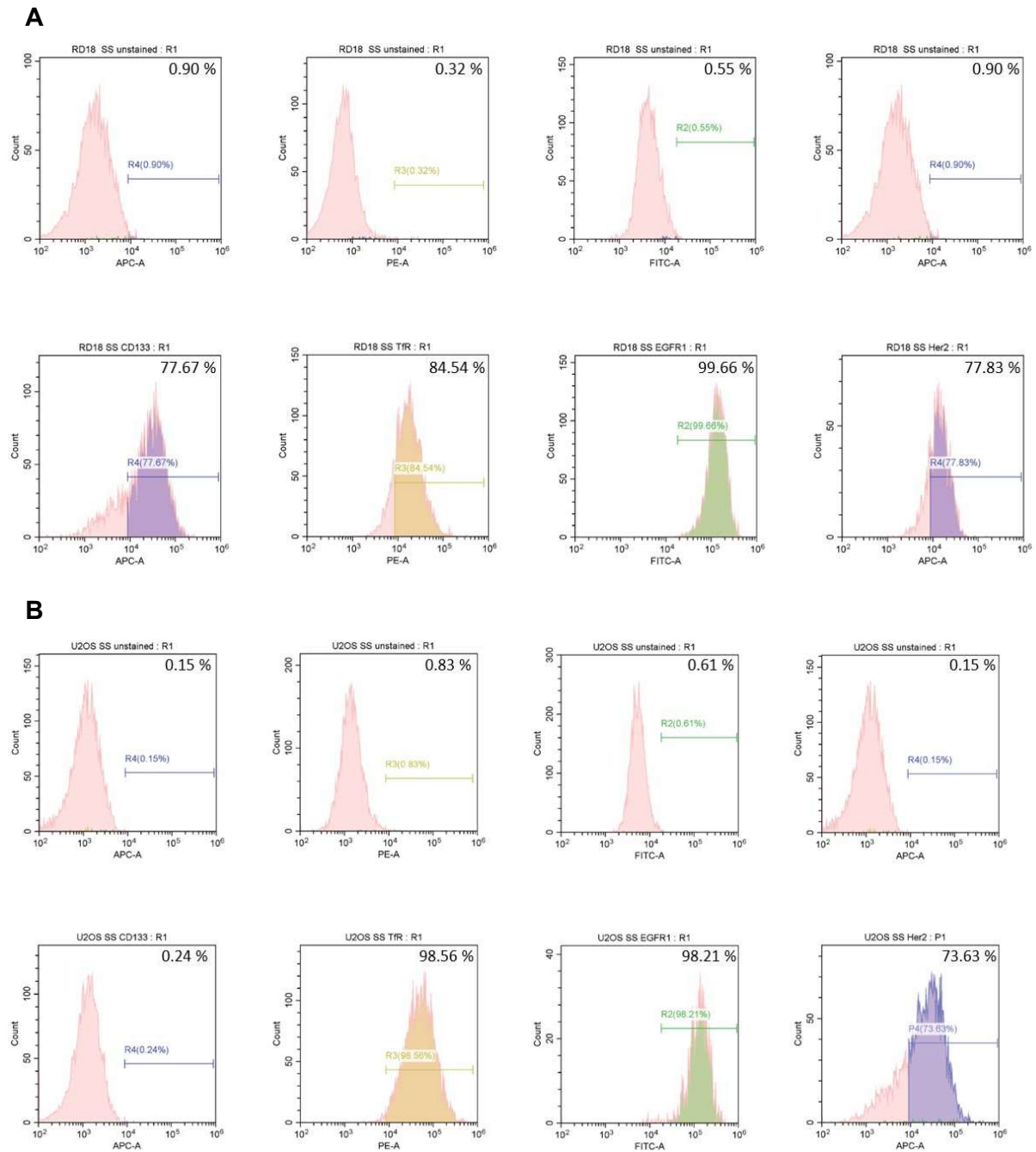
Figure 9. A) Flow cytometry expression of CD133, TfR1, EGFR1 and Her2 on RD18 single spheroids. **B)** Flow cytometry expression of CD133, TfR1, EGFR1 and Her2 on U2OS single spheroids. Samples were incubated with antiCD133-APC (1:20), antiTfR1-PE (1:50), antiEGFR1-FITC (1:10) and antiHer2-APC (1:10) in PBS containing 1% FBS. Above, negative control for each fluorophore represented by unstained samples, below stained cells with fluorophore-conjugated antibodies. Results are representative of 3 independent experiments. Samples were analyzed by flow cytometry Cytoflex analyzer (CRBA).

4.2.3 Cell viability assays in single-spheroid 3D model

We performed ATP viability assay in RD18 and U2OS single spheroids to evaluate if ITs could have a possible antitumor effect also on this 3D model, and compared the toxic action of conjugates between adherent cells and single spheroids. After appropriate formation times, single spheroids were treated for 72 h with the indicated scalar dilutions of ITs, unconjugated RIPs or carrier alone (Figure 10 and 11). In RD18 single spheroids, Tf-SO6 conjugate showed a great targeted efficacy compared to unconjugated saporin or transferrin (Figure 10A). Indeed, for each concentration tested, the cytotoxicity of Tf-SO6 was significantly higher compared to unconjugated RIP or carrier (Figure 10A). Tf-SO6 had an IC_{50} value of 5.4 nM, while unconjugated SO6 and Tf alone had values of 314.6 nM and >100 nM, respectively (Table 4), meaning that IT was 58 times more toxic than unconjugated RIP. Also, αEGFR1-Ocy IT was more cytotoxic than unconjugated ocymoidine or αEGFR1. For each concentration tested, the cytotoxicity of αEGFR1-ocy was significantly higher compared to unconjugated RIP or carrier (Figure 10B). αEGFR1-Ocy had an IC_{50} value of 2.8 nM, while unconjugated Ocy and αEGFR1 alone had values of 751.9 nM and >100 nM, respectively. Thus, the IT was 268 times more cytotoxic than unconjugated RIP (Table 4). In addition, αHer2-Ocy showed a great cytotoxic effect compared to unconjugated RIP saporin or carrier alone αHer2. Indeed, Figure 10C clearly showed that for each concentration tested, αHer2-Ocy toxicity was significantly higher compared to unconjugated RIP or carrier. αHer2-Ocy had an IC_{50} value of 6.8 nM, while unconjugated Ocy and αHer2 had values of 751.9 nM and >100 nM, respectively, showing a specific toxicity 110 times greater than unconjugated RIP (Table 4). In U2OS single spheroids, Tf-SO6 conjugate showed remarkable targeted efficacy compared to unconjugated saporin or transferrin (Figure 11A). As showed in Figure 11A, for each concentration tested, Tf-SO6 cytotoxicity was significantly higher compared to unconjugated RIP or carrier. Tf-SO6 had an IC_{50} value of 4.2 nM, while unconjugated SO6 and Tf alone had values of 473.3 nM and >100 nM, respectively (Table 5), meaning that IT was 112 times more toxic than unconjugated RIP. αEGFR1-Ocy IT was more cytotoxic than unconjugated ocymoidine or αEGFR1 (Figure 11B). In this case, the cytotoxicity induced by αEGFR1-Ocy was significantly higher respect to RIP or carrier alone at 10 nM (Figure 11B). In addition, αEGFR1-Ocy had an IC_{50} value of 12.1 nM, while unconjugated Ocy and αEGFR1 alone had values of 593.5 nM and >100 nM, respectively, meaning that IT was 49 times more cytotoxic than unconjugated RIP (Table 5). αHer2-Ocy showed a greater cytotoxic effect compared to unconjugated RIP saporin or carrier alone αHer2 (Figure 11C).

At 10 nM, αHer2-Ocy induced a higher cytotoxicity compared to RIP or carrier alone; moreover, αHer2-Ocy had an IC_{50} value of 11.1 nM, while unconjugated Ocy and αHer2 alone had values of 593.5 nM and >100 nM, respectively, showing a specific toxicity 53 times greater than unconjugated RIP (Table 5). Unfortunately, non-target U937 cell line was not able to grow as single spheroids; as demonstrated by ATP assay performed every 24 h after seeding, U937 gradually died beginning 48 h after seeding in a statistically significant way (Figure 12). Indeed, we considered valid results previously obtained in viability curves of U937 2D model to demonstrate the selectivity of the conjugates. Both in RD18 and U2OS single spheroids, all tested conjugates showed an enhanced efficacy compared to corresponding unconjugated RIP or carrier alone. Among ITs used, looking at IC_{50} values, αEGFR1-Ocy resulted the most cytotoxic in RD18 single spheroids while in U2OS single spheroids was Tf-SO6. In addition, the IC_{50} difference between RIP and IT was higher in single spheroids rather than adherent cells. Overview of IT and RIP IC_{50} values among cell models is reported in Table 10.

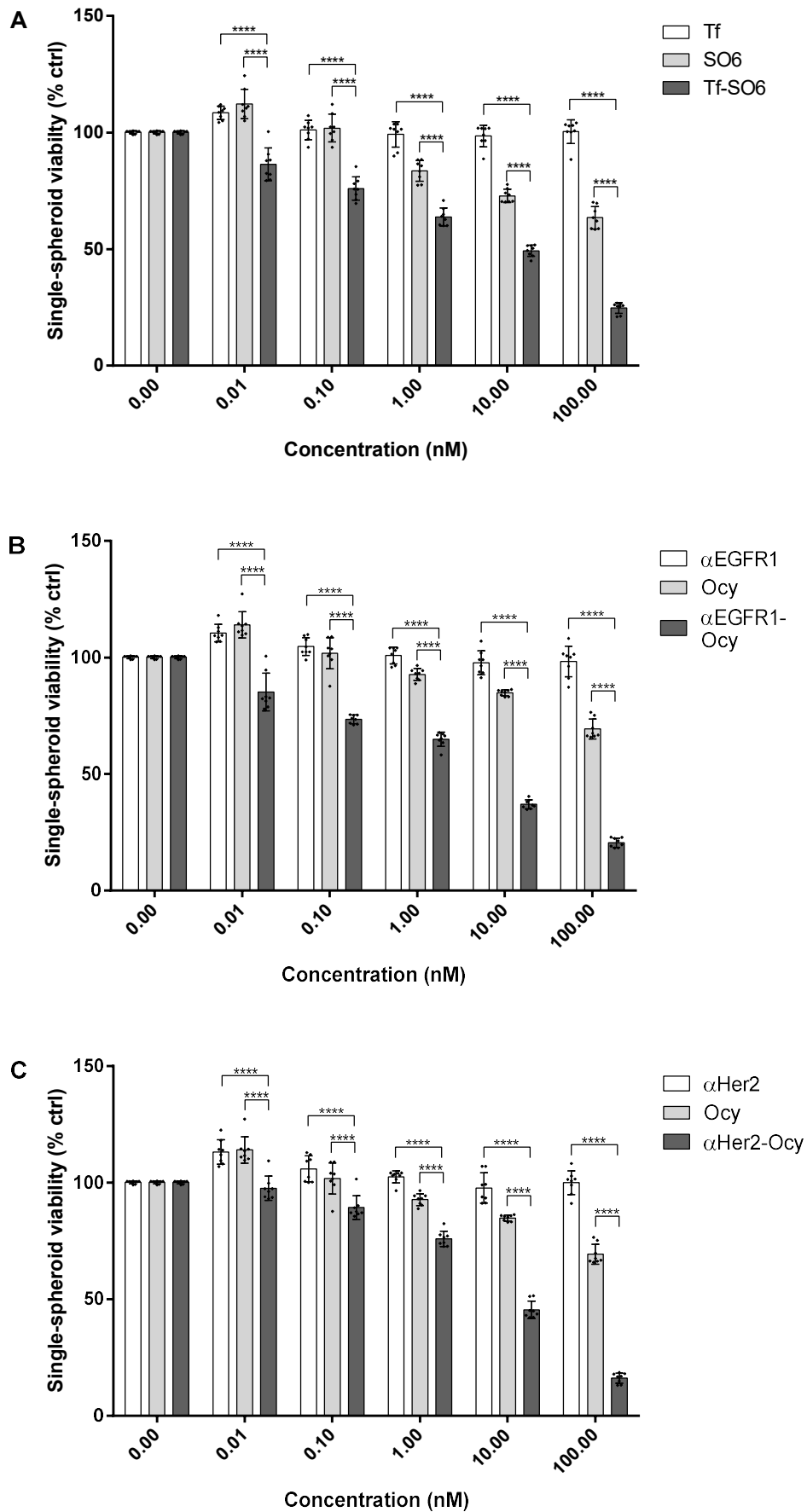**RD18**

Figure 10. Dose-response curves on RD18 single spheroids. **A)** Single spheroids were treated for 72 h with Tf-SO6, unconjugated SO6 and Tf. **B)** Single spheroids were treated for 72 h with αEGFR1-Ocy, unconjugated Ocy and αEGFR1. **C)** Single spheroids were treated for 72 h with αHer2-Ocy, unconjugated Ocy and αHer2. Cells (5000/well) were seeded in ultra-low attachments black 96-well U-bottom plates in a final volume of 100 μl of DMEM-F12 complete medium containing appropriate concentration of compounds. Viability was evaluated using the 3D luminometric ATP assay. Results are the means of four independent experiments, each performed in duplicate. Statistical analysis was performed with Prism 9 using ANOVA/Tukey's multiple comparison test (**** $p < 0.0001$). Data have been normalized to vehicle values (PBS) and plotted with Prism 9.

Table 4. IC_{50} values related to RD18 single spheroids treated for 72 h with ITs, unconjugated RIPs and carriers. IC_{50} were calculated using non-linear regression (Prism 9).

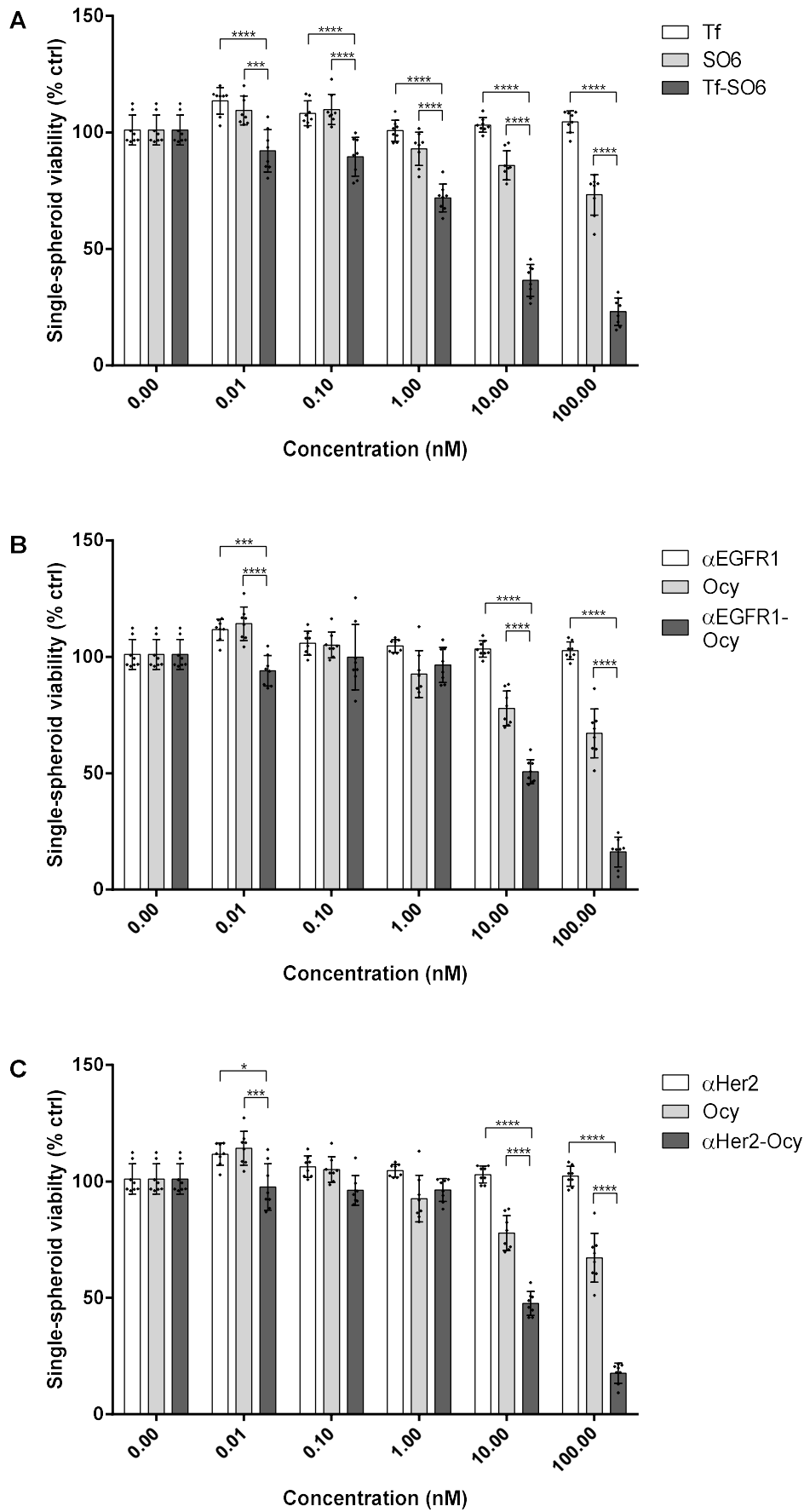|	Tf	SO6	Tf-SO6	αEGFR1	Ocy	αEGFR1-Ocy	αHer2	αHer2-Ocy
IC_{50} (nM)	>100	314.6	5.4	>100	751.9	2.8	>100	6.8

U2OS

Figure 11. Dose-response curves on U2OS single spheroids. **A)** Single spheroids were treated for 72 h with Tf-SO6, unconjugated so6 and Tf. **B)** Single spheroids were treated for 72 h with αEGFR1-Ocy, unconjugated Ocy and αEGFR1. **C)** Single spheroids were treated for 72 h with αHer2-Ocy, unconjugated Ocy and αHer2. Cells (5000/well) were seeded in ultra-low attachments black 96-well U-bottom plates in a final volume of 100 μl of DMEM-F12 complete medium containing appropriate concentration of compounds. Viability was evaluated using the 3D luminometric ATP assay. Results are the means of four independent experiments, each performed in duplicate. Statistical analysis was performed with Prism 9 using ANOVA/Tukey's multiple comparison test (**** $p < 0.0001$). Data have been normalized to vehicle values (PBS) and plotted with Prism 9.

Table 5. IC_{50} values related to U2OS single spheroids treated for 72 h with ITs, unconjugated RIPs and carriers. IC_{50} were calculated using non-linear regression (Prism 9).

	Tf	SO6	Tf-SO6	αEGFR1	Ocy	αEGFR1-Ocy	αHer2	αHer2-Ocy
IC_{50} (nM)	>100	473.3	4.2	>100	593.5	12.1	>100	11.1

U937
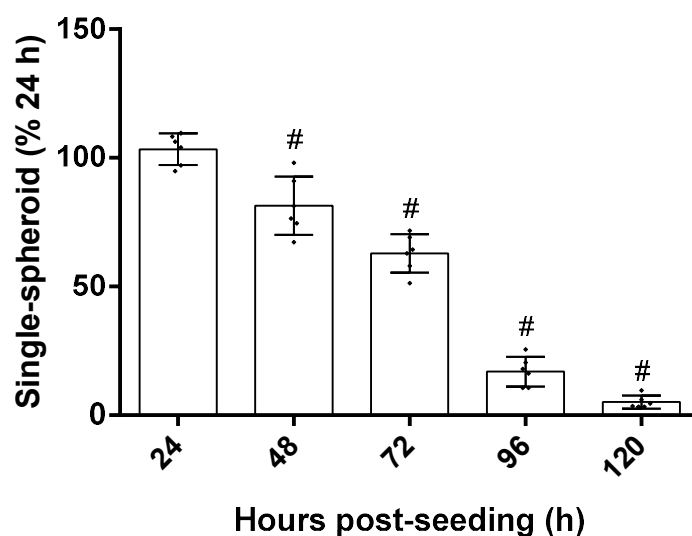
Figure 12. U937 cells (5000/well) were seeded in ultra-low attachments black 96-well U-bottom plates in a final volume of 100 μl of DMEM-F12 complete medium Viability was evaluated using the 3D luminometric ATP assay every 24 h. Results are the means of two independent experiments, each performed in triplicate. Statistical analysis was performed with Prism 9 using ANOVA/Dunnett's multiple comparison test (# $p < 0.0001$ compared to 24 h). Data have been normalized to viability at 24 h post-seeding and plotted with Prism 9.

4.2.4 Representative imaging of viability experiments in RD18 single spheroids

RD18 single spheroids imaging, relative to ATP viability assay, represents the morphological analysis of single spheroids treated with indicated IT, RIP or carrier for 72 h at the concentration of 100 nM, the highest dose used. The toxic action induced by each IT was compared to that one induced by the corresponding unconjugated RIP and carrier. As clearly reported in Figure 13, representative imaging confirmed the results already obtained in viability assay.
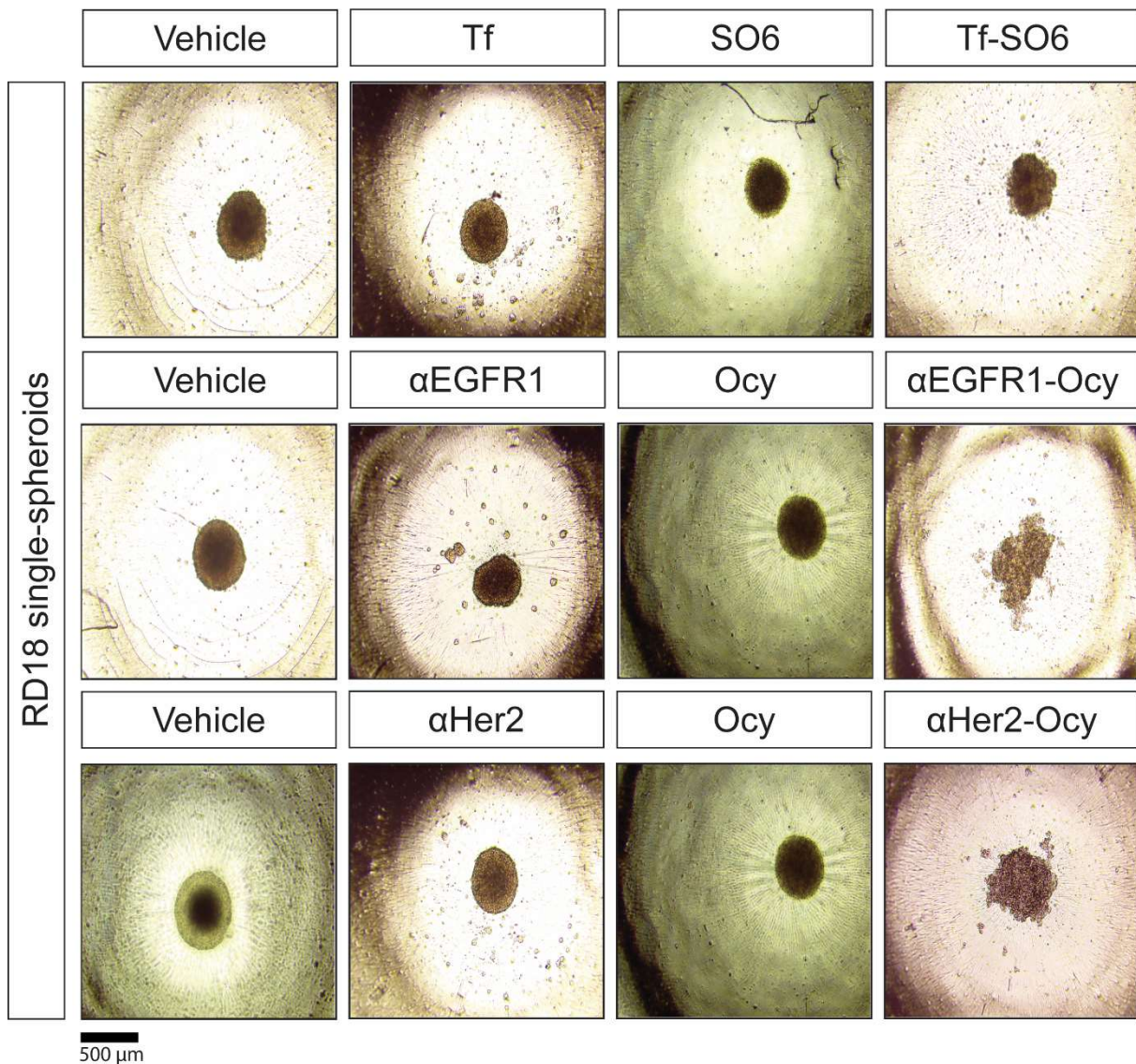

Figure 13. Representative imaging of ATP assay on RD18 single spheroids. Single spheroids were treated with the indicated IT and RIP or carrier alone for 72 h at 100 nM. Vehicle represents control samples (PBS). Imaging was performed using a phase-contrast microscope with a digital camera from Nikon Eclipse TS100 with 40× magnification.

4.2.5 Time-dependent effect of ITs on caspase 3/7 activation in RD18 and U2OS single spheroids

To verify if ITs could induce the activation of apoptosis also on RD18 and U2OS single spheroids and eventually compare the timing of activation between them and adherent cells, we decided to evaluate effector caspase 3/7 activation in IT or RIP-treated single spheroids. To further verify the correlation between caspase activation and viability, we performed in parallel a cell viability assay. Activation of effector caspases 3/7 was measured in RD18 and U2OS single spheroids after 8, 16 and 24 h of treatment. Spheroids were treated with the IC_{50} of each IT (see Table 10). For unconjugated RIPs, it was chosen the same concentration of the corresponding IT. All ITs induced a significantly strong activation of caspase 3/7 compared to control (PBS) at 24 h (Figure 14 and 15). However, at 16 h, effector caspase activation induced by αEGFR1-Ocy and αHer2-Ocy was poor but statistically significant (compared to control, PBS) in both RD18 and U2OS single spheroids ($p < 0.0001$). After 24 h of treatment, all ITs induced similar intensity of caspase 3/7 activation reaching values around 300% (compared to control, PBS) for RD18 single spheroids and around 350-400% (compared to control, PBS) for U2OS single spheroids (Figure 14 and 15). RIPs were not able to activate effector caspase at any time tested (respect to control, PBS), as already seen in adherent cells (Figure 14 and 15). We compared IT-deriving caspase activation with that one induced by RIPs alone at 8, 16, and 24 h. At 24 h, all ITs induced a significantly higher caspase 3/7 activation compared to that one induced by RIP alone at the same time ($p < 0.0001$) (Figure 14 and 15). Differently from adherent cells, we noticed that after 16 h in single spheroids, there was a poorer apoptosis activation even if statistically significant, while at 24 h, it was extremely high with a similar intensity observed in adherent cells at the same time. IT-dependent apoptosis activation proceeded in parallel with the decrease of viability (Figure 14 and 15). In single spheroids we observed a strong activation of caspase 3/7 delayed of 8h compared to what observed in 2D model. Nevertheless, these results clearly indicated that type I RIP-based ITs can induce caspase-dependent apoptosis also in single-spheroid 3D model.
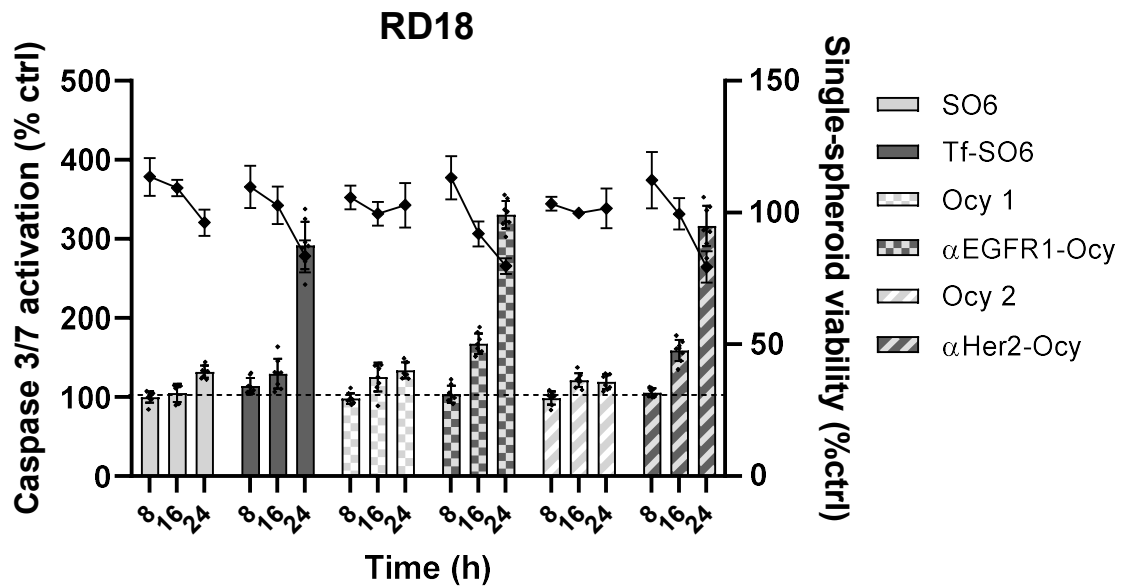
Figure 14. Caspases 3/7 activation in RD18 single spheroids exposed to IC50 of Tf-SO6, αEGFR1-Ocy and αHer2-Ocy or corresponding RIPs. Single spheroids (5000/well) were seeded in ultra-low attachment black 96-well U-bottom plates in a final volume of 100 μl of DMEM-F12 complete medium containing appropriate concentration of compounds. Caspase activity was compared to viability and expressed as the percentage of control values (PBS). Results of caspase 3/7 activation assay (bars) and viability assay (lines) are the means of four independent experiments, each performed in duplicate. Statistical analysis was performed with Prism 9 using ANOVA/Tukey's multiple comparison test (p < 0.0001). Data have been plotted with Prism 9.

Figure 15. Caspases 3/7 activation in U2OS single spheroids exposed to IC_{50} of Tf-SO6, αEGFR1-Ocy and αHer2-Ocy or corresponding RIPs. Single spheroids (5000/well) were seeded in ultra-low attachment black 96-well U-bottom plates in a final volume of 100 μl of DMEM-F12 complete medium containing appropriate concentration of compounds. Caspase activity was compared to viability and expressed as the percentage of control values (PBS). Results of caspase 3/7 activation assay (bars) and viability assay (lines) are the means of four independent experiments each performed in duplicate. Statistical analysis was performed with Prism 9 using ANOVA/Tukey's multiple comparison test (p < 0.0001). Data have been plotted with Prism 9.
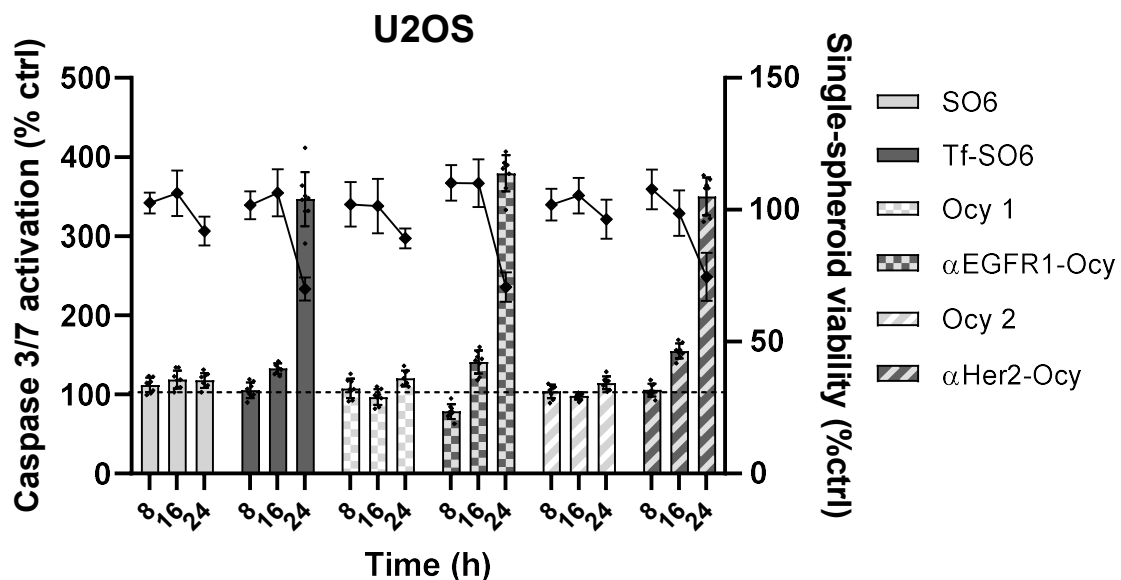
4.2.6   Matrigel-based establishment of cell or patient-derived organoids: ring strategy

In order to verify if ITs could have a specific toxic effect also on 3D organoids, thus understanding if the results obtained in adherent cells and single spheroids could be also translated to this model, we established 3D organoids using the "ring strategy" developed by Prof. Alice Soragni's laboratory. This method allows for 3D tumor organoids formation using a miniaturized ring geometry with no need of functionalized plates or dissociation to single-cell suspension before final assay. To generate organoids, we seeded cells, by plating in a ring shape around the rim of 96 or 24-well plates (mini-rings or maxi-rings respectively), single-cell suspensions pre-mixed with cold Mammocult-Matrigel (1:1.33 ratio). Thanks to small volume plated and surface tension of the well, cells were held on the rim of the well until Matrigel solidifies upon incubation at 37°C. After this, pre-warmed Mammocult complete medium was added using EpMotion. Ring geometry allowed for media addition and removal directly in the center of the well without disrupting Matrigel-containing organoids. For viability and apoptosis assays, RD18 and U2OS-derived organoids were established by generating mini-ring in 96-well plates. Organoids were generated by plating, in a final volume of 10 μl, 1000 cells/well of RD18 or U2OS single-cell suspensions pre-mixed with cold Mammocult-Matrigel. This seeding concentration was chosen among the others tested because gave rise to organized tumor organoids without allowing adherent cells formation in the center of the well (Figure 16). This problem was observed with all the other seeding concentration tested: 5000, 3000, 2000 cells/well. For flow-cytometry, H&E and IHC analysis, maxi-ring organoids were created in 24-well plates by plating, in a final volume of 70 μl, 20.000 cells/well of RD18 or U2OS single-cell suspensions pre-mixed with cold Mammocult-Matrigel. This seeding concentration was chosen among the other tested because gave rise to organized tumor organoids without adherent cells presence in the center of the well. This problem was observed with the other seeding concentration tested, 50.000 cells/well. For viability assay performed on patient-derived SARC0116 organoids, human tumor tissue biopsy was processed as described in Methods. After digestion and red blood cell lysis, mini-rings were generated by plating, in 96-well plates, 5000 cells/well in a final volume of 10 μl of the single-cell suspension pre-mixed with cold Mammocult-Matrigel. The seeding concentration was chosen considering the availability of tumor sample.
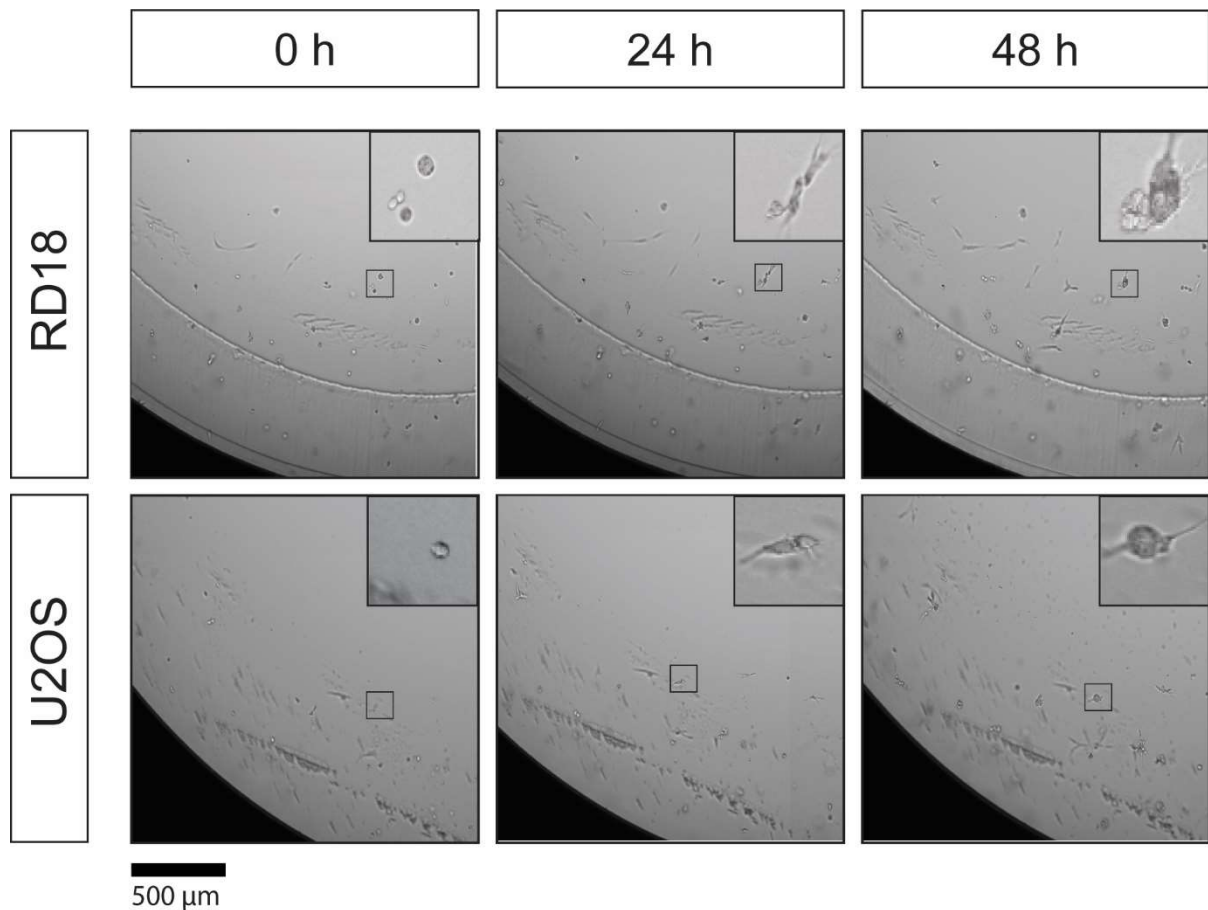
Figure 16. Time-course formation assay of RD18 and U2OS-derived organoids. 1000 cells/well were seeded in white 96-well plates. Organoids formation was monitored daily using Celigo software.

4.2.7 Flow cytometry analysis of CD133, TfR1, EGFR1 and Her2 expression in 3D sarcoma organoids

To assess if RD18 and U2OS organoids maintained an overexpression of the selected antigens, as already observed in the other cell models (adherent cells and single spheroids), flow-cytometry analysis was performed. In addition, we also analyzed the expression of staminal marker CD133. As described in methods, cell line derived-organoids were created by plating, in 24-well plate, 20.000 cells/well of Mammocult-Matrigel-cell mixture and keeping them in culture with Mammocult complete medium for 6 days to allow maxi-ring organoids formation. Then, 2 well for each sample were harvested (Dispase and pipetting) as described in methods and stained. Expression of selected markers, CD133, TfR1, EGFR1 and Her2, was examined by flow cytometry after staining with fluorophore-conjugated primary antibodies.

Overview of the results obtained among models are reported in Table 9 while organoids flow cytometry graphs are reported in Figure 17A (RD18 organoids) and 17B (U2OS organoids).
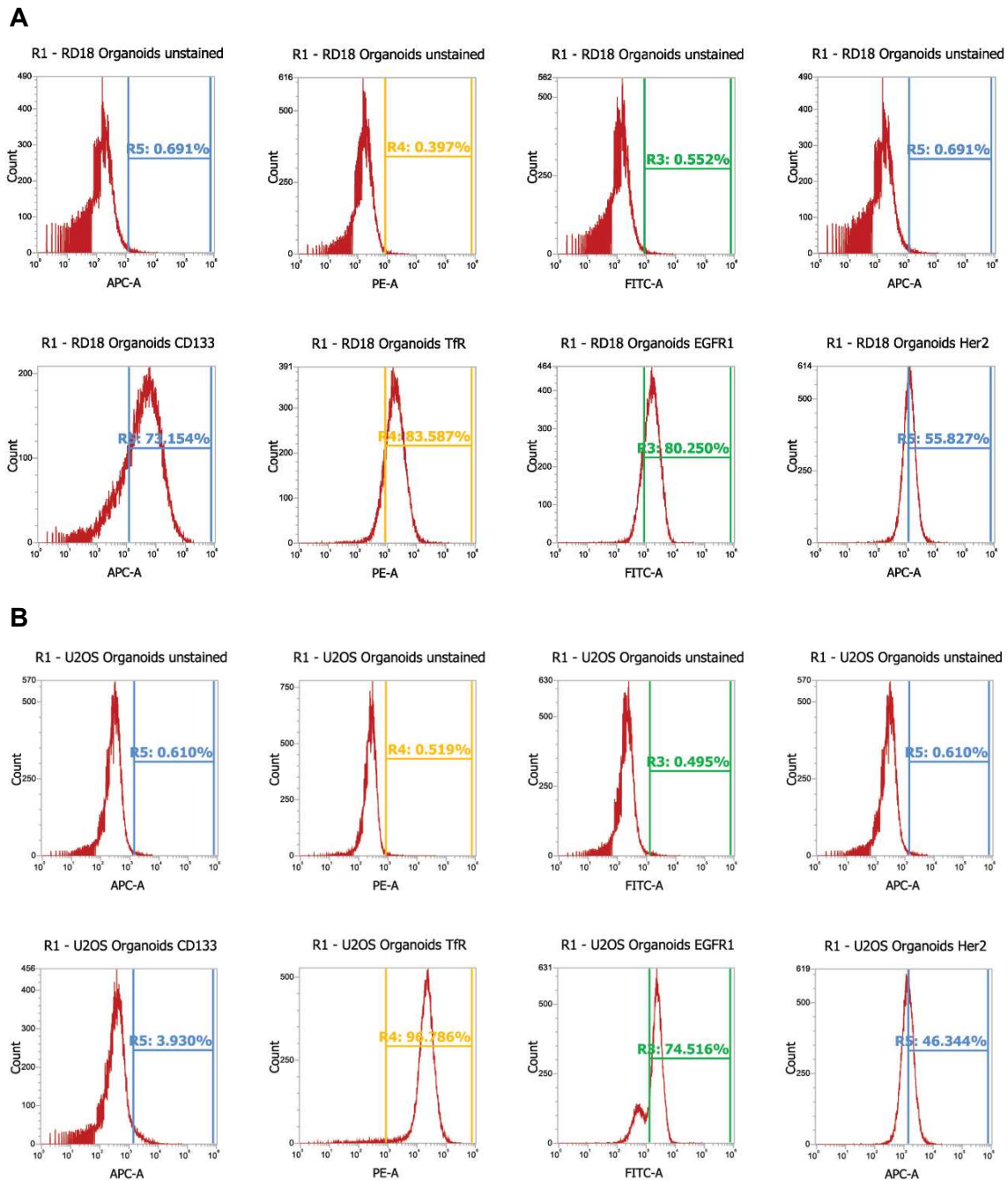
Figure 17. A) Flow cytometry expression of CD133, TfR1, EGFR1 and Her2 on RD18 organoids. **B**) Flow cytometry expression of CD133, TfR1, EGFR1 and Her2 on U2OS organoids. Samples were incubated with antiCD133-APC (1:20), antiTfR1-PE (1:50), antiEGFR1-FITC (1:10) and antiHer2-APC (1:10) in PBS containing 1% FBS. Above, negative control for each fluorophore represented by unstained organoids, below stained organoids with fluorophore-conjugated antibodies. Results are representative of 3 independent experiments. Organoids were analyzed by flow cytometry Attune NxT cell analyzer (UCLA).

Results showed that CD133 stem cell marker is overexpressed only in the organoids deriving from the RD18 cell line (73%) and not in those deriving from the U2OS line. As for single spheroids, this does not exclude a priori that the latter do not overexpress other staminal markers that we have not taken into consideration in this phase of the research project. There was also a strong overexpression of TfR1 and EGFR1 in RD18 (83% and 80% respectively) and U2OS organoids (96% and 74% respectively), while Her2 was expressed at lower levels on both of them (55% in RD18 and 46% in U2OS).

4.2.8 Cell-derived organoids morphology: first evidence of saporin-induced toxicity

In order to assess cell-derived organoids morphology and evaluate if saporin could induce morphological changes compatible with cell death, we performed Hematoxylin & Eosin staining on paraffin-embedded slides of RD18 and U2OS-derived organoids. As described in methods, we established maxi-rings in 24-well plates and, after 2 days, we treated them with the IC_{50} of saporin (calculated in related dose-response viability curves) for 72h. Organoids were embedded in paraffin, cut and stained with Hematoxilin for 1 minute, followed by Bluing for 5 minutes and Eosin Y for 2 minutes. Then, slides were dehydrated and mounted before to proceed with imaging. As reported in Figure 16, vehicle RD18 and U2OS organoids are characterized by a peculiar shape of small clusters grouped in a ring, maintaining cell-cell and cell-matrix interaction. The same morphology can be observed in a very similar way to the corresponding sarcomas in vivo. Treatment of RD18 and U2OS organoids with the IC_{50} of saporin for 72 h determined organoid architecture disruption with nuclear alteration such as pyknosis, karyorrhexis and karyolysis. All these features are compatible with cell death (Figure 18).
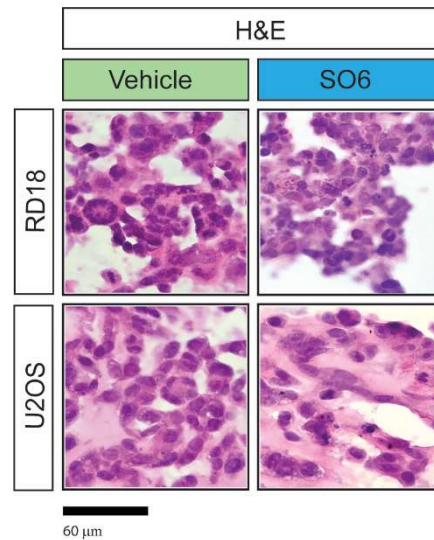
Figure 18. H&E staining of paraffin-embedded slides of RD18 and U2OS-derived organoids. Organoids were treated with vehicle (PBS) or the IC_{50} of saporin for 72 h. Images were acquired through a revolve upright and inverted microscope system. (400× magnification).

4.2.9 Ki-67/Caspase 3 molecular characterization of cell-derived organoids: first proof of saporin-induced apoptosis

To evaluate the molecular characterization of organoids and further assess the effect of saporin on tumor cells proliferation and apoptosis activation, we performed ki67/Caspase 3 immunohistochemistry staining on paraffin-embedded slides of RD18 and U2OS-derived organoids. We established maxi-rings in 24-well plates and after 2 days, we treated them with the IC_{50} of saporin (calculated in related viability experiments) for 72h. As showed in Figure 19, vehicle RD18 and U2OS organoids are characterized by a high expression of the tumor proliferation marker ki67, and by a small presence of the apoptotic marker, Caspase 3, thus showing a typical molecular tumor profile. Interestingly, treatment of RD18 and U2OS organoids with the IC_{50} of saporin for 72 h caused a high reduction of the ki67 marker and a significant increase of Caspase 3. Together with nuclear alteration observed in H&E experiments, these results demonstrated that type I RIP saporin had an anti-proliferative effect and was able to induce apoptosis in cell-derived organoids.
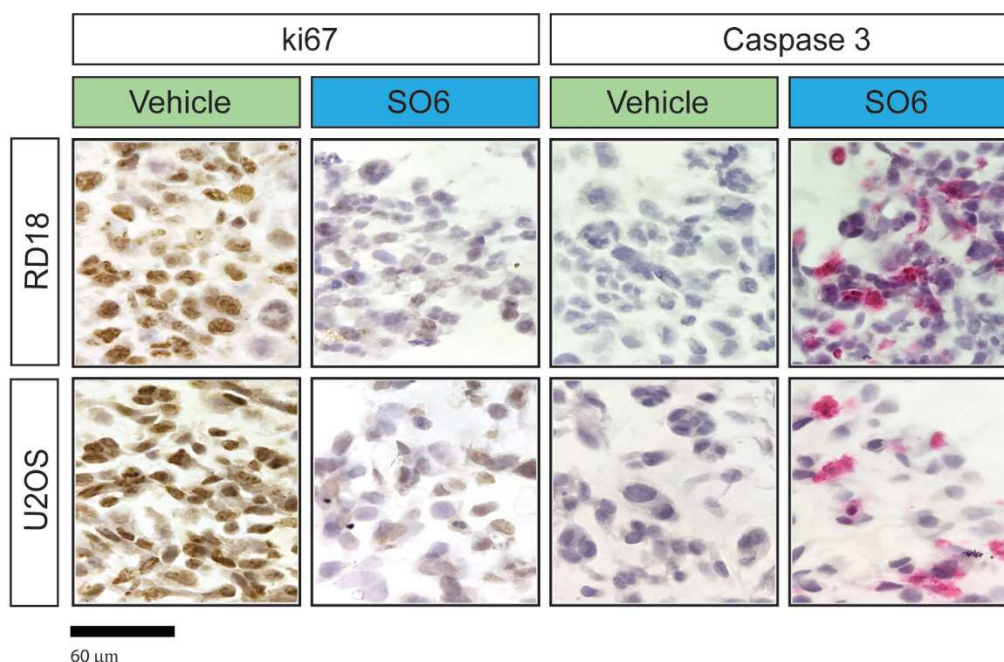
Figure 19. ki67/Caspase 3 staining of paraffin-embedded slides of RD18 and U2OS-derived organoids. Organoids were treated with vehicle (PBS) or the IC_{50} of saporin for 72 h. Images were acquired through a revolve upright and inverted microscope system. (400× magnification).

4.2.10 Cell viability assays in 3D sarcoma organoids

To evaluate the cytotoxicity induced by ITs on RD18 and U2OS organoids and compare the results with those ones already obtained in adherent cell lines and single spheroids, we proceeded by performing ATP viability assay on cell line-derived organoids. Specific cytotoxicity induced by IT was compared to non-specific one related to corresponding unconjugated carriers or RIPs. After appropriate formation time (2 days), organoids were treated with the indicated scalar dilutions for 72 h with ITs, unconjugated RIP or carrier alone. In RD18 organoids, all the conjugates tested showed a mayor targeted efficacy compared to unconjugated RIP or carrier alone. Indeed, at 10 nM concentration, while all ITs killed 50% of organoids, RIP or carrier alone maintained organoids viability around 100% (Figure 20A, 20B, 20C). Tf-SO6 had an IC_{50} value of 9.8 nM, while unconjugated SO6 and Tf alone had values of 740.6 nM and >100 nM, respectively (Table 6), meaning that IT was 75 times more toxic than unconjugated RIP. αEGFR1-Ocy IT was more cytotoxic than unconjugated ocymoidine or αEGFR1 (Figure 20B); αEGFR1-Ocy had an IC_{50} value of 9.1 nM, while unconjugated Ocy and αEGFR1 alone had values of 1219 nM and >100 nM, respectively, meaning that IT was 133 times more cytotoxic than unconjugated RIP (Table 6). Also, αHer2-Ocy showed a remarkable cytotoxic effect than unconjugated Ocy or αHer2 (Figure 20C). In fact, αHer2-Ocy had an IC_{50} value of 28.8 nM, while unconjugated Ocy and

αHer2 alone had values of 1219 nM and >100 nM, respectively, showing a specific toxicity 42 times greater than unconjugated RIP (Table 6). Tf-SO6, αEGFR1-Ocy and αHer2-Ocy, showed a mayor targeted efficacy compared to unconjugated RIP or carrier alone also in U2OS organoids, with higher sensitivity compared to RD18 organoids. Indeed, at 1 nM concentration, all tested ITs killed 50% of organoids, while RIP or carrier alone maintained viability around 100% (Figure 21A, 21B, 21C). Tf-SO6 had an IC_{50} value of 1 nM, while unconjugated SO6 and Tf alone had values of 236.8 nM and >100 nM, respectively (Table 7), meaning that IT was 236 times more cytotoxic than unconjugated RIP. Also, αEGFR1-Ocy IT was more cytotoxic than unconjugated ocymoidine or αEGFR1 (Figure 21B); moreover, αEGFR1-Ocy had an IC_{50} value of 1.8 nM, while unconjugated Ocy and αEGFR1 alone had values of 196.7 nM and >100 nM, respectively, meaning that IT was 109 times more cytotoxic than unconjugated RIP (Table 7). In addition, αHer2-Ocy showed a greater cytotoxic effect compared to unconjugated saporin or αHer2 (Figure 21C); in fact, αHer2-Ocy had an IC_{50} value of 0.7 nM, while unconjugated Ocy and αHer2 alone had values of 197.6 nM and >100 nM, respectively, showing a specific toxicity 282 times greater than unconjugated RIP (Table 7). Unfortunately, as found for spheroids, non-target U937 were not able to grow as organoids (Figure 22). In both RD18 and U2OS organoids, all tested ITs showed a greater efficacy compared to unconjugated RIP or carrier alone. Among ITs tested, looking at IC_{50}, αEGFR1-Ocy resulted the most effective in RD18 organoids while in U2OS organoids was αHer2-Ocy. As observed in single spheroids, also in cell-derived organoids the IC_{50} difference between RIP and IT was higher compared to adherent cells. Overview of IT and RIP IC_{50} values among cell models is reported in Table 10.
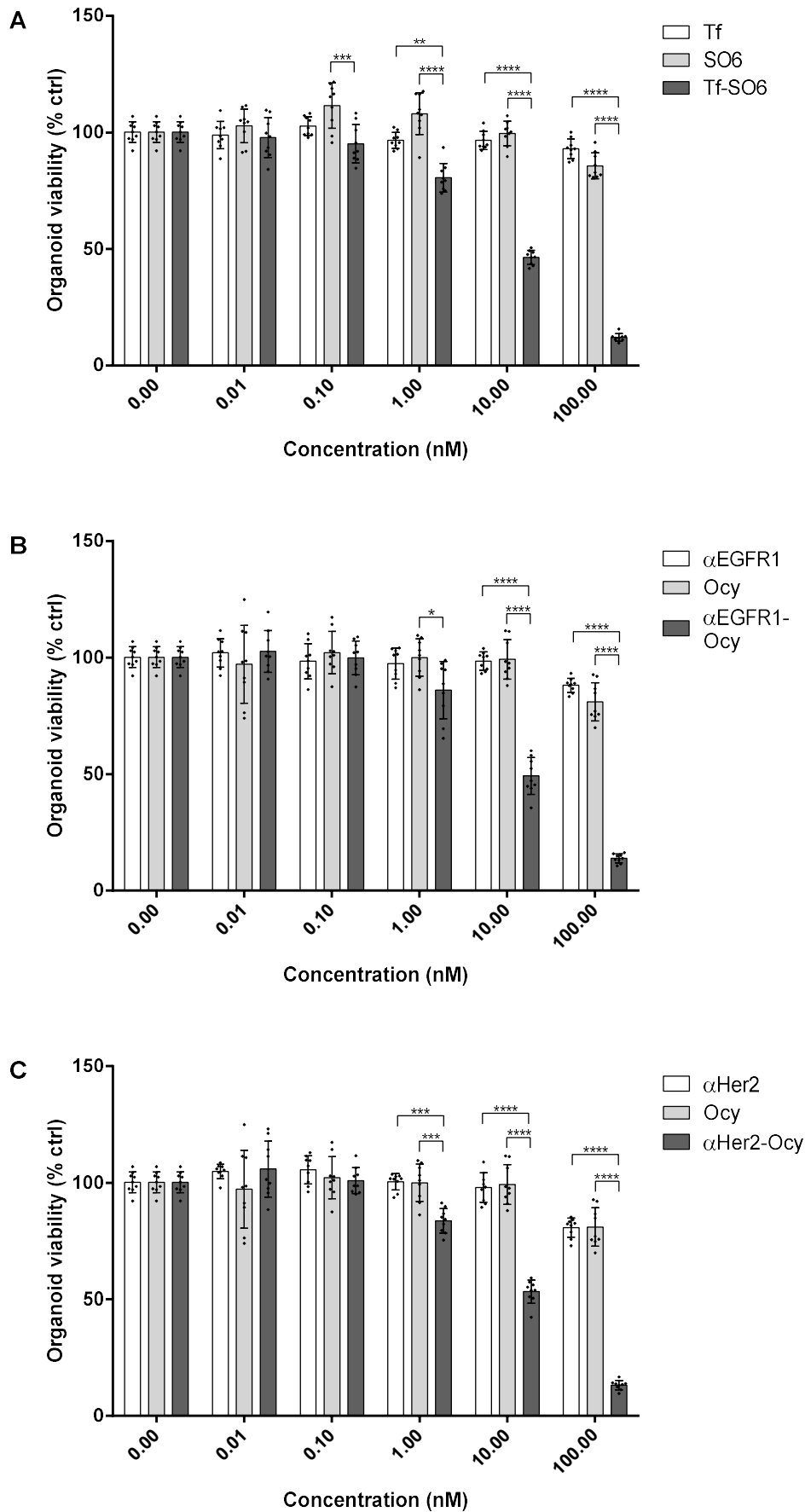
RD18

Figure 20. Dose-response curves on RD18 organoids. **A)** Organoids were treated for 72 h with Tf-SO6, unconjugated SO6 and Tf. **B)** Organoids were treated for 72 h with αEGFR1-Ocy, unconjugated Ocy and αEGFR1. **C)** Organoids were treated for 72 h with αHer2-Ocy, unconjugated Ocy and αHer2. Cells (1000/well) were seeded in white 96-well plates in a final volume of 100 μl of Mammocult complete medium containing appropriate concentration of compounds. Viability was evaluated using the 3D luminometric ATP assay. Results are the means of three independent experiments, each performed in triplicate. Statistical analysis was performed with Prism 9 using ANOVA/Tukey's multiple comparison test (**** $p < 0.0001$). Data have been normalized to vehicle values (PBS) and plotted with Prism 9.

Table 6. IC_{50} values related to RD18 organoids treated for 72 h with ITs, unconjugated RIPs and carriers. IC_{50} were calculated using non-linear regression (Prism 9).

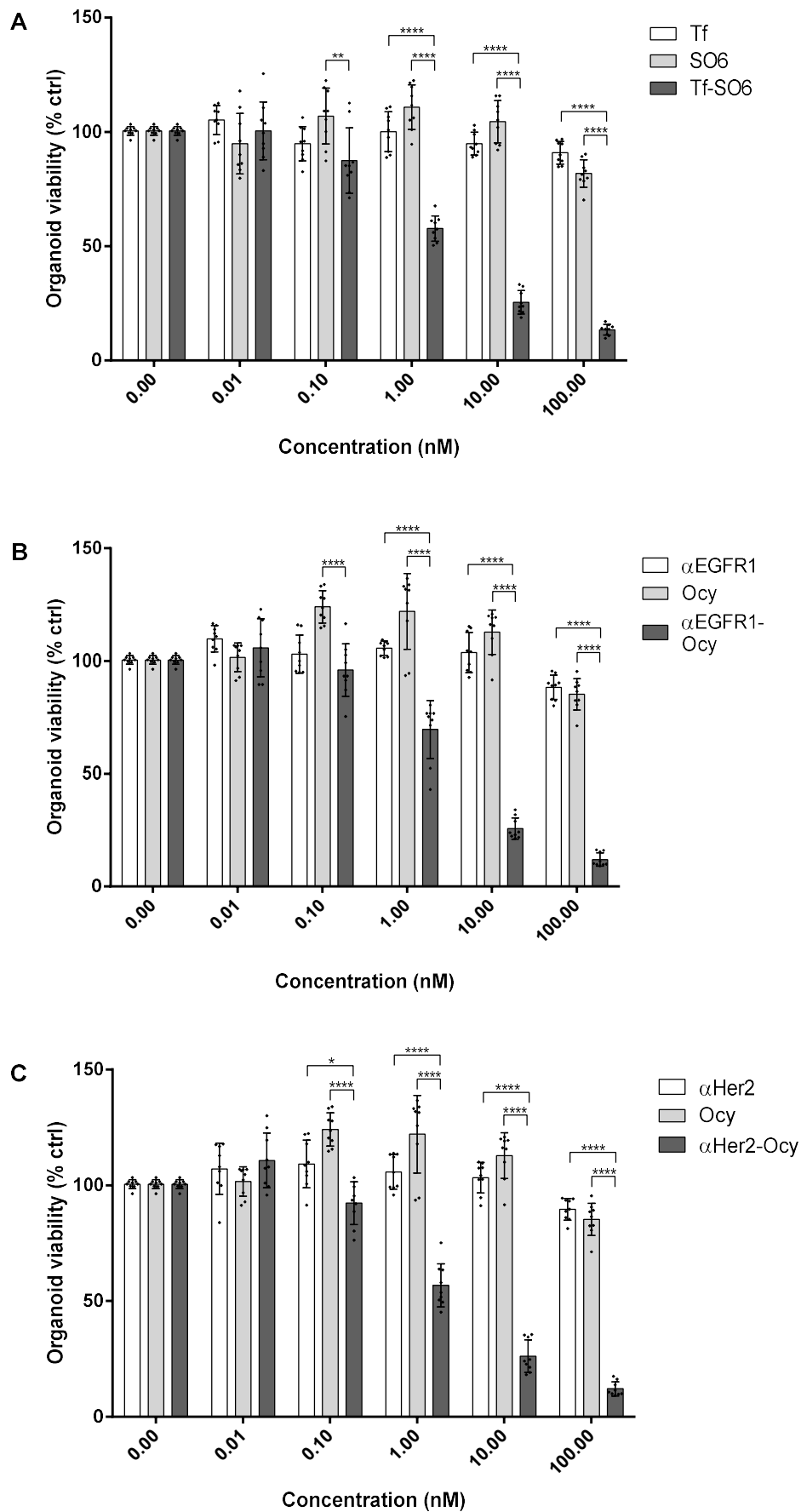|	**Tf**	**SO6**	**Tf-SO6**	**αEGFR1**	**Ocy**	**αEGFR1-Ocy**	**αHer2**	**αHer2-Ocy**
IC_{50} (nM)	>100	740.6	9.8	>100	1219	9.1	>100	28.8

U2OS

Figure 21. Dose-response curves on U2OS organoids. **A)** Organoids were treated for 72 h with Tf-SO6, unconjugated SO6 and Tf. **B)** Organoids were treated for 72 h with αEGFR1-Ocy, unconjugated Ocy and αEGFR1. **C)** Organoids treated for 72 h with αHer2-Ocy, unconjugated Ocy and αHer2. Cells (1000/well) were seeded in white 96-well plates in a final volume of 100 μl of Mammocult complete medium containing appropriate concentration of compounds. Viability was evaluated using the 3D luminometric ATP assay. Results are the means of three independent experiments, each performed in triplicate. Statistical analysis was performed with Prism 9 using ANOVA/Tukey's multiple comparison test (**** p < 0.0001). Data have been normalized to vehicle values (PBS) and plotted with Prism 9.

Table 7. IC_{50} values related to U2OS organoids treated for 72 h with ITs, unconjugated RIPs and carriers. IC_{50} were calculated using non-linear regression (Prism 9).

	Tf	SO6	Tf-SO6	αEGFR1	Ocy	αEGFR1-Ocy	αHer2	αHer2-Ocy
IC_{50} (nM)	>100	236.8	1.0	>100	196.7	1.8	>100	0.7

U937
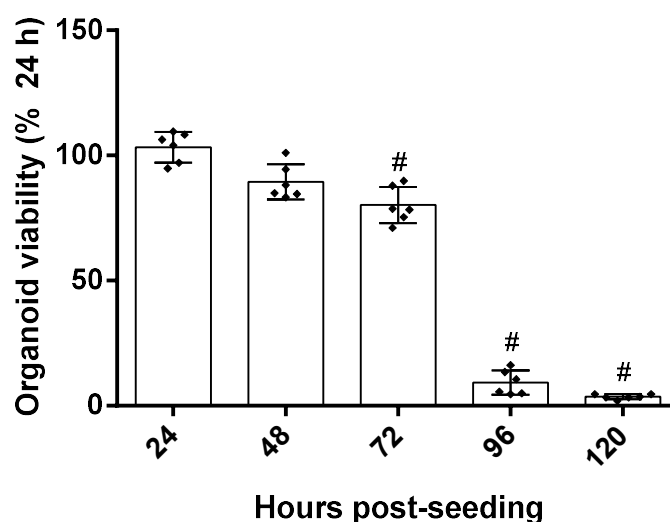
Figure 22. U937 cells (1000/well) were seeded in white 96-well plates in a final volume of 100 μl of Mammocult complete medium. Viability was evaluated using the luminometric ATP assay every 24 h. Results are the means of two independent experiments, each performed in triplicate. Statistical analysis was performed with Prism 9 using ANOVA/Dunnett's multiple comparison test (# p < 0.0001 compared to 24 h). Data have been normalized to viability at 24 h post-seeding and plotted with Prism 9.

4.2.11 Representative imaging of viability experiments in RD18 organoids

RD18 organoids imaging, relative to ATP viability assay, represents the morphological analysis of organoids treated with indicated IT, RIP or carrier for 72 h at the concentration of 100 nM, the highest dose used. The toxic action induced by each IT was compared to that one

induced by the corresponding unconjugated RIP and carrier. As clearly reported in Figure 23, representative imaging confirmed the results already obtained in viability assay.
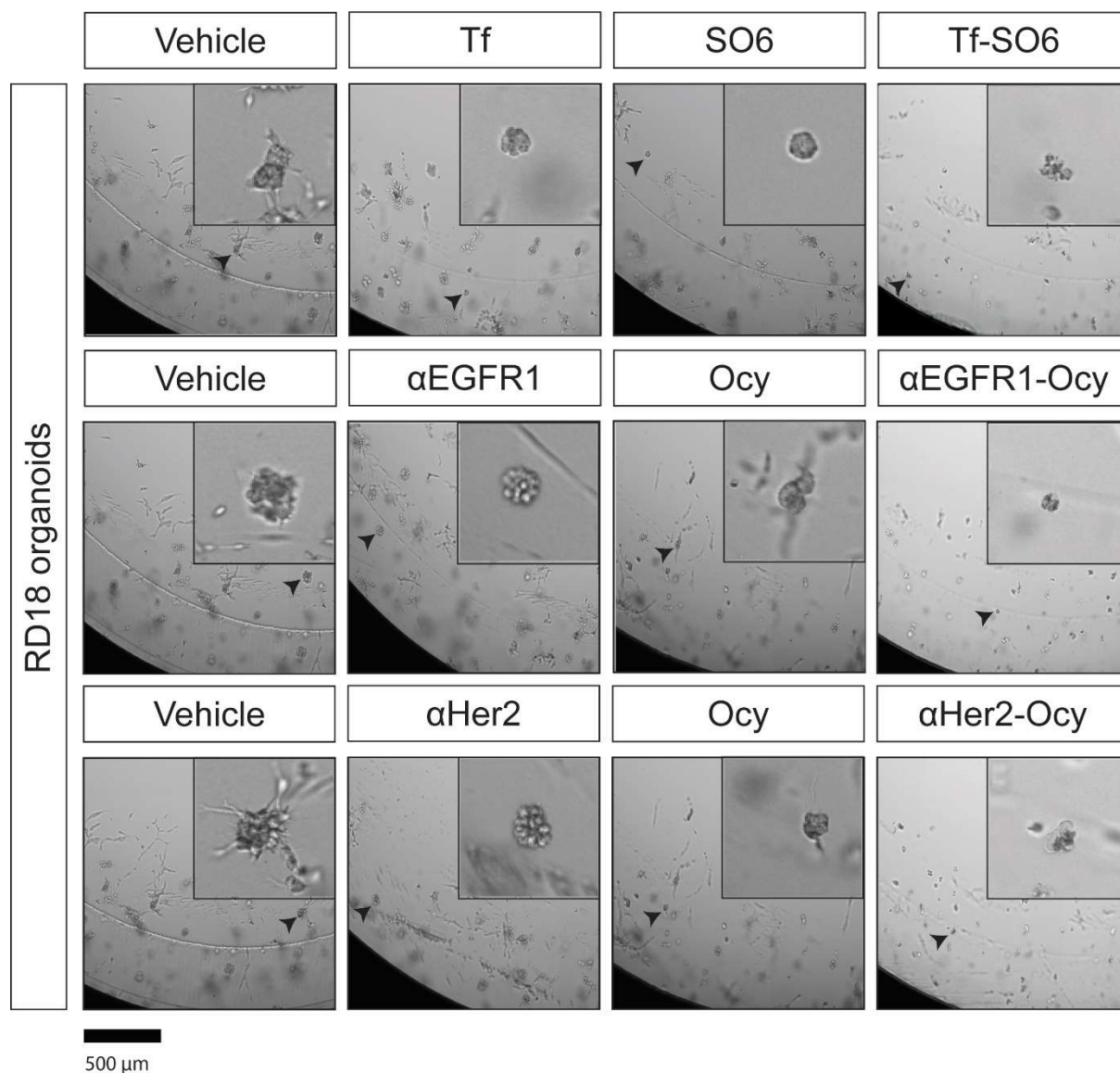
Figure 23. Representative imaging of ATP assay on RD18 organoids. Organoids were treated with the indicated IT and RIP or carrier alone for 72 h at 100 nM. Vehicle represents control samples (PBS). Imaging was performed using Celigo.

4.2.12 Time-dependent effect of ITs on caspase 3/7 activation in RD18 and U2OS-derived organoids

To evaluate if ITs could induce apoptosis also on 3D sarcoma organoids, we further proceed by assessing the effector caspase 3/7 activation in IT or RIP treated RD18 and U2OS-derived organoids, also comparing the apoptosis starting activation time among all cell models used, 2D (adherent cells) and 3D models (single spheroids and organoids). To further verify the

correlation between caspase activation and viability, we performed in parallel a cell viability assay. In RD18 and U2OS organoids, effector caspase 3/7 activation was initially measured after 8, 16 and 24 h of treatment with the IC_{50} of each IT (previously calculated in organoids dose-response curves). For unconjugated RIPs, it was chosen the same concentration of the corresponding ITs. No activation of caspase 3/7 was detected at 8 h and 16 h while it was very poor or no present at all at 24 h. Considering this, we decided to further proceed by assessing apoptosis involvement also at 48 and 72 h. In RD18 organoids, all ITs induced a significant strong activation of caspase 3/7 compared to control (PBS) at 48 h and 72 h (p < 0.0001) (Figure 24). In U2OS organoids, αHer2-Ocy induced a higher significant caspase 3/7 activation compared to control (PBS) at 48 h and 72 h while Tf-SO6 and αEGFR1-Ocy only at 72 h (p < 0.0001) (Figure 25). In RD18 organoids, after 48 h of treatment, Tf-SO6 and αHer2-Ocy induced similar intensity of caspase 3/7 activation reaching values around 200% (compared to control) while αEGFR1-Ocy around 160%. In U2OS organoids, after 72 h, αEGFR1-Ocy and αHer2-Ocy induced similar intensity of caspase 3/7 activation reaching values around 270% (compared to control) while Tf-SO6 around 200% (compared to control). RIPs were not able to activate effector caspase at any time tested compared to control (PBS) as for adherent cells and single spheroids. We also compared IT-deriving caspase activation with that one induced by RIPs alone at 48 h and 72 h. In RD18 organoids, all ITs induced a significantly higher caspase 3/7 activation compared to RIP at 48 h and 72 h (p < 0.0001). In U2OS organoids, αHer2-Ocy induced a significantly higher caspase 3/7 activation compared to that one induced by corresponding RIP at 48 h and 72 h while Tf-SO6 and EGFR1-ocy only at 72 h (p < 0.0001). IT-dependent apoptosis activation proceeded in parallel with the decrease of viability (Figure 24 and 25). In organoids, we observed a strong activation of caspase 3/7, with a delayed induction-time compared to what observed in adherent cells and in single spheroids. Nevertheless, these results clearly indicated that type I RIP-based ITs can induce caspase-dependent apoptosis also in 3D organoids.
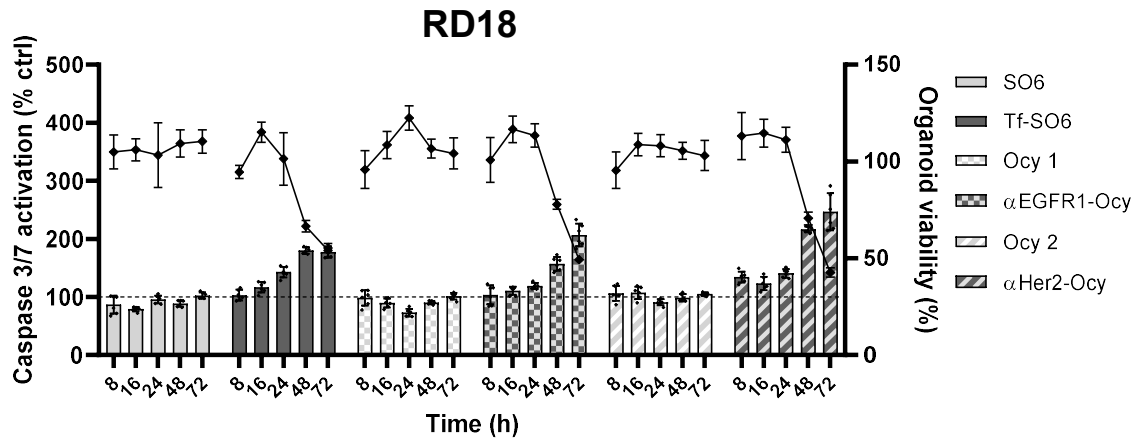
Figure 24. Caspases 3/7 activation in RD18 organoids exposed to IC_{50} of Tf-SO6, αEGFR1-Ocy and αHer2-Ocy or corresponding RIPs. Organoids (1000/well) were seeded in white 96-well plates and treated in a final volume of 100 μl of Mammocult complete medium containing appropriate concentration of compounds. Caspase activity was compared to viability and expressed as the percentage of control values. Results of caspase 3/7 activation assay (bars) and viability assay (lines) are the means of two independent experiments, each performed in triplicate. Statistical analysis was performed with Prism 9 using ANOVA/Tukey's multiple comparison test ($p < 0.0001$). Data have been plotted with Prism 9.
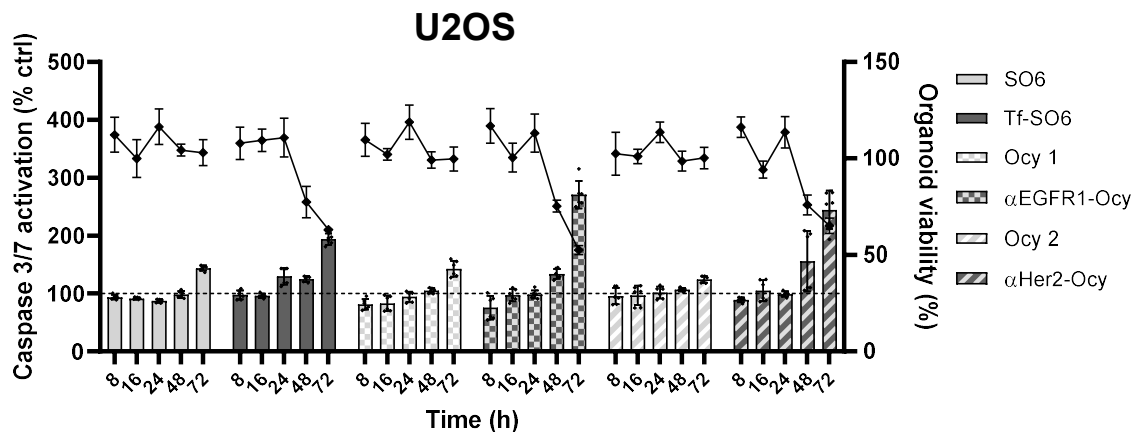
Figure 25. Caspases 3/7 activation in U2OS organoids exposed to IC_{50} of Tf-SO6, αEGFR1-Ocy and αHer2-Ocy or corresponding RIPs. Organoids (1000/well) were seeded white 96-well plates and treated in a final volume of 100 μl of Mammocult complete medium containing appropriate concentration of compounds. Caspase activity was compared to viability and expressed as the percentage of control values. Results of caspase 3/7 activation assay (bars) and viability assay (lines) are the means of two independent experiments, each performed in triplicate. Statistical analysis was performed with Prism 9 using ANOVA/Tukey's multiple comparison test ($p < 0.0001$). Data have been plotted with Prism 9.

4.2.13 Cytotoxic effect of ITs on SARC0116 patient-derived organoids

To verify that ITs could be cytotoxic in nM range also on embryonal rhabdomyosarcoma patient-derived organoids, we proceeded by performing ATP viability assay on SARC0116 patient-derived organoids. SARC116 is a male patient with left arm amputation surgery for recurrent, metastatic alveolar rhabdomyosarcoma 15 years after the diagnosis of the primary. The tumor was first diagnosed when the patient was 3 years old and was removed one year after diagnosis with adjuvant chemotherapy, but the patient kept getting recurrences and metastasis of the tumor multiple times. Patient had been treated with the following drugs: Bevacizumab + Vinorelbine + Cyclophosphamide combination, radiation therapy, and Vinorelbine + Mocetinostat combination. After Collagenase IV digestion of SARC0116 tumor sample and appropriate organoids formation time (3 days), organoids were treated for 72 h with ITs, unconjugated RIP or carrier alone. Tf-SO6 conjugate showed a higher targeted efficacy than unconjugated saporin or transferrin (Figure 26A). Tf-SO6 had an IC_{50} value of 80.8 nM, while unconjugated SO6 and Tf alone had values of 7509 nM and >100 nM, respectively (Table 8), meaning that IT was 93 times more toxic than unconjugated RIP. αEGFR1-Ocy IT was more cytotoxic than unconjugated ocymoidine or αEGFR1 (Figure 26B). αEGFR1-Ocy had an IC_{50} value of 59.6 nM, while unconjugated Ocy and αEGFR1 alone had values of 1391 nM and >100 nM, respectively, meaning that IT was 23 times more cytotoxic than unconjugated RIP (Table 8). Also, αHer2-Ocy showed a greater cytotoxic effect compared to unconjugated RIP Ocy or carrier alone αHer (Figure 26C); in fact, αHer2-Ocy had an IC_{50} value of 95.2 nM, while unconjugated Ocy and αHer2 alone had values of 1391 nM and >100 nM, respectively, showing a specific toxicity 15 times greater than unconjugated RIP (Table 8). These results highlighted that, also in the patient-derived organoids, all ITs tested had an enhanced efficacy compared to corresponding unconjugated RIP or carrier alone. Among ITs tested, αEGFR1-Ocy was the most effective one. We did not perform flow cytometry analysis, IHC and apoptosis assay on SARC0116 patient-derived organoids because of the lack of sufficient biological tumor material.
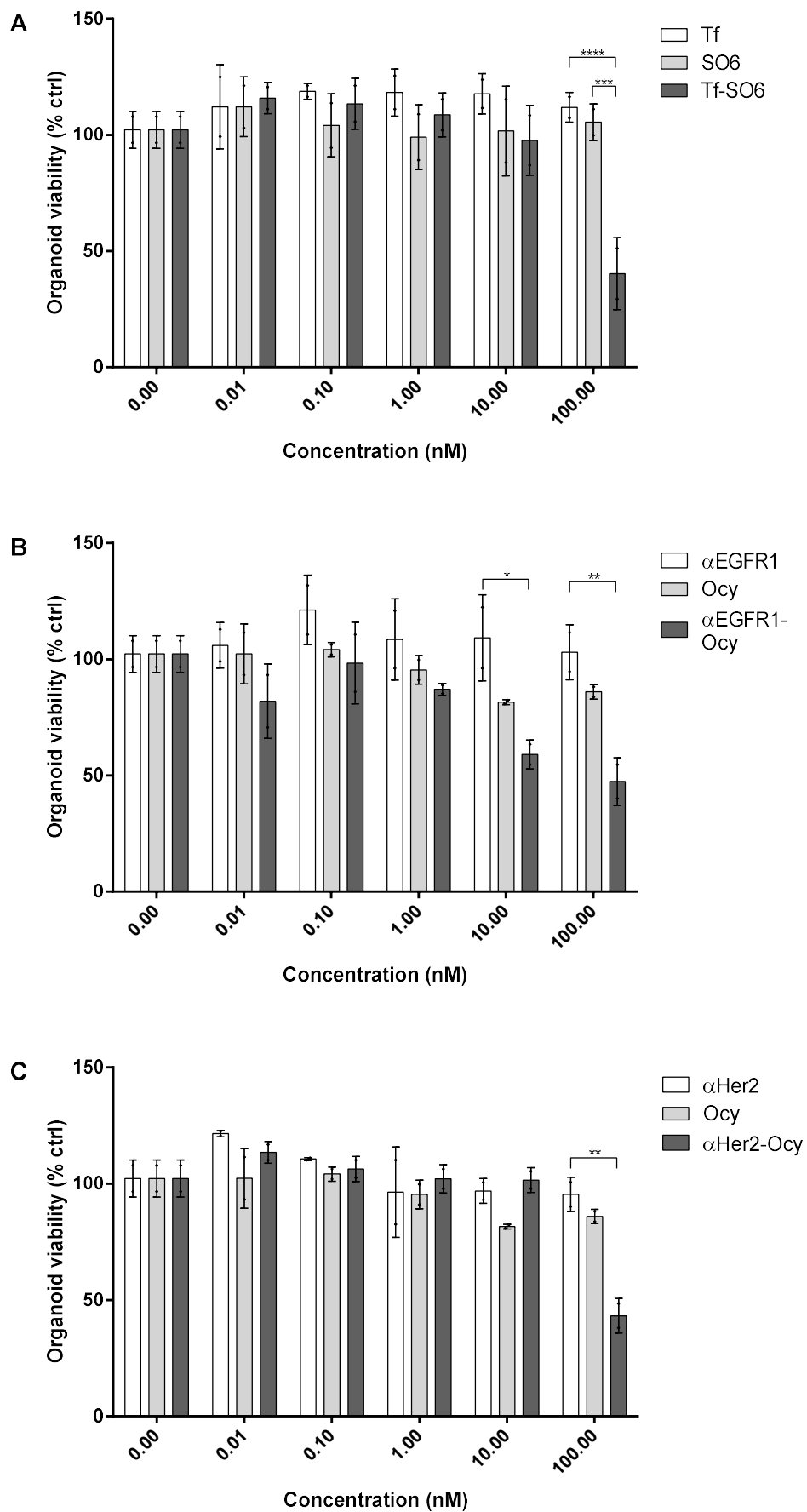
Figure 26. Dose-response curves on SARC0116 organoids. **A)** Organoids were treated for 72 h with Tf-SO6, unconjugated SO6 and Tf. **B)** Organoids were treated for 72 h with αEGFR1-Ocy, unconjugated Ocy and αEGFR1. **C)** Organoids treated for 72 h with αHer2-Ocy, unconjugated Ocy and αHer2. Cells (5000/well) were seeded in white 96-well plates in a final volume of 100 μl of Mammocult complete medium containing appropriate concentration of compounds. Viability was evaluated using the luminometric ATP assay. Results are the means of one experiment, performed in triplicate. We excluded one value from each concentration point because it was out of scale. Statistical analysis was performed with Prism 9 using ANOVA/Tukey's multiple comparison test (**** $p < 0.0001$). Data have been normalized to vehicle values (PBS) and plotted with Prism 9.

Table 8. IC_{50} values related to SARC0116 organoids treated for 72 h with ITs, unconjugated RIPs and carriers. IC_{50} were calculated using non-linear regression (Prism 9).

	Tf	SO6	Tf-SO6	αEGFR1	Ocy	αEGFR1-Ocy	αHer2	αHer2-Ocy
IC_{50} (nM)	>100	236.8	1.0	>100	196.7	1.8	>100	0.7

4.2.14 Comparison of antigens expression between adherent cells, single spheroids and organoids

Comparison of flow cytometry results, performed on adherent cells, single spheroids and organoids, showed a peculiar expression of the selected antigens (Table 1). CD133 is overexpressed only on RD18 single spheroids and RD18 organoids while no considerable level of expression on adherent cell lines and on U2OS single spheroids and U2OS organoids was observed. As anticipated before, the fact that U2OS single spheroids and U2OS organoids showed low levels of CD133 expression, did not necessarily mean that they did not recapitulate staminal tumor characteristic, but that we probably should proceed with a panel of expression analysis of all staminal sarcoma markers to see which of them is present or not. TfR1 and EGFR1 were strongly present on all the models tested for both cell lines. Her2 was expressed at around 50% in RD18 and U2OS adherent cells and organoids, while in single spheroids its level was around 75%. In addition, non-target U937 cells showed low or no expression at all for all antigens tested, confirming that TfR1, EGFR1 and Her2 were selectively overexpressed on target-cells.

Table 9. Overview of antigens expression, in RD18 and U2OS adherent cells, single spheroids and organoids and non-target U937 cells. Values are expressed as percentage of FITC, APC or PE intensity. Experiments were repeated 3 times. Adherent cell lines and organoids were analyzed by flow cytometry Attune NxT cell analyzer (UCLA) while single spheroids by flow cytometry Cytoflex analyzer (CRBA).

	Antigen expression (FITC, PE or APC %)						
	RD18			U2OS			U937 non-target cells
Antigens	**Adherent cells**	**Single spheroids**	**Organoids**	**Adherent cells**	**Single spheroids**	**Organoids**	
CD133	0.3	77.7	73.1	0.1	0.2	3.9	1.2
TfR	98.9	84.5	83.5	99.7	98.6	96.8	0.01
EGFR1	91.8	99.7	80.3	87.9	98.2	74.5	1.4
Her2	56.7	77.8	55.8	57.2	73.6	46.3	0.6

4.2.15 Comparison of IC$_{50}$: overview

Overview of IC$_{50}$, calculated through non-linear regression with Prism 9, showed that selective toxicity induced by ITs is more prominent than the non-specific one induced by RIP administered alone (Table 10). This statement was valid for all the cell models used, except for non-target U937 cell line. Among cell line-derived 2D and 3D models, Tf-SO6, αEGFR1-Ocy and αHer2-Ocy showed IC$_{50}$ values in nM range. Although 3D models are much more complex than 2D ones, ITs are still cytotoxic in a similar way among cell models used. Interestingly, αHer2-Ocy shows the best cytotoxic effect on U2OS organoids. In particular, except for αEGFR1-Ocy, U2OS adherent cells are more sensitive than RD18; RD18 single spheroids are more sensitive respect to U2OS, except for Tf-SO6; for all the tested ITs, U2OS organoids respond better to treatments compared to RD18. In addition, the IC$_{50}$ difference between RIP and IT was higher in 3D models rather than 2D models. A similar cytotoxic profile was obtained in SARC0116 patient-derived organoids where ITs had IC$_{50}$ values in nM range.

Table 10. Overview of IC_{50} related to dose-response curves of 2D and 3D models treated for 72 with ITs or unconjugated RIPs. IC_{50} were calculated using non-linear regression (Prism 9).

Payloads	IC_{50} (nM)							
	RD18			U2OS			SARC-0116 Organoids	U937 Non-target cells
	Adherent cells	Single spheroids	Organoids	Adherent cells	Single spheroids	Organoids		
SO6	24.2	314.6	740.6	13.1	473.3	236.8	7509	47.7
Tf-SO6	1.3	5.4	9.8	0.1	4.2	1.0	80.8	>100
Ocy	58.9	751.9	1219	73.9	593.5	196.7	1391	1076
αEGFR1-Ocy	0.3	2.8	9.1	1.3	12.1	1.8	59.6	>100
αHer2-Ocy	8.8	6.8	28.8	3.7	11.1	0.7	95.2	>100

Chapter 5 – Discussion and conclusions

Although rare, sarcomas are very common types of cancer in children. The standard treatment regimen does not often prove to be conclusive, as many patients with localized primary sarcoma can undergo relapse, progression and metastasis [236, 237, 238]. In order to improve patient outcome, new therapeutic strategies are being evaluated today. Combining RIP high cytotoxicity and mAb selectivity, RIP-containing immunotoxins (ITs) are a promising tool for cancer therapy [239, 240]. To investigate novel personalized treatments for cancer patients, tridimensional models as spheroids and organoids are considered an essential tool for translation of results obtained in basic cancer research, because they are able to recapitulate the histological and genetic features of tumor from which they derive [241, 242].

In this project, we tested and compare the antitumor effect of three RIP-containing ITs, Tf-SO6, αEGFR1-Ocy and αHer2-Ocy, in two sarcoma adherent cell lines, single spheroids and organoids. To perform our analysis, we choose two commonly used sarcoma cell lines for preclinical studies, embryonal rhabdomyosarcoma cell line RD18 and osteosarcoma cell line U2OS, representative of the two main sarcoma subtypes. The choice of immunoconjugates was made based on three considerations: i) TfR1, EGFR1 and Her2 are frequently used in targeted cancer therapy [243, 244, 245, 246]; ii) some authors reported the overexpression of these antigens on primary or advanced sarcoma [247, 248, 249]; iii) ITs directed against those antigens were previously evaluated in carcinoma cancer cells and in some sarcoma cell lines, showing high cytotoxicity [250, 251, 252]. For our study, we choose single spheroids and organoids as tridimensional models. Single spheroids were mostly chosen for their ability to recapitulate staminal features of tumors thank to an elevate presence of cancer stem cells, a cancer cell subpopulation with elevate self-renewal and differentiation properties as well as tumorigenic potential causative of mechanisms of resistance [253, 254]. Organoids were used because they can better recapitulate original tumor features and predict, with high accuracy, sensibility to drugs compared to monolayer cells [255, 256]. Starting from adherent cells, we established RD18 and U2OS-derived single spheroids using ultra-low attachment plates [257] and organoids using ring-strategy [258]. The conjugation of RIP with carrier allows to obtain a conjugate that acquires specificity toward the corresponding antigen and, consequently, to increase the cytotoxicity towards target cells expressing the antigen at high levels. To assess if RD18 and U2OS cell lines could be considered as "target cells" and verify that the overexpression of selected antigens was maintained also in 3D models, we proceed by analyzing TfR1, EGFR1 and Her2 expression in RD18 and U2OS adherent cells, single spheroids and organoids through flow cytometry. Flow cytometry analysis clearly indicated that TfR1 and EGFR1 were highly expressed in RD18 (98.9 % and 91.8 %, respectively) and

U2OS (99.7 % and 87.9 %, respectively) adherent cell lines, while Her2 has an expression, albeit high, slightly lower than the other two antigens, meaning that RD18 and U2OS were effectively target cells. The data obtained in adherent cell lines agree with those ones reported in literature. Indeed, it was shown that, on RD18 and U2OS/osteosarcoma adherent cells, EGFR1 is highly expressed while Her2 presents an intermediate expression level [259, 260, 261, 262]. TfR1 was found to be expressed at high levels in some osteosarcoma patient samples, correlating to a short overall survival [263]. Relevant were the results of flow cytometry analysis obtained in single spheroids and organoids, where, for the first time, we discovered that RD18 and U2OS-derived single spheroids and organoids maintained the high expression of TfR1, EGFR1 and the intermediate expression of Her2, already observed for corresponding adherent model. The analysis also revealed that RD18 single spheroids and organoids, but not U2OS, presented high level of the staminal marker CD133, validating the hypothesis that 3D models are able to recapitulate staminal features of tumor. It was demonstrated that CD133 expression was heterogeneous among Ewing sarcoma with only 4/48 samples characterized by high-expression levels [264]. Considering this, the fact that U2OS single spheroids and organoids did not have a high expression of CD133 did not surprise us, suggesting that it is probably necessary analyzing the expression of a multitude of staminal tumor markers before to arrive at any conclusion [265]. We proceeded by selecting the three conjugates Tf-SO6, αEGFR1-Ocy and αHer2-Ocy, directed against TfR1, EGFR1 and Her2, respectively. The two main goals were: i.) evaluating the increase in cytotoxicity and efficacy of the three conjugates compared to the corresponding unconjugated RIPs or carriers in RD18 and U2OS adherent cells, single spheroids and organoids; ii.) verifying if IT-induced cytotoxicity obtained in adherent cells could be maintained, with similar toxic range, also in more complex 3D tumor models represented by single spheroids and organoids. The conjugates, previously designed and produced in our laboratory, had already shown an enhanced antitumor effect in "in vivo" models of carcinoma and in glioblastoma cell lines [266, 267]. Moreover, EGFR-specific ITs were found to be effective in rhabdomyosarcoma cells [268, 269, 270]. In this study, IC_{50} values, related to viability assays, clearly indicated that the conjugation of RIP to carrier enhanced the cytotoxic effect of the conjugate compared to RIP alone in RD18 and U2OS adherent cells. In fact, in RD18 adherent cells, Tf-SO6, αEGFR1-Ocy and αHer2-Ocy had IC_{50} values ranging from 0.3 to 8.8 nM, while corresponding unconjugated RIP from 24.2 to 58.9 nM. A similar cytotoxic activity was observed in U2OS adherent cells, where the conjugates showed IC_{50} values ranging from 0.1 to 3.7 nM, while corresponding RIP alone from 13.1 to 73.9 nM. Interestingly, our results showed that, IT-cytotoxic profile was

maintained with similar toxic ranges also in the more heterogeneous and complex 3D models, single spheroids and organoids. Our results agreed with toxicity data relative to other immunoconjugates reported in literature (ADC, PE-IT). In 2014, it was shown a similar efficacy of a bispecific PE-immunotoxins in carcinoma adherent cells and spheroids [271]. Moreover, another study demonstrated the similar cytotoxic effect of the ADC trastuzumab emtansine (T-DM1) in MCF-7 adherent cells and spheroids [272]. The same ADC was also found to be highly cytotoxic on lung patient-derived tumor organoids [273]. However, some studies reported the decrease of conjugate activity in tridimensional model compared to adherent cells, meaning that, basing on the internalization efficacy of IT as well as the type of target and tumor, there is not a homogeneous response in 3D models [274, 275,]. Therefore, considering that ITs not always maintain their cytotoxicity in 3D models, which possess a more complex configuration than adherent cells, our study revealed promising results. Moreover, we notice that, at the maximum IT tested dose, a residual viability of about 10-20% was present in single spheroids and organoids but not in adherent cells. Partially, this fact could be explained considering the difficulties encountered by drugs to penetrate 3D models, thus decreasing its efficacy [276]. In addition, it is widely reported that the presence of CSCs correlates with greater resistance to anticancer treatments than other tumor populations [277, 278]. It is important underlying that RD18 and U2OS adherent cells, spheroids and organoids, as cell lines and cell-derived 3D models, did not contain elements (effector cells of the immune system and complement factors) responsible for mAb-induced ADCC or CDC, the two main cytotoxic pathways that can be activated after mAbs-antigen binding [279]. However, some antibodies can directly kill the target cells by triggering the apoptotic pathway [280]. Interestingly, cell viability assays showed that treatment with the unconjugated ligand or mAbs (Tf, αEGFR1 and αHer2) had never induced, even at the highest concentration tested (100 nM), a decrease of viability in target adherent cells, single spheroids and organoids (IC_{50} > 100 nM). This mean that, at least at the dosed used, the treatment with carrier is not sufficient to trigger cell death, while the conjugation of carrier to RIP is fundamental to enhance its cytotoxicity.

Due to the possibility of acting on different molecular targets, inducing cell death through multiple pathways, RIPs have a high antitumor potential, because they can overcome the ability of tumor cells to acquire a resistant phenotype to RIP-induced cell death mechanisms [281, 282, 283]. Apoptosis represents the most studied RIP-induced cell death mechanism. It has been already reported that RIP-containing IT can induce apoptosis in lymphoma cells, bladder cancer and rhabdomyosarcoma cells [284, 285, 286, 287]. Considering this, we decided to

investigate whether the selected ITs could induce apoptosis in our 2D and 3D cell models. Results of caspase 3/7 assays demonstrated that Tf-SO6, αEGFR1-Ocy and αHer2-Ocy were able to induce effector caspase activation in RD18 and U2OS adherent cells, single spheroids and organoids, with similar range but different timing. Indeed, we observed a significantly strong caspase 3/7 activation induced by ITs (both compared to control and to unconjugated RIP) at 16 h in adherent cell lines, at 24 h in single spheroids and at 48 h or 72 h in organoids. Moreover, we notice that the activation of caspase 3/7 goes hand in hand with the decrease of viability. The delayed apoptosis activation and decrease of viability observed in single spheroids and organoids could be caused by the difficulties encountered by payloads to penetrate spheroid mass and matrigel-based matrix, respectively. A promising result was obtained in the patient-derived alveolar rhabdomyosarcoma organoids, where all the ITs showed a good cytotoxic effect compared to corresponding RIP or carrier alone.

In conclusion, this work is the first attempt to assess RIP-containing IT efficacy on sarcoma derived single spheroids and organoids. Basing on our results, we can assess that EGFR1, Her2 and Tf-R are highly expressed in all sarcoma models used and are possible targets for immunotherapy. We can also state that the Tf-SO6, αEGFR1-Ocy and αHer2-Ocy can exert a highly significant cytotoxic effect in 2D (adherent cells) and 3D (single spheroids and organoids) sarcoma models, with similar toxic range values. Considering that tridimensional models recapitulate also staminal features of tumor, we could suppose that ITs are cytotoxic for both sarcoma cancer cells and sarcoma cancer stem cells. Moreover, apoptosis is widely involved in IT-induced cell death and it is activated after conjugate treatments in all sarcoma models with different timing.

Finally, our work allowed us to conclude that RIP-containing ITs can be considered agents of potential interest, and therefore deserving of furthermore in-depth study, for the development of new therapies for treatment of sarcomas.

References

1 Stirpe F. On the action of ribosome-inactivating proteins: are plant ribosomes species-specific? *Biochem J*. 1982;202(1):279-280. doi:10.1042/bj2020279.

2 Endo Y, Mitsui K, Motizuki M, Tsurugi K. The mechanism of action of ricin and related toxic lectins on eukaryotic ribosomes. The site and the characteristics of the modification in 28 S ribosomal RNA caused by the toxins. *J Biol Chem*. 1987;262(12):5908-5912.

3 Barbieri L, Gorini P, Valbonesi P, Castiglioni P, Stirpe F. Unexpected activity of saporins. *Nature*. 1994;372(6507):624. doi:10.1038/372624a0.

4 Barbieri L, Brigotti M, Perocco P, et al. Ribosome-inactivating proteins depurinate poly(ADP-ribosyl)ated poly(ADP-ribose) polymerase and have transforming activity for 3T3 fibroblasts. *FEBS Lett*. 2003;538(1-3):178-182. doi:10.1016/s0014-5793(03)00176-5.

5 Barbieri L, Valbonesi P, Bonora E, Gorini P, Bolognesi A, Stirpe F. Polynucleotide:adenosine glycosidase activity of ribosome-inactivating proteins: effect on DNA, RNA and poly(A). *Nucleic Acids Res*. 1997;25(3):518-522. doi:10.1093/nar/25.3.518.

6 Stirpe F. Ribosome-inactivating proteins: from toxins to useful proteins. Toxicon. 2013;67:12-16. doi:10.1016/j.toxicon.2013.02.005.

7 Nielsen K, Boston RS. RIBOSOME-INACTIVATING PROTEINS: A Plant Perspective. *Annu Rev Plant Physiol Plant Mol Biol*. 2001;52:785-816. doi:10.1146/annurev.arplant.52.1.785.

8 Polito L, Bortolotti M, Mercatelli D, et al. Protein synthesis inhibition activity by strawberry tissue protein extracts during plant life cycle and under biotic and abiotic stresses. *Int J Mol Sci*. 2013;14(8):15532-15545. Published 2013 Jul 25. doi:10.3390/ijms140815532.

9 Chan YS, Ng TB. Shiga toxins: from structure and mechanism to applications. *Appl Microbiol Biotechnol*. 2016;100(4):1597-1610. doi:10.1007/s00253-015-7236-3.

10 Walsh MJ, Dodd JE, Hautbergue GM. Ribosome-inactivating proteins: potent poisons and molecular tools. *Virulence*. 2013;4(8):774-784. doi:10.4161/viru.26399.

11 Zhou R, Liu ZK, Zhang YN, Wong JH, Ng TB, Liu F. Research Progress of Bioactive Proteins from the Edible and Medicinal Mushrooms. *Curr Protein Pept Sci*. 2019;20(3):196-219. doi:10.2174/1389203719666180613090710.

12 Xu X, Yan H, Chen J, Zhang X. Bioactive proteins from mushrooms. *Biotechnol Adv*. 2011;29(6):667-674. doi:10.1016/j.biotechadv.2011.05.003.

13 Battelli MG. Cytotoxicity and toxicity to animals and humans of ribosome-inactivating proteins. *Mini Rev Med Chem*. 2004;4(5):513-521. doi:10.2174/1389557043403819.

14 Rust A, Partridge LJ, Davletov B, Hautbergue GM. The Use of Plant-Derived Ribosome Inactivating Proteins in Immunotoxin Development: Past, Present and Future Generations. Toxins (Basel). 2017;9(11):344. Published 2017 Oct 27. doi:10.3390/toxins9110344

15 Stirpe F, Barbieri L, Battelli MG, Soria M, Lappi DA. Ribosome-inactivating proteins from plants: present status and future prospects. *Biotechnology (N Y)*. 1992;10(4):405-412. doi:10.1038/nbt0492-405.

16 Polito L, Djemil A, Bortolotti M. Plant Toxin-Based Immunotoxins for Cancer Therapy: A Short Overview. Biomedicines. 2016;4(2):12. Published 2016 Jun 1. doi:10.3390/biomedicines4020012.

17 Stirpe F. Ribosome-inactivating proteins: from toxins to useful proteins. *Toxicon*. 2013;67:12-16. doi:10.1016/j.toxicon.2013.02.005.

18 Ng TB, Chan WY, Yeung HW. Proteins with abortifacient, ribosome inactivating, immunomodulatory, antitumor and anti-AIDS activities from Cucurbitaceae plants. *Gen Pharmacol*. 1992;23(4):579-590. doi:10.1016/0306-3623(92)90131-3.

19 Kaur I, Gupta RC, Puri M. Ribosome inactivating proteins from plants inhibiting viruses. *Virol Sin*. 2011;26(6):357-365. doi:10.1007/s12250-011-3223-8.

20 Parikh BA, Tumer NE. Antiviral activity of ribosome inactivating proteins in medicine. *Mini Rev Med Chem*. 2004;4(5):523-543. doi:10.2174/1389557043403800.

21 Zhu F, Zhou YK, Ji ZL, Chen XR. The Plant Ribosome-Inactivating Proteins Play Important Roles in Defense against Pathogens and Insect Pest Attacks. *Front Plant Sci*. 2018;9:146. Published 2018 Feb 9. doi:10.3389/fpls.2018.00146.

22 Barbieri L, Battelli MG, Stirpe F. Ribosome-inactivating proteins from plants. Biochim Biophys Acta. 1993;1154(3-4):237-282. doi:10.1016/0304-4157(93)90002-6.

23 Walsh MJ, Dodd JE, Hautbergue GM. Ribosome-inactivating proteins: potent poisons and molecular tools. *Virulence*. 2013;4(8):774-784. doi:10.4161/viru.26399.

24 Schrot J, Weng A, Melzig MF. Ribosome-inactivating and related proteins. *Toxins (Basel)*. 2015;7(5):1556-1615. Published 2015 May 8. doi:10.3390/toxins7051556.

25 Shi WW, Mak AN, Wong KB, Shaw PC. Structures and Ribosomal Interaction of Ribosome-Inactivating Proteins. Molecules. 2016;21(11):1588. Published 2016 Nov 21. doi:10.3390/molecules21111588.

26 Peumans WJ, Van Damme EJ, Barre A, Rougé P. Classification of plant lectins in families of structurally and evolutionary related proteins. *Adv Exp Med Biol*. 2001;491:27-54. doi:10.1007/978-1-4615-1267-7_3.

27 Hey TD, Hartley M, Walsh TA. Maize ribosome-inactivating protein (b-32). Homologs in related species, effects on maize ribosomes, and modulation of activity by pro-peptide deletions. *Plant Physiol*. 1995;107(4):1323-1332. doi:10.1104/pp.107.4.1323.

28 Chaudhry B, Müller-Uri F, Cameron-Mills V, et al. The barley 60 kDa jasmonate-induced protein (JIP60) is a novel ribosome-inactivating protein. *Plant J*. 1994;6(6):815-824. doi:10.1046/j.1365-313x.1994.6060815.x.

29 Schrot J, Weng A, Melzig MF. Ribosome-inactivating and related proteins. *Toxins (Basel)*. 2015;7(5):1556-1615. Published 2015 May 8. doi:10.3390/toxins7051556.

30 Nielsen K, Boston RS. RIBOSOME-INACTIVATING PROTEINS: A Plant Perspective. *Annu Rev Plant Physiol Plant Mol Biol*. 2001;52:785-816. doi:10.1146/annurev.arplant.52.1.785.

31 Hartley MR, Lord JM. Cytotoxic ribosome-inactivating lectins from plants. *Biochim Biophys Acta*. 2004;1701(1-2):1-14. doi:10.1016/j.bbapap.2004.06.004.

32 Carzaniga R, Sinclair L, Fordham-Skelton AP, Harris N, Croy RRD. Cellular and subcellular distribution of saporins, type-1 ribosome-inactivating proteins in soapwort (Saponaria officinalis L.). Planta. 1994 ;194:461- 470.

33 Barbieri L, Stoppa C, Bolognesi A. Large scale chromatographic purification of ribosome-inactivating proteins. J. Chromat. A. 1987; 408: 235-243.

[34] Olsnes S, Pihl A. Different biological properties of the two constituent peptide chains of ricin, a toxic protein inhibiting protein synthesis. Biochemistry. 1973;12(16):3121-3126. doi:10.1021/bi00740a028.

[35] Van Damme EJM, Hao Q, Chen Y, Barre A, Vandenbussche F, Desmyter S, Rougé P, Peumans WJ. Ribosome-inactivating proteins: a family of plant proteins that do more than inactivate ribosomes. Crit Rev Plant Sci. 2001; 20:395-465.

[36] Lord JM, Roberts LM, Robertus JD. Ricin: structure, mode of action, and some current applications. *FASEB J*. 1994;8(2):201-208.

[37] Frigerio L, Jolliffe NA, Di Cola A, et al. The internal propeptide of the ricin precursor carries a sequence-specific determinant for vacuolar sorting. *Plant Physiol*. 2001;126(1):167-175. doi:10.1104/pp.126.1.167.

[38] Lamb FI, Roberts LM, Lord JM. Nucleotide sequence of cloned cDNA coding for preproricin. Eur J Biochem. 1985; 148(2):265-70.

[39] Puri M, Kaur I, Perugini MA, Gupta RC. Ribosome-inactivating proteins: current status and biomedical applications. Drug Discov Today. 2012;17(13-14):774-783. doi:10.1016/j.drudis.2012.03.007.

[40] Ferreras JM, Citores L, Iglesias R, Jiménez P, Girbés T. Use of ribosome-inactivating proteins from Sambucus for the construction of immunotoxins and conjugates for cancer therapy. *Toxins (Basel)*. 2011;3(5):420-441. doi:10.3390/toxins3050420.

[41] Citores L, Muñoz R, Rojo MA, Jiménez P, Ferreras JM, Girbés T. Evidence for distinct cellular internalization pathways of ricin and nigrin b. Cell Mol Biol (Noisy-le-grand). 2003;49 Online Pub:OL461-OL465.

[42] De Zaeytijd J, Van Damme EJ. Extensive Evolution of Cereal Ribosome-Inactivating Proteins Translates into Unique Structural Features, Activation Mechanisms, and Physiological Roles. Toxins (Basel). 2017;9(4):123. Published 2017 Mar 29. doi:10.3390/toxins9040123.

[43] Walsh TA, Morgan AE, Hey TD. Characterization and molecular cloning of a proenzyme form of a ribosome-inactivating protein from maize. Novel mechanism of proenzyme activation by proteolytic removal of a 2.8-kilodalton internal peptide segment. J Biol Chem. 1991;266(34):23422-23427.

44 Van Damme EJM, Hao Q, Chen Y, Barre A, Vandenbussche F, Desmyter S, Rougé P, Peumans WJ. Ribosome-inactivating proteins: a family of plant proteins that do

more than inactivate ribosomes. Crit Rev Palnt Sci. 2001; 20:395-465.

[45] Lord JM, Hartley MR, Roberts LM. Ribosome inactivating proteins of plants. Semin Cell Biol. 1991;2(1):15-22.

[46] Skilleter DN, Paine AJ, Stirpe F. A comparison of the accumulation of ricin by hepatic parenchymal and non-parenchymal cells and its inhibition of protein synthesis. Biochim Biophys Acta. 1981;677(3-4):495-500. doi:10.1016/0304-4165(81)90264-6.

[47] Simmons BM, Stahl PD, Russell JH. Mannose receptor-mediated uptake of ricin toxin and ricin A chain by macrophages. Multiple intracellular pathways for a chain translocation. J Biol Chem. 1986;261(17):7912-7920.

[48] Stirpe F. Ribosome-inactivating proteins. *Toxicon*. 2004;44(4):371-383. doi:10.1016/j.toxicon.2004.05.004.

[49] Roberts LM, Lord JM. Ribosome-inactivating proteins: entry into mammalian cells and intracellular routing. Mini Rev Med Chem. 2004;4(5):505-512. doi:10.2174/1389557043403846.

[50] Sandvig K, van Deurs B. Endocytosis, intracellular transport, and cytotoxic action of Shiga toxin and ricin. *Physiol Rev*. 1996;76(4):949-966. doi:10.1152/physrev.1996.76.4.949.

[51] Sandvig K, van Deurs B. Transport of protein toxins into cells: pathways used by ricin, cholera toxin and Shiga toxin. FEBS Lett. 2002;529(1):49-53. doi:10.1016/s0014-5793(02)03182-4.

[52] Mayerhofer PU, Cook JP, Wahlman J, Pinheiro TT, Moore KA, Lord JM, Johnson AE, Roberts LM. Ricin A chain insertion into endoplasmic reticulum membranes is triggered by a temperature increase to 37ºC. J. Biol. Chem. 2009; 284, 10232–10242.

[53] Sandvig K, van Deurs B. Delivery into cells: lessons learned from plant and bacterial toxins. *Gene Ther*. 2005;12(11):865-872. doi:10.1038/sj.gt.3302525.

[54] Johannes L, Popoff V. Tracing the retrograde route in protein trafficking. *Cell*. 2008;135(7):1175-1187. doi:10.1016/j.cell.2008.12.009.

[55] Bolognesi A, Polito L, Scicchitano V, et al. Endocytosis and intracellular localisation of type 1 ribosome-inactivating protein saporin-s6. J Biol Regul Homeost Agents. 2012;26(1):97-109.

[56] Cavallaro U, Soria MR. Targeting plant toxins to the urokinase and alpha 2-macroglobulin receptors. *Semin Cancer Biol*. 1995;6(5):269-278. doi:10.1006/scbi.1995.0035.

[57] Madan S, Ghosh PC. Enhancing potency of liposomal monensin on ricin cytotoxicity in mouse macrophage tumor cells. *Biochem Int*. 1992;28(2):287-295.

[58] Vago R, Marsden CJ, Lord JM, et al. Saporin and ricin A chain follow different intracellular routes to enter the cytosol of intoxicated cells. *FEBS J*. 2005;272(19):4983-4995. doi:10.1111/j.1742-4658.2005.04908.x.

[59] Bolognesi A, Polito L, Scicchitano V, et al. Endocytosis and intracellular localisation of type 1 ribosome-inactivating protein saporin-s6. *J Biol Regul Homeost Agents*. 2012;26(1):97-109.

[60] Parikh BA, Baykal U, Di R, Tumer NE. Evidence for retro-translocation of pokeweed antiviral protein from endoplasmic reticulum into cytosol and separation of its activity on ribosomes from its activity on capped RNA. *Biochemistry*. 2005;44(7):2478-2490. doi:10.1021/bi048188c.

[61] Endo Y, Mitsui K, Motizuki M, Tsurugi K. The mechanism of action of ricin and related toxic lectins on eukaryotic ribosomes. The site and the characteristics of the modification in 28 S ribosomal RNA caused by the toxins. *J Biol Chem*. 1987;262(12):5908-5912.

[62] Girbés T, Ferreras JM, Arias FJ, Stirpe F. Description, distribution, activity and phylogenetic relationship of ribosome-inactivating proteins in plants, fungi and bacteria. *Mini Rev Med Chem*. 2004;4(5):461-476. doi:10.2174/1389557043403891.

[63] Stirpe F. Ribosome-inactivating proteins: from toxins to useful proteins. Toxicon. 2013;67:12-16. doi:10.1016/j.toxicon.2013.02.005.

[64] Endo Y, Mitsui K, Motizuki M, Tsurugi K. The mechanism of action of ricin and related toxic lectins on eukaryotic ribosomes. The site and the characteristics of the modification in 28 S ribosomal RNA caused by the toxins. *J Biol Chem*. 1987;262(12):5908-5912.

[65] Stirpe F, Battelli MG. Ribosome-inactivating proteins: progress and problems. *Cell Mol Life Sci*. 2006;63(16):1850-1866. doi:10.1007/s00018-006-6078-7.

[66] Tumer NE, Li XP. Interaction of ricin and Shiga toxins with ribosomes. Curr Top

Microbiol Immunol. 2012;357:1-18. doi: 10.1007/82_2011_174.

[67] Barbieri L, Battelli MG, Stirpe F. Ribosome-inactivating proteins from plants. *Biochim Biophys Acta*. 1993;1154(3-4):237-282. doi:10.1016/0304-4157(93)90002-6.

[68] Barbieri L, Gorini P, Valbonesi P, Castiglioni P, Stirpe F. Unexpected activity of saporins. *Nature*. 1994;372(6507):624. doi:10.1038/372624a0.

[69] Barbieri L, Valbonesi P, Bonora E, Gorini P, Bolognesi A, Stirpe F. Polynucleotide:adenosine glycosidase activity of ribosome-inactivating proteins: effect on DNA, RNA and poly(A). *Nucleic Acids Res*. 1997;25(3):518-522. doi:10.1093/nar/25.3.518.

[70] Barbieri L, Valbonesi P, Bonora E, Gorini P, Bolognesi A, Stirpe F. Polynucleotide:adenosine glycosidase activity of ribosome-inactivating proteins: effect on DNA, RNA and poly(A). *Nucleic Acids Res*. 1997;25(3):518-522. doi:10.1093/nar/25.3.518.

[71] Barbieri L, Brigotti M, Perocco P, et al. Ribosome-inactivating proteins depurinate poly(ADP-ribosyl)ated poly(ADP-ribose) polymerase and have transforming activity for 3T3 fibroblasts. *FEBS Lett*. 2003;538(1-3):178-182. doi:10.1016/s0014-5793(03)00176-5.

[72] Endo Y, Mitsui K, Motizuki M, Tsurugi K. The mechanism of action of ricin and related toxic lectins on eukaryotic ribosomes. The site and the characteristics of the modification in 28 S ribosomal RNA caused by the toxins. *J Biol Chem*. 1987;262(12):5908-5912.

[73] Rajamohan F, Kurinov IV, Venkatachalam TK, Uckun FM. Deguanylation of human immunodeficiency virus (HIV-1) RNA by recombinant pokeweed antiviral protein. *Biochem Biophys Res Commun*. 1999;263(2):419-424. doi:10.1006/bbrc.1999.1335.

[74] Olsnes S, Refsnes K, Pihl A. Mechanism of action of the toxic lectins abrin and ricin. Nature. 1974;249(458):627-631. doi:10.1038/249627a0.

[75] Griffiths GD, Leek MD, Gee DJ. The toxic plant proteins ricin and abrin induce apoptotic changes in mammalian lymphoid tissues and intestine. *J Pathol*. 1987;151(3):221-229. doi:10.1002/path.1711510310.

[76] Bolognesi A, Tazzari PL, Olivieri F, Polito L, Falini B, Stirpe F. Induction of apoptosis by ribosome-inactivating proteins and related immunotoxins. *Int J Cancer*. 1996;68(3):349-355. doi:10.1002/(SICI)1097-0215(19961104)68:3<349::AID-IJC13>3.0.CO;2-3.

[77] Kim WH, Park WB, Gao B, Jung MH. Critical role of reactive oxygen species and mitochondrial membrane potential in Korean mistletoe lectin-induced apoptosis in human hepatocarcinoma cells. *Mol Pharmacol*. 2004;66(6):1383-1396. doi:10.1124/mol.104.001347.

[78] Narayanan S, Surendranath K, Bora N, Surolia A, Karande AA. Ribosome inactivating proteins and apoptosis. *FEBS Lett*. 2005;579(6):1324-1331. doi:10.1016/j.febslet.2005.01.038

[79] Sikriwal D, Ghosh P, Batra JK. Ribosome inactivating protein saporin induces apoptosis through mitochondrial cascade, independent of translation inhibition. *Int J Biochem Cell Biol*. 2008;40(12):2880-2888. doi:10.1016/j.biocel.2008.06.004.

[80] Das MK, Sharma RS, Mishra V. Induction of apoptosis by ribosome inactivating proteins: importance of N-glycosidase activity. *Appl Biochem Biotechnol*. 2012;166(6):1552-1561. doi:10.1007/s12010-012-9550-x.

[81] Mercatelli D, Bortolotti M, Andresen V, et al. Early Response to the Plant Toxin Stenodactylin in Acute Myeloid Leukemia Cells Involves Inflammatory and Apoptotic Signaling. Front Pharmacol. 2020;11:630. Published 2020 May 8. doi:10.3389/fphar.2020.00630.

[82] Polito L, Bortolotti M, Pedrazzi M, Mercatelli D, Battelli MG, Bolognesi A. Apoptosis and necroptosis induced by stenodactylin in neuroblastoma cells can be completely prevented through caspase inhibition plus catalase or necrostatin-1. Phytomedicine. 2016;23(1):32-41. doi:10.1016/j.phymed.2015.11.006.

83 Iordanov MS, Pribnow D, Magun JL, et al. Ribotoxic stress response: activation of the stress-activated protein kinase JNK1 by inhibitors of the peptidyl transferase reaction and by sequence-specific RNA damage to the alpha-sarcin/ricin loop in the 28S rRNA. *Mol Cell Biol*. 1997;17(6):3373-3381. doi:10.1128/MCB.17.6.3373.

[84] Jandhyala DM, Thorpe CM, Magun B. Ricin and Shiga toxins: effects on host cell signal transduction. *Curr Top Microbiol Immunol*. 2012;357:41-65. doi:10.1007/82_2011_181.

[85] Jetzt AE, Cheng JS, Tumer NE, Cohick WS. Ricin A-chain requires c-Jun N-terminal kinase to induce apoptosis in nontransformed epithelial cells. *Int J Biochem Cell Biol*. 2009;41(12):2503-2510. doi:10.1016/j.biocel.2009.08.007.

[86] Higuchi S, Tamura T, Oda T. Cross-talk between the pathways leading to the induction of apoptosis and the secretion of tumor necrosis factor-alpha in ricin-treated RAW 264.7 cells. *J Biochem*. 2003;134(6):927-933. doi:10.1093/jb/mvg224.

[87] Tabas I, Ron D. Integrating the mechanisms of apoptosis induced by endoplasmic reticulum stress. Nat Cell Biol. 2011;13(3):184-190. doi:10.1038/ncb0311-184.

[88] Szegezdi E, Logue SE, Gorman AM, Samali A. Mediators of endoplasmic reticulum stress-induced apoptosis. EMBO Rep. 2006;7(9):880-885. doi:10.1038/sj.embor.7400779.

[89] Shi Y, Vattem KM, Sood R, et al. Identification and characterization of pancreatic eukaryotic initiation factor 2 alpha-subunit kinase, PEK, involved in translational control. Mol Cell Biol. 1998;18(12):7499-7509. doi:10.1128/MCB.18.12.7499.

[90] Yadav RK, Chae SW, Kim HR, Chae HJ. Endoplasmic reticulum stress and cancer. *J Cancer Prev*. 2014;19(2):75-88. doi:10.15430/JCP.2014.19.2.75.

[91] Horrix C, Raviv Z, Flescher E, Voss C, Berger MR. Plant ribosome-inactivating proteins type II induce the unfolded protein response in human cancer cells. *Cell Mol Life Sci*. 2011;68(7):1269-1281. doi:10.1007/s00018-010-0524-2.

[92] Zhang C, Gong Y, Ma H, An C, Chen D, Chen ZL. Reactive oxygen species involved in trichosanthin-induced apoptosis of human choriocarcinoma cells [published correction appears in Biochem J 2001 Sep 15;358(Pt 3):792]. *Biochem J*. 2001;355(Pt 3):653-661. doi:10.1042/bj3550653.

[93] Kim MS, Lee J, Lee KM, et al. Involvement of hydrogen peroxide in mistletoe lectin-II-induced apoptosis of myeloleukemic U937 cells. *Life Sci*. 2003;73(10):1231-1243. doi:10.1016/s0024-3205(03)00418-1.

94 Bhaskar AS, Gupta N, Rao PV. Transcriptomic profile of host response in mouse brain after exposure to plant toxin abrin. *Toxicology*. 2012;299(1):33-43. doi:10.1016/j.tox.2012.05.005.

95 Shih SF, Wu YH, Hung CH, Yang HY, Lin JY. Abrin triggers cell death by inactivating a thiol-specific antioxidant protein. *J Biol Chem*. 2001;276(24):21870-21877. doi:10.1074/jbc.M100571200.

96 Parikh BA, Tumer NE. Antiviral activity of ribosome inactivating proteins in medicine.

Mini Rev Med Chem. 2004 Jun;4(5):523-43.

97 Parikh BA, Tumer NE. Antiviral activity of ribosome inactivating proteins in medicine.

Mini Rev Med Chem. 2004 Jun;4(5):523-43.

98 Fernández-Puentes C, Carrasco L. Viral infection permeabilizes mammalian cells to protein toxins. *Cell*. 1980;20(3):769-775. doi:10.1016/0092-8674(80)90323-2.

99 Stirpe F, Battelli MG. Ribosome-inactivating proteins: progress and problems. Cell. Mol.

Life Sci. 2006; 63: 1850–1866.

100 Uckun FM, Rajamohan F, Pendergrass S, Ozer Z, Waurzyniak B, Mao C. Structure-based design and engineering of a nontoxic recombinant pokeweed antiviral protein with potent anti-human immunodeficiency virus activity. *Antimicrob Agents Chemother*. 2003;47(3):1052-1061. doi:10.1128/AAC.47.3.1052-1061.2003.

101 Barnett BB, Smee DF, Malek SM, Sidwell RW. Selective cytotoxicity of ricin A chain immunotoxins towards murine cytomegalovirus-infected cells. *Antimicrob Agents Chemother*. 1996;40(2):470-472. doi:10.1128/AAC.40.2.470.

102 Barnett BB, Smee DF, Malek SM, Sidwell RW. Selective cytotoxicity towards cytomegalovirus-infected cells by immunotoxins consisting of gelonin linked to anti-cytomegalovirus antibody. Antiviral Res. 1995;28(1):93-100. doi:10.1016/0166-3542(95)00034-j.

103 Kaur I, Gupta RC, Puri M. Ribosome inactivating proteins from plants inhibiting viruses. *Virol Sin*. 2011;26(6):357-365. doi:10.1007/s12250-011-3223-8.

104 Frankel AE, Kreitman RJ, Sausville EA. Targeted toxins. Clin Cancer Res. 2000;6(2):326-334.

105 Fracasso G, Stirpe F, Colombatti M. Ribosome-Inactivating Protein-Containing Conjugates for Therapeutic Use. In: Lord J.M., Hartley R.M., editors. Toxic Plant Proteins, Plant Cell Monographs. Springer-Verlag; Heidelberg, Berlin, German: 2010. pp. 225–263.

106 Barbieri L, Brigotti M, Perocco P, et al. Ribosome-inactivating proteins depurinate poly(ADP-ribosyl)ated poly(ADP-ribose) polymerase and have transforming activity for 3T3 fibroblasts. FEBS Lett. 2003;538(1-3):178-182. doi:10.1016/s0014-5793(03)00176-5.

107 Polito L, Bortolotti M, Mercatelli D, Battelli MG, Bolognesi A. Saporin-S6: a useful tool in cancer therapy. Toxins (Basel). 2013;5(10):1698-1722. Published 2013 Oct 7. doi:10.3390/toxins5101698.

108 Madhumathi J, Verma RS. Therapeutic targets and recent advances in protein immunotoxins. Curr Opin Microbiol. 2012; 15(3):300-9.

[109] Polito L, Djemil A, Bortolotti M. Plant Toxin-Based Immunotoxins for Cancer Therapy: A Short Overview. *Biomedicines*. 2016;4(2):12. Published 2016 Jun 1. doi:10.3390/biomedicines4020012.

[110] Bolognesi A, Polito L. Immunotoxins and other conjugates: pre-clinical studies. *Mini Rev Med Chem*. 2004;4(5):563-583. doi:10.2174/1389557043403864.

[111] Fracasso G, Bellisola G, Castelletti D, Tridente G, Colombatti M. Immunotoxins and other conjugates: preparation and general characteristics. Mini Rev Med Chem. 2004;4(5):545-562. doi:10.2174/1389557043403909.

[112] Polito L, Bortolotti M, Mercatelli D, Battelli MG, Bolognesi A. Saporin-S6: a useful tool in cancer therapy. Toxins (Basel). 2013;5(10):1698-1722. Published 2013 Oct 7. doi:10.3390/toxins5101698.

[113] Maleki LA, Baradaran B, Majidi J, Mohammadian M, Shahneh FZ. Future prospects of monoclonal antibodies as magic bullets in immunotherapy. Hum Antibodies. 2013;22(1-2):9-13. doi:10.3233/HAB-130266.

[114] Fracasso G, Stirpe F, Colombatti M. Ribosome-Inactivating Protein-Containing Conjugates for Therapeutic Use. In: Lord J.M., Hartley R.M., editors. Toxic Plant Proteins, Plant Cell Monographs. Springer-Verlag; Heidelberg, Berlin, German: 2010. pp. 225–263.

[115] Polito L, Bortolotti M, Pedrazzi M, Bolognesi A. Immunotoxins and other conjugates

containing saporin-s6 for cancer therapy. Toxins (Basel). 2011 Jun;3(6):697-720.

[116] Palanca-Wessels MC, Press OW. Advances in the treatment of hematologic malignancies using immunoconjugates. *Blood*. 2014;123(15):2293-2301. doi:10.1182/blood-2013-10 492223.

[117] Lambert JM, Blättler WA, McIntyre GD, Goldmacher VS, Scott CF Jr. Immunotoxins containing single-chain ribosome-inactivating proteins. Cancer Treat Res. 1988;37:175-209. doi:10.1007/978-1-4613-1083-9_12.

[118] Siena S, Lappi DA, Bregni M, et al. Synthesis and characterization of an antihuman T-lymphocyte saporin immunotoxin (OKT1-SAP) with in vivo stability into nonhuman primates. *Blood*. 1988;72(2):756-765.

[119] Bolognesi A, Tazzari PL, Tassi C, Gromo G, Gobbi M, Stirpe F. A comparison of anti-lymphocyte immunotoxins containing different ribosome-inactivating proteins and antibodies. *Clin Exp Immunol*. 1992;89(3):341-346. doi:10.1111/j.1365-2249.1992.tb06959.x.

[120] Polito L, Bortolotti M, Pedrazzi M, Bolognesi A. Immunotoxins and other conjugates containing saporin-s6 for cancer therapy. *Toxins (Basel)*. 2011;3(6):697-720. doi:10.3390/toxins3060697.

[121] Glennie MJ, McBride HM, Stirpe F, Thorpe PE, Worth AT, Stevenson GT. Emergence of immunoglobulin variants following treatment of a B cell leukemia with an immunotoxin composed of antiidiotypic antibody and saporin. *J Exp Med*. 1987;166(1):43-62. doi:10.1084/jem.166.1.43.

122 Stirpe F. Ribosome-inactivating proteins. Toxicon. 2004;44(4):371-383. doi:10.1016/j.toxicon.2004.05.004.

[123] Fracasso G, Stirpe F, Colombatti M. Ribosome-Inactivating Protein- containing conjugates

for therapeutic use. In: Lord J.M., Hartley R.M., editors. Toxic Plant Proteins, Plant Cell

Monographs. Springer-Verlag; Heidelberg, Berlin, German: 2010; pp. 225–263.

[124] Polito L, Bortolotti M, Pedrazzi M, Bolognesi A. Immunotoxins and other conjugates containing saporin-s6 for cancer therapy. *Toxins (Basel)*. 2011;3(6):697-720. doi:10.3390/toxins3060697.

[125] Stirpe F. Ribosome-inactivating proteins. *Toxicon*. 2004;44(4):371-383. doi:10.1016/j.toxicon.2004.05.004.

[126] Baluna R, Rizo J, Gordon BE, Ghetie V, Vitetta ES. Evidence for a structural motif in toxins and interleukin-2 that may be responsible for binding to endothelial cells and initiating vascular leak syndrome. Proc Natl Acad Sci U S A. 1999;96(7):3957-3962. doi:10.1073/pnas.96.7.3957.

[127] Pincus SH, Smallshaw JE, Song K, Berry J, Vitetta ES. Passive and active vaccination strategies to prevent ricin poisoning. *Toxins (Basel)*. 2011;3(9):1163-1184. doi:10.3390/toxins3091163.

[128] Baluna R, Coleman E, Jones C, Ghetie V, Vitetta ES. The effect of a monoclonal antibody coupled to ricin A chain-derived peptides on endothelial cells in vitro: insights into toxin-mediated vascular damage. *Exp Cell Res*. 2000;258(2):417-424. doi:10.1006/excr.2000.4954.

[129] Wang H, Song S, Kou G, et al. Treatment of hepatocellular carcinoma in a mouse xenograft model with an immunotoxin which is engineered to eliminate vascular leak syndrome. *Cancer Immunol Immunother*. 2007;56(11):1775-1783. doi:10.1007/s00262-007-0321-4.

[130] Weldon JE, Xiang L, Zhang J, et al. A recombinant immunotoxin against the tumor-associated antigen mesothelin reengineered for high activity, low off-target toxicity, and reduced antigenicity. *Mol Cancer Ther*. 2013;12(1):48-57. doi:10.1158/1535-7163.MCT-12-0336.

[131] Battelli MG, Buonamici L, Bolognesi A, Stirpe F. In vivo and in vitro uptake of an anti-CD30/saporin immunotoxin by rat liver parenchymal and nonparenchymal cells. *Hepatology*. 1994;20(4 Pt 1):940-947. doi:10.1002/hep.1840200424.

[132] Hoogenboom HR, Marks JD, Griffiths AD, Winter G. Building antibodies from their genes. *Immunol Rev*. 1992;130:41-68. doi:10.1111/j.1600-065x.1992.tb01520.x.

[133] Hoogenboom HR, Marks JD, Griffiths AD, Winter G. Building antibodies from their genes. *Immunol Rev*. 1992;130:41-68. doi:10.1111/j.1600-065x.1992.tb01520.x.

[134] Alewine C, Hassan R, Pastan I. Advances in anticancer immunotoxin therapy. *Oncologist*. 2015;20(2):176-185. doi:10.1634/theoncologist.2014-0358.

[135] Stirpe F. Ribosome-inactivating proteins. *Toxicon*. 2004;44(4):371-383. doi:10.1016/j.toxicon.2004.05.004.

[136] Pirker R. Immunotoxins against solid tumors. J Cancer Res Clin Oncol. 1988;114(4):385-393. doi:10.1007/BF02128183.

[137] Stirpe F. Ribosome-inactivating proteins. *Toxicon*. 2004;44(4):371-383. doi:10.1016/j.toxicon.2004.05.004.

[138] Gilabert-Oriol R, Weng A, Mallinckrodt Bv, Melzig MF, Fuchs H, Thakur M. Immunotoxins constructed with ribosome-inactivating proteins and their enhancers: a lethal cocktail with tumor specific efficacy. *Curr Pharm Des*. 2014;20(42):6584-6643. doi:10.2174/1381612820666140826153913.

[139] Weyergang A, Selbo PK, Berstad ME, Bostad M, Berg K. Photochemical internalization of tumor-targeted protein toxins. *Lasers Surg Med*. 2011;43(7):721-733. doi:10.1002/lsm.21084.

[140] Barta SK, Zou Y, Schindler J, et al. Synergy of sequential administration of a deglycosylated ricin A chain-containing combined anti-CD19 and anti-CD22 immunotoxin (Combotox) and cytarabine in a murine model of advanced acute lymphoblastic leukemia. Leuk Lymphoma. 2012;53(10):1999-2003. doi:10.3109/10428194.2012.679267.

[141] Shen GL, Li JL, Ghetie MA, et al. Evaluation of four CD22 antibodies as ricin A chain-containing immunotoxins for the in vivo therapy of human B-cell leukemias and lymphomas. Int J Cancer. 1988;42(5):792-797. doi:10.1002/ijc.2910420527.

[142] Phan GQ, Yang JC, Sherry RM, et al. Cancer regression and autoimmunity induced by cytotoxic T lymphocyte-associated antigen 4 blockade in patients with metastatic melanoma. Proc Natl Acad Sci U S A. 2003;100(14):8372-8377. doi:10.1073/pnas.1533209100.

[143] Solomon SR, Mielke S, Savani BN, et al. Selective depletion of alloreactive donor lymphocytes: a novel method to reduce the severity of graft-versus-host disease in older patients undergoing matched sibling donor stem cell transplantation. Blood. 2005;106(3):1123-1129. doi:10.1182/blood-2005-01-0393.

[144] Madhumathi J, Verma RS. Therapeutic targets and recent advances in protein immunotoxins. Curr Opin Microbiol. 2012;15(3):300-309. doi:10.1016/j.mib.2012.05.006.

[145] Strand V, Lipsky PE, Cannon GW, et al. Effects of administration of an anti-CD5 plus immunoconjugate in rheumatoid arthritis. Results of two phase II studies. The CD5 Plus Rheumatoid Arthritis Investigators Group. *Arthritis Rheum*. 1993;36(5):620-630. doi:10.1002/art.1780360508.

[146] Stafford FJ, Fleisher TA, Lee G, et al. A pilot study of anti-CD5 ricin A chain immunoconjugate in systemic lupus erythematosus. *J Rheumatol*. 1994;21(11):2068-2070.

[147] Skyler JS, Lorenz TJ, Schwartz S, et al. Effects of an anti-CD5 immunoconjugate (CD5-plus) in recent onset type I diabetes mellitus: a preliminary investigation. The CD5 Diabetes Project Team. *J Diabetes Complications*. 1993;7(4):224-232.

[148] Madhumathi J, Verma RS. Therapeutic targets and recent advances in protein immunotoxins. Curr Opin Microbiol. 2012;15(3):300-309. doi:10.1016/j.mib.2012.05.006.

[149] Rennie DP, McGregor AM, Wright J, Weetman AP, Hall R, Thorpe P. An immunotoxin of ricin A chain conjugated to thyroglobulin selectively suppresses the antithyroglobulin autoantibody response. *Lancet*.1983;2(8363):1338-1340.doi:10.1016/s0140-6736(83)91094-2

[150] Pincus SH. Therapeutic potential of anti-HIV immunotoxins. *Antiviral Res*. 1996;33(1):1-9. doi:10.1016/s0166-3542(96)00995-3.

[151] Hossann M, Li Z, Shi Y, et al. Novel immunotoxin: a fusion protein consisting of gelonin and an acetylcholine receptor fragment as a potential immunotherapeutic agent for the treatment of Myasthenia gravis. *Protein Expr Purif*. 2006;46(1):73-84. doi:10.1016/j.pep.2005.08.029.

[152] Polito L, Bortolotti M, Farini V, Pedrazzi M, Tazzari PL, Bolognesi A. ATG-saporin-S6 immunotoxin: a new potent and selective drug to eliminate activated lymphocytes and lymphoma cells. *Br J Haematol*. 2009;147(5):710-718. doi:10.1111/j.1365-2141.2009.07904.x.

153 Tazzari PL, Polito L, Bolognesi A, et al. Immunotoxins containing recombinant anti-CTLA-4 single-chain fragment variable antibodies and saporin: in vitro results and in vivo effects in an acute rejection model. *J Immunol*. 2001;167(8):4222-4229. doi:10.4049/jimmunol.167.8.4222.

154 Polito L, Calafato G, Bortolotti M, Chiarelli Olivari C, Maiello S, Bolognesi A. Antibody Conjugates for Sarcoma Therapy: How Far along Are We?. *Biomedicines*. 2021;9(8):978. Published 2021 Aug 8. doi:10.3390/biomedicines9080978.

155 Breslin S, O'Driscoll L. Three-dimensional cell culture: the missing link in drug discovery. *Drug Discov Today*. 2013;18(5-6):240-249. doi:10.1016/j.drudis.2012.10.003.

156 Wong CH, Siah KW, Lo AW. Estimation of clinical trial success rates and related parameters [published correction appears in Biostatistics. 2019 Apr 1;20(2):366]. *Biostatistics*. 2019;20(2):273-286. doi:10.1093/biostatistics/kxx069.

157 Imamura Y, Mukohara T, Shimono Y, et al. Comparison of 2D- and 3D-culture models as drug-testing platforms in breast cancer. *Oncol Rep*. 2015;33(4):1837-1843. doi:10.3892/or.2015.3767.

158 Duval K, Grover H, Han LH, et al. Modeling Physiological Events in 2D vs. 3D Cell Culture. *Physiology (Bethesda)*. 2017;32(4):266-277. doi:10.1152/physiol.00036.2016

159 Ryu NE, Lee SH, Park H. Spheroid Culture System Methods and Applications for Mesenchymal Stem Cells. *Cells*. 2019;8(12):1620. Published 2019 Dec 12. doi:10.3390/cells8121620.

160 Ivascu A, Kubbies M. Rapid generation of single-tumor spheroids for high-throughput cell function and toxicity analysis. J Biomol Screen. 2006;11(8):922-932. doi:10.1177/1087057106292763.

161 Zanoni M, Pignatta S, Arienti C, Bonafè M, Tesei A. Anticancer drug discovery using multicellular tumor spheroid models. *Expert Opin Drug Discov*. 2019;14(3):289-301. doi:10.1080/17460441.2019.1570129.

162 Sant S, Johnston PA. The production of 3D tumor spheroids for cancer drug discovery. *Drug Discov Today Technol*. 2017;23:27-36. doi:10.1016/j.ddtec.2017.03.002.

163 Costa EC, Moreira AF, de Melo-Diogo D, Gaspar VM, Carvalho MP, Correia IJ. 3D tumor spheroids: an overview on the tools and techniques used for their analysis. *Biotechnol Adv*. 2016;34(8):1427-1441. doi:10.1016/j.biotechadv.2016.11.002.

164 Warburg O, Wind F, Negelein E. THE METABOLISM OF TUMORS IN THE BODY. *J Gen Physiol*. 1927;8(6):519-530. doi:10.1085/jgp.8.6.519.

165 Jeanes A, Gottardi CJ, Yap AS. Cadherins and cancer: how does cadherin dysfunction promote tumor progression?. *Oncogene*. 2008;27(55):6920-6929. doi:10.1038/onc.2008.343.

166 Nederman T, Norling B, Glimelius B, Carlsson J, Brunk U. Demonstration of an extracellular matrix in multicellular tumor spheroids. *Cancer Res*. 1984;44(7):3090-3097.

167 S Franco S, Szczesna K, Iliou MS, et al. In vitro models of cancer stem cells and clinical applications. *BMC Cancer*. 2016;16(Suppl 2):738. Published 2016 Sep 30. doi:10.1186/s12885-016-2774-3.

168 Tirino V, Desiderio V, Paino F, et al. Cancer stem cells in solid tumors: an overview and new approaches for their isolation and characterization. *FASEB J*. 2013;27(1):13-24. doi:10.1096/fj.12-218222.

[169] Laranjo M, Carvalho MJ, Serambeque B, et al. Obtaining Cancer Stem Cell Spheres from Gynecological and Breast Cancer Tumors. *J Vis Exp*. 2020;(157):10.3791/60022. Published 2020 Mar 1. doi:10.3791/60022.

[170] Zhou Y, Xia L, Wang H, et al. Cancer stem cells in progression of colorectal cancer. *Oncotarget*. 2017;9(70):33403-33415. Published 2017 Dec 22. doi:10.18632/oncotarget.23607.

[171] Tannock IF, Lee CM, Tunggal JK, Cowan DS, Egorin MJ. Limited penetration of anticancer drugs through tumor tissue: a potential cause of resistance of solid tumors to chemotherapy. *Clin Cancer Res*. 2002;8(3):878-884.

[172] Trédan O, Galmarini CM, Patel K, Tannock IF. Drug resistance and the solid tumor microenvironment. *J Natl Cancer Inst*. 2007;99(19):1441-1454. doi:10.1093/jnci/djm135.

[173] Vidal SJ, Rodriguez-Bravo V, Galsky M, Cordon-Cardo C, Domingo-Domenech J. Targeting cancer stem cells to suppress acquired chemotherapy resistance. *Oncogene*. 2014;33(36):4451-4463. doi:10.1038/onc.2013.411.

[174] Zanoni M, Cortesi M, Zamagni A, Arienti C, Pignatta S, Tesei A. Modeling neoplastic disease with spheroids and organoids. *J Hematol Oncol*. 2020;13(1):97. Published 2020 Jul 16. doi:10.1186/s13045-020-00931-0.

[175] Ivascu A, Kubbies M. Rapid generation of single-tumor spheroids for high-throughput cell function and toxicity analysis. *J Biomol Screen*. 2006;11(8):922-932. doi:10.1177/1087057106292763.

[176] Nunes AS, Barros AS, Costa EC, Moreira AF, Correia IJ. 3D tumor spheroids as in vitro models to mimic in vivo human solid tumors resistance to therapeutic drugs. *Biotechnol Bioeng*. 2019;116(1):206-226. doi:10.1002/bit.26845.

[177] Drost J, Clevers H. Organoids in cancer research. *Nat Rev Cancer*. 2018;18(7):407-418. doi:10.1038/s41568-018-0007-6.

[178] Bleijs M, van de Wetering M, Clevers H, Drost J. Xenograft and organoid model systems in cancer research. *EMBO J*. 2019;38(15):e101654. doi:10.15252/embj.2019101654.

[179] Takahashi T. Organoids for Drug Discovery and Personalized Medicine. *Annu Rev Pharmacol Toxicol*. 2019;59:447-462. doi:10.1146/annurev-pharmtox-010818-021108.

[180] Zanoni M, Cortesi M, Zamagni A, Arienti C, Pignatta S, Tesei A. Modeling neoplastic disease with spheroids and organoids. *J Hematol Oncol*. 2020;13(1):97. Published 2020 Jul 16. doi:10.1186/s13045-020-00931-0.

[181] Clevers H. Modeling Development and Disease with Organoids. *Cell*. 2016;165(7):1586-1597. doi:10.1016/j.cell.2016.05.082.

[182] van de Wetering M, Francies HE, Francis JM, et al. Prospective derivation of a living organoid biobank of colorectal cancer patients. *Cell*. 2015;161(4):933-945. doi:10.1016/j.cell.2015.03.053.

[183] Phan N, Hong JJ, Tofig B, et al. A simple high-throughput approach identifies actionable drug sensitivities in patient-derived tumor organoids. *Commun Biol*. 2019;2:78. Published 2019 Feb 25. doi:10.1038/s42003-019-0305-x.

[184] Bartfeld S, Clevers H. Stem cell-derived organoids and their application for medical research and patient treatment. *J Mol Med (Berl)*. 2017;95(7):729-738. doi:10.1007/s00109-017-1531-7.

[185] Phan N, Hong JJ, Tofig B, et al. A simple high-throughput approach identifies actionable drug sensitivities in patient-derived tumor organoids. *Commun Biol*. 2019;2:78. Published 2019 Feb 25. doi:10.1038/s42003-019-0305-x.

[186] Letai A. Functional precision cancer medicine-moving beyond pure genomics. *Nat Med*. 2017;23(9):1028-1035. doi:10.1038/nm.4389.

[187] Drost J, Clevers H. Organoids in cancer research. *Nat Rev Cancer*. 2018;18(7):407-418. doi:10.1038/s41568-018-0007-6.

[188] Huang L, Holtzinger A, Jagan I, et al. Ductal pancreatic cancer modeling and drug screening using human pluripotent stem cell- and patient-derived tumor organoids. *Nat Med*. 2015;21(11):1364-1371. doi:10.1038/nm.3973.

[189] Phan N, Hong JJ, Tofig B, et al. A simple high-throughput approach identifies actionable drug sensitivities in patient-derived tumor organoids. *Commun Biol*. 2019;2:78. Published 2019 Feb 25. doi:10.1038/s42003-019-0305-x.

[190] Phan N, Hong JJ, Tofig B, et al. A simple high-throughput approach identifies actionable drug sensitivities in patient-derived tumor organoids. *Commun Biol*. 2019;2:78. Published 2019 Feb 25. doi:10.1038/s42003-019-0305-x.

[191] Nguyen HTL, Soragni A. Patient-Derived Tumor Organoid Rings for Histologic Characterization and High-Throughput Screening. *STAR Protoc*. 2020;1(2):100056. doi:10.1016/j.xpro.2020.100056.

[192] Matano M, Date S, Shimokawa M, et al. Modeling colorectal cancer using CRISPR-Cas9-mediated engineering of human intestinal organoids. *Nat Med*. 2015;21(3):256-262. doi:10.1038/nm.3802.

[193] Drost J, van Boxtel R, Blokzijl F, et al. Use of CRISPR-modified human stem cell organoids to study the origin of mutational signatures in cancer. *Science*. 2017;358(6360):234-238. doi:10.1126/science.aao3130.

[194] Neal JT, Li X, Zhu J, et al. Organoid Modeling of the Tumor Immune Microenvironment. *Cell*. 2018;175(7):1972-1988.e16. doi:10.1016/j.cell.2018.11.021.

[195] Zumwalde NA, Haag JD, Sharma D, et al. Analysis of Immune Cells from Human Mammary Ductal Epithelial Organoids Reveals Vδ2+ T Cells That Efficiently Target Breast Carcinoma Cells in the Presence of Bisphosphonate. *Cancer Prev Res (Phila)*. 2016;9(4):305-316. doi:10.1158/1940-6207.CAPR-15-0370-T.

[196] Schnalzger TE, de Groot MH, Zhang C, et al. 3D model for CAR-mediated cytotoxicity using patient-derived colorectal cancer organoids. *EMBO J*. 2019;38(12):e100928. doi:10.15252/embj.2018100928.

[197] Endo Y, Mitsui K, Motizuki M, Tsurugi K. The mechanism of action of ricin and related toxic lectins on eukaryotic ribosomes. The site and the characteristics of the modification in 28 S ribosomal RNA caused by the toxins. *J Biol Chem*. 1987;262(12):5908-5912.

[198] Barbieri L, Valbonesi P, Bonora E, Gorini P, Bolognesi A, Stirpe F. Polynucleotide:adenosine glycosidase activity of ribosome-inactivating proteins: effect on DNA, RNA and poly(A). *Nucleic Acids Res*. 1997;25(3):518-522. doi:10.1093/nar/25.3.518.

[199] Polito L, Djemil A, Bortolotti M. Plant Toxin-Based Immunotoxins for Cancer Therapy: A Short Overview. *Biomedicines*. 2016;4(2):12. Published 2016 Jun 1. doi:10.3390/biomedicines4020012.

[200] Dyson KA, Stover BD, Grippin A, et al. Emerging trends in immunotherapy for pediatric sarcomas. J Hematol Oncol. 2019;12(1):78. Published 2019 Jul 16. doi:10.1186/s13045-019-0756-z.

[201] Ferrari A, Dirksen U, Bielack S. Sarcomas of Soft Tissue and Bone. *Prog Tumor Res*. 2016;43:128-141. doi:10.1159/000447083.

[202] Gronchi A, Maki RG, Jones RL. Treatment of soft tissue sarcoma: a focus on earlier stages. *Future Oncol*. 2017;13(1s):13-21. doi:10.2217/fon-2016-0499.

[203] https://www.cancer.net/cancer-types/sarcomas-soft-tissue/statistics.

[204] van den Bulk J, Verdegaal EM, de Miranda NF. Cancer immunotherapy: broadening the scope of targetable tumours. *Open Biol*. 2018;8(6):180037. doi:10.1098/rsob.180037.

[205] Bolognesi A, Polito L. Immunotoxins and other conjugates: pre-clinical studies. *Mini Rev Med Chem*. 2004;4(5):563-583. doi:10.2174/1389557043403864.

[206] Polito L, Bortolotti M, Pedrazzi M, Bolognesi A. Immunotoxins and other conjugates containing saporin-s6 for cancer therapy. Toxins (Basel). 2011;3(6):697-720. doi: 10.3390/toxins3060697.

[207] Polito L, Calafato G, Bortolotti M, Chiarelli Olivari C, Maiello S, Bolognesi A. Antibody Conjugates for Sarcoma Therapy: How Far along Are We?. *Biomedicines*. 2021;9(8):978. Published 2021 Aug 8. doi:10.3390/biomedicines9080978.

[208] Imamura Y, Mukohara T, Shimono Y, et al. Comparison of 2D- and 3D-culture models as drug-testing platforms in breast cancer. *Oncol Rep*. 2015;33(4):1837-1843. doi:10.3892/or.2015.3767.

[209] Duval K, Grover H, Han LH, et al. Modeling Physiological Events in 2D vs. 3D Cell Culture. *Physiology (Bethesda)*. 2017;32(4):266-277. doi:10.1152/physiol.00036.2016.

[210] Ryu NE, Lee SH, Park H. Spheroid Culture System Methods and Applications for Mesenchymal Stem Cells. *Cells*. 2019;8(12):1620. Published 2019 Dec 12. doi:10.3390/cells8121620.

[211] Zanoni M, Cortesi M, Zamagni A, Arienti C, Pignatta S, Tesei A. Modeling neoplastic disease with spheroids and organoids. *J Hematol Oncol*. 2020;13(1):97. Published 2020 Jul 16. doi:10.1186/s13045-020-00931-0.

[212] Wu H, Zhang J, Dai R, Xu J, Feng H. Transferrin receptor-1 and VEGF are prognostic factors for osteosarcoma. J Orthop Surg Res. 2019;14(1):296. Published 2019 Sep 4. doi:10.1186/s13018-019-1301-z.

[213] Ahmed N, Brawley VS, Hegde M, et al. Human Epidermal Growth Factor Receptor 2 (HER2) -Specific Chimeric Antigen Receptor-Modified T Cells for the Immunotherapy of HER2-Positive Sarcoma. J Clin Oncol. 2015;33(15):1688-1696. doi:10.1200/JCO.2014.58.0225.

[214] Ricci C, Polito L, Nanni P, et al. HER/erbB receptors as therapeutic targets of immunotoxins in human rhabdomyosarcoma cells. J Immunother. 2002;25(4):314-323. doi:10.1097/00002371-200207000-0000.

[215] Braun AC, de Mello CAL, Corassa M, et al. EGFR expression in circulating tumor cells from high-grade metastatic soft tissue sarcomas. Cancer Biol Ther. 2018;19(6):454-460. doi:10.1080/15384047.2018.1433498.

[216] Daniels-Wells TR, Penichet ML. Transferrin receptor 1: a target for antibody-mediated cancer therapy. *Immunotherapy*. 2016;8(9):991-994. doi:10.2217/imt-2016-0050.

[217] Candelaria PV, Leoh LS, Penichet ML, Daniels-Wells TR. Antibodies Targeting the Transferrin Receptor 1 (TfR1) as Direct Anti-cancer Agents. *Front Immunol*. 2021;12:607692. Published 2021 Mar 17. doi:10.3389/fimmu.2021.607692.

[218] Maennling AE, Tur MK, Niebert M, et al. Molecular Targeting Therapy against EGFR Family in Breast Cancer: Progress and Future Potentials. *Cancers (Basel)*. 2019;11(12):1826. Published 2019 Nov 20. doi:10.3390/cancers11121826.

[219] Shen Y, Li X, Dong D, Zhang B, Xue Y, Shang P. Transferrin receptor 1 in cancer: a new sight for cancer therapy. *Am J Cancer Res*. 2018;8(6):916-931. Published 2018 Jun 1.

[220] Stirpe F, Gasperi-Campani A, Barbieri L, Falasca A, Abbondanza A, Stevens WA. Ribosome-inactivating proteins from the seeds of Saponaria officinalis L. (soapwort), of Agrostemma githago L. (corn cockle) and of Asparagus officinalis L. (asparagus), and from the latex of Hura crepitans L. (sandbox tree). Biochem J. 1983;216(3):617-625. doi:10.1042/bj2160617.

[221] Bolognesi A, Olivieri F, Battelli MG, et al. Ribosome-inactivating proteins (RNA N-glycosidases) from the seeds of Saponaria ocymoides and Vaccaria pyramidata. Eur J Biochem. 1995;228(3):935-940. doi:10.1111/j.1432-1033.1995.tb20343.xandbox tree). Biochem J. 1983;216(3):617-625. doi:10.1042/bj2160617.

[222] Gosselaar PH, van-Dijk AJ, de-Gast GC, et al. Transferrin toxin but not transferrin receptor immunotoxin is influenced by free transferrin and iron saturation. Eur J Clin Invest. 2002;32 Suppl 1:61-69. doi:10.1046/j.1365-2362.2002.0320s1061.x.

[223] Di Massimo AM, Di Loreto M, Pacilli A, et al. Immunoconjugates made of an anti-EGF receptor monoclonal antibody and type 1 ribosome-inactivating proteins from Saponaria ocymoides or Vaccaria pyramidata. Br J Cancer. 1997;75(6):822-828. doi:10.1038/bjc.1997.147.

[224] Nguyen HTL, Soragni A. Patient-Derived Tumor Organoid Rings for Histologic Characterization and High-Throughput Screening. STAR Protoc. 2020;1(2):100056. doi:10.1016/j.xpro.2020.100056.

[225] Wu H, Zhang J, Dai R, Xu J, Feng H. Transferrin receptor-1 and VEGF are prognostic factors for osteosarcoma. J Orthop Surg Res. 2019;14(1):296. Published 2019 Sep 4. doi:10.1186/s13018-019-1301-z.

[226] Ahmed N, Brawley VS, Hegde M, et al. Human Epidermal Growth Factor Receptor 2 (HER2) -Specific Chimeric Antigen Receptor-Modified T Cells for the Immunotherapy of HER2-Positive Sarcoma. J Clin Oncol. 2015;33(15):1688-1696. doi:10.1200/JCO.2014.58.0225.

[227] Ricci C, Polito L, Nanni P, et al. HER/erbB receptors as therapeutic targets of immunotoxins in human rhabdomyosarcoma cells. J Immunother. 2002;25(4):314-323. doi:10.1097/00002371-200207000-0000.

228 Braun AC, de Mello CAL, Corassa M, et al. EGFR expression in circulating tumor cells from high-grade metastatic soft tissue sarcomas. Cancer Biol Ther. 2018;19(6):454-460. doi:10.1080/15384047.2018.1433498.

[229] Barzegar Behrooz A, Syahir A, Ahmad S. CD133: beyond a cancer stem cell biomarker. J Drug Target. 2019;27(3):257-269. doi:10.1080/1061186X.2018.1479756.

[230] Niesen J, Brehm H, Stein C, et al. In vitro effects and ex vivo binding of an EGFR-specific immunotoxin on rhabdomyosarcoma cells. J Cancer Res Clin Oncol. 2015;141(6):1049-1061. doi:10.1007/s00432-014-1884-z.

[231] Leone F, Perissinotto E, Cavalloni G, et al. Expression of the c-ErbB-2/HER2 proto-oncogene in normal hematopoietic cells. J Leukoc Biol. 2003;74(4):593-601. doi:10.1189/jlb.0203068.

[232] Bolognesi A, Tazzari PL, Olivieri F, Polito L, Falini B, Stirpe F. Induction of apoptosis by ribosome-inactivating proteins and related immunotoxins. Int J Cancer. 1996;68(3):349-55.

[233] Bergamaschi G, Perfetti V, Tonon L, et al. Saporin, a ribosome-inactivating protein used to prepare immunotoxins, induces cell death via apoptosis. Br J Haematol. 1996;93(4):789-794. doi:10.1046/j.1365-2141.1996.d01-1730.x.

[234] Polito L, Mercatelli D, Bortolotti M, et al. Two Saporin-Containing Immunotoxins Specific for CD20 and CD22 Show Different Behavior in Killing Lymphoma Cells. Toxins (Basel). 2017;9(6):182. Published 2017 May 30. doi:10.3390/toxins9060182.

[235] Ishiguro T, Ohata H, Sato A, Yamawaki K, Enomoto T, Okamoto K. Tumor-derived spheroids: Relevance to cancer stem cells and clinical applications. Cancer Sci. 2017;108(3):283-289. doi:10.1111/cas.13155.

[236] Ferrari A, Dirksen U, Bielack S. Sarcomas of Soft Tissue and Bone. *Prog Tumor Res*. 2016;43:128-141. doi:10.1159/000447083.

[237] Gronchi A, Maki RG, Jones RL. Treatment of soft tissue sarcoma: a focus on earlier stages. *Future Oncol*. 2017;13(1s):13-21. doi:10.2217/fon-2016-0499.

[238] https://www.cancer.net/cancer-types/sarcomas-soft-tissue/statistics.

[239] Polito L, Djemil A, Bortolotti M. Plant Toxin-Based Immunotoxins for Cancer Therapy: A Short Overview. *Biomedicines*. 2016;4(2):12. doi:10.3390/biomedicines4020012.

[240] Gilabert-Oriol R, Weng A, Mallinckrodt Bv, Melzig MF, Fuchs H, Thakur M. Immunotoxins constructed with ribosome-inactivating proteins and their enhancers: a lethal cocktail with tumor specific efficacy. *Curr Pharm Des*. 2014;20(42):6584-6643. doi:10.2174/1381612820666140826153913.

241 Kimlin LC, Casagrande G, Virador VM. In vitro three-dimensional (3D) models in cancer research: an update. Mol Carcinog. 2013;52(3):167-182. doi:10.1002/mc.21844.

[242] Zanoni M, Cortesi M, Zamagni A, Arienti C, Pignatta S, Tesei A. Modeling neoplastic disease with spheroids and organoids. *J Hematol Oncol*. 2020;13(1):97. Published 2020 Jul 16. doi:10.1186/s13045-020-00931-0.

[243] Daniels-Wells TR, Penichet ML. Transferrin receptor 1: a target for antibody-mediated cancer therapy. *Immunotherapy*. 2016;8(9):991-994. doi:10.2217/imt-2016-0050.

[244] Candelaria PV, Leoh LS, Penichet ML, Daniels-Wells TR. Antibodies Targeting the Transferrin Receptor 1 (TfR1) as Direct Anti-cancer Agents. *Front Immunol*. 2021;12:607692. Published 2021 Mar 17. doi:10.3389/fimmu.2021.607692.

[245] Maennling AE, Tur MK, Niebert M, et al. Molecular Targeting Therapy against EGFR Family in Breast Cancer: Progress and Future Potentials. *Cancers (Basel)*. 2019;11(12):1826. Published 2019 Nov 20. doi:10.3390/cancers11121826.

[246] Shen Y, Li X, Dong D, Zhang B, Xue Y, Shang P. Transferrin receptor 1 in cancer: a new sight for cancer therapy. *Am J Cancer Res*. 2018;8(6):916-931. Published 2018 Jun 1.

[247] Braun AC, de Mello CAL, Corassa M, et al. EGFR expression in circulating tumor cells from high-grade metastatic soft tissue sarcomas. *Cancer Biol Ther*. 2018;19(6):454-460. doi:10.1080/15384047.2018.1433498.

[248] Ahmed N, Brawley VS, Hegde M, et al. Human Epidermal Growth Factor Receptor 2 (HER2) -Specific Chimeric Antigen Receptor-Modified T Cells for the Immunotherapy of HER2-Positive Sarcoma. *J Clin Oncol*. 2015;33(15):1688-1696. doi:10.1200/JCO.2014.58.0225.

[249] Wu H, Zhang J, Dai R, Xu J, Feng H. Transferrin receptor-1 and VEGF are prognostic factors for osteosarcoma. *J Orthop Surg Res*. 2019;14(1):296. Published 2019 Sep 4. doi:10.1186/s13018-019-1301-z.

[250] Ricci C, Polito L, Nanni P, et al. HER/erbB receptors as therapeutic targets of immunotoxins in human rhabdomyosarcoma cells. *J Immunother*. 2002;25(4):314-323. doi:10.1097/00002371-200207000-00003.

[251] Cazzola M, Bergamaschi G, Dezza L, et al. Cytotoxic activity of an anti-transferrin receptor immunotoxin on normal and leukemic human hematopoietic progenitors. *Cancer Res*. 1991;51(2):536-541.

[252] Simon N, FitzGerald D. Immunotoxin Therapies for the Treatment of Epidermal Growth Factor Receptor-Dependent Cancers. *Toxins (Basel)*. 2016;8(5):137. Published 2016 May 4. doi:10.3390/toxins8050137.

[253] Ishiguro T, Ohata H, Sato A, Yamawaki K, Enomoto T, Okamoto K. Tumor-derived spheroids: Relevance to cancer stem cells and clinical applications. *Cancer Sci*. 2017;108(3):283-289. doi:10.1111/cas.13155.

[254] Bai X, Ni J, Beretov J, Graham P, Li Y. Cancer stem cell in breast cancer therapeutic resistance. *Cancer Treat Rev*. 2018;69:152-163. doi:10.1016/j.ctrv.2018.07.004.

[255] Brancato V, Oliveira JM, Correlo VM, Reis RL, Kundu SC. Could 3D models of cancer enhance drug screening? Biomaterials. 2020. 232:119744.doi:10.1016/j.biomaterials.

2019.119744.

[256] Phan N, Hong JJ, Tofig B, et al. A simple high-throughput approach identifies actionable drug sensitivities in patient-derived tumor organoids. *Commun Biol*. 2019;2:78. Published 2019 Feb 25. doi:10.1038/s42003-019-0305-x.

[257] Sant S, Johnston PA. The production of 3D tumor spheroids for cancer drug discovery. *Drug Discov Today Technol*. 2017;23:27-36. doi:10.1016/j.ddtec.2017.03.002.

[258] Nguyen HTL, Soragni A. Patient-Derived Tumor Organoid Rings for Histologic Characterization and High-Throughput Screening. *STAR Protoc*. 2020;1(2):100056. doi:10.1016/j.xpro.2020.100056.

[259] Ricci C, Polito L, Nanni P, et al. HER/erbB receptors as therapeutic targets of immunotoxins in human rhabdomyosarcoma cells. *J Immunother*. 2002;25(4):314-323. doi:10.1097/00002371-200207000-00003.

[260] Ricci C, Landuzzi L, Rossi I, et al. Expression of HER/erbB family of receptor tyrosine kinases and induction of differentiation by glial growth factor 2 in human rhabdomyosarcoma cells. *Int J Cancer*. 2000;87(1):29-36.

[261] Liu M, Sun LL, Li YJ, et al. Trastuzumab enhanced the cytotoxicity of Vγ9Vδ2 T cells against zoledronate-sensitized osteosarcoma cells. *Int Immunopharmacol*. 2015;28(1):160-167. doi:10.1016/j.intimp.2015.06.002.

[262] Wang J, Wang G, Li B, Qiu C, He M. miR-141-3p is a key negative regulator of the EGFR pathway in osteosarcoma. *Onco Targets Ther*. 2018;11:4461-4478. Published 2018 Jul 31. doi:10.2147/OTT.S171304.

[263] Wu H, Zhang J, Dai R, Xu J, Feng H. Transferrin receptor-1 and VEGF are prognostic factors for osteosarcoma. J Orthop Surg Res. 2019;14(1):296. Published 2019 Sep 4. doi:10.1186/s13018-019-1301-z

[264] Jiang X, Gwye Y, Russell D, et al. CD133 expression in chemo-resistant Ewing sarcoma cells. *BMC Cancer*. 2010;10:116. Published 2010 Mar 26. doi:10.1186/1471-2407-10-116.

[265] Walcher L, Kistenmacher AK, Suo H, et al. Cancer Stem Cells-Origins and Biomarkers: Perspectives for Targeted Personalized Therapies. *Front Immunol*. 2020;11:1280. Published 2020 Aug 7. doi:10.3389/fimmu.2020.01280.

[266] Di Massimo AM, Di Loreto M, Pacilli A, et al. Immunoconjugates made of an anti-EGF receptor monoclonal antibody and type 1 ribosome-inactivating proteins from Saponaria ocymoides or Vaccaria pyramidata. *Br J Cancer*. 1997;75(6):822-828. doi:10.1038/bjc.1997.147.

[267] Gosselaar PH, van-Dijk AJ, de-Gast GC, et al. Transferrin toxin but not transferrin receptor immunotoxin is influenced by free transferrin and iron saturation. *Eur J Clin Invest*. 2002;32 Suppl 1:61-69. doi:10.1046/j.1365-2362.2002.0320s1061.x.

[268] Niesen J, Brehm H, Stein C, et al. In vitro effects and ex vivo binding of an EGFR-specific immunotoxin on rhabdomyosarcoma cells. *J Cancer Res Clin Oncol*. 2015;141(6):1049-1061. doi:10.1007/s00432-014-1884-z.

[269] Niesen J, Stein C, Brehm H, et al. Novel EGFR-specific immunotoxins based on panitumumab and cetuximab show in vitro and ex vivo activity against different tumor entities. *J Cancer Res Clin Oncol*. 2015;141(12):2079-2095. doi:10.1007/s00432-015-1975-5.

[270] Pilbeam K, Wang H, Taras E, et al. Targeting pediatric sarcoma with a bispecific ligand immunotoxin targeting urokinase and epidermal growth factor receptors. *Oncotarget*. 2017;9(15):11938-11947. Published 2017 Sep 23. doi:10.18632/oncotarget.21187.

[271] Waldron NN, Barsky SH, Dougherty PR, Vallera DA. A bispecific EpCAM/CD133-targeted toxin is effective against carcinoma. *Target Oncol*. 2014;9(3):239-249. doi:10.1007/s11523-013-0290-9.

[272] Boyer JZ, Phillips GDL, Nitta H, et al. Activity of trastuzumab emtansine (T-DM1) in 3D cell culture. *Breast Cancer Res Treat*. 2021;188(1):65-75. doi:10.1007/s10549-021-06272-x.

[273] Takahashi N, Hoshi H, Higa A, et al. An In Vitro System for Evaluating Molecular Targeted Drugs Using Lung Patient-Derived Tumor Organoids. Cells. 2019;8(5):481. Published 2019 May 20. doi:10.3390/cells8050481

[274] Balalaeva IV, Sokolova EA, Puzhikhina AD, Brilkina AA, Deyev SM. Spheroids of HER2-Positive Breast Adenocarcinoma for Studying Anticancer Immunotoxins In Vitro. *Acta Naturae*. 2017;9(1):38-43.

[275] Xiang X, Phung Y, Feng M, et al. The development and characterization of a human mesothelioma in vitro 3D model to investigate immunotoxin therapy. *PLoS One*. 2011;6(1):e14640. Published 2011 Jan 31. doi:10.1371/journal.pone.0014640.

[276] Nath S, Devi GR. Three-dimensional culture systems in cancer research: Focus on tumor spheroid model. *Pharmacol Ther*. 2016;163:94-108. doi:10.1016/j.pharmthera.2016.03.013.

[277] Phi LTH, Sari IN, Yang YG, et al. Cancer Stem Cells (CSCs) in Drug Resistance and their Therapeutic Implications in Cancer Treatment. *Stem Cells Int*. 2018;2018:5416923. Published 2018 Feb 28. doi:10.1155/2018/5416923.

[278] Najafi M, Mortezaee K, Majidpoor J. Cancer stem cell (CSC) resistance drivers. *Life Sci*. 2019;234:116781. doi:10.1016/j.lfs.2019.116781.

[279] Golay J, Taylor RP. The Role of Complement in the Mechanism of Action of Therapeutic Anti-Cancer mAbs. *Antibodies (Basel)*. 2020;9(4):58. Published 2020 Oct 28. doi:10.3390/antib9040058.

[280] Smith MR. Rituximab (monoclonal anti-CD20 antibody): mechanisms of action and resistance. *Oncogene*. 2003;22(47):7359-7368. doi:10.1038/sj.onc.1206939.

[281] Chen S, Lóssio CF, Verbeke I, et al. The type-1 ribosome-inactivating protein OsRIP1 triggers caspase-independent apoptotic-like death in HeLa cells [published online ahead of print, 2021 Sep 30]. *Food Chem Toxicol*. 2021;157:112590. doi:10.1016/j.fct.2021.112590.

[282] Polito L, Bortolotti M, Farini V, Battelli MG, Barbieri L, Bolognesi A. Saporin induces multiple death pathways in lymphoma cells with different intensity and timing as compared to ricin. *Int J Biochem Cell Biol*. 2009;41(5):1055-1061. doi:10.1016/j.biocel.2008.09.021.

[283] Polito L, Bortolotti M, Pedrazzi M, Mercatelli D, Battelli MG, Bolognesi A. Apoptosis and necroptosis induced by stenodactylin in neuroblastoma cells can be completely prevented through caspase inhibition plus catalase or necrostatin-1. *Phytomedicine*. 2016;23(1):32-41. doi:10.1016/j.phymed.2015.11.006.

[284] Polito L, Mercatelli D, Bortolotti M, et al. Two Saporin-Containing Immunotoxins Specific for CD20 and CD22 Show Different Behavior in Killing Lymphoma Cells. *Toxins (Basel)*. 2017;9(6):182. Published 2017 May 30. doi:10.3390/toxins9060182.

[285] Polito L, Bolognesi A, Tazzari PL, et al. The conjugate Rituximab/saporin-S6 completely inhibits clonogenic growth of CD20-expressing cells and produces a synergistic toxic effect with Fludarabine. *Leukemia*. 2004;18(7):1215-1222. doi:10.1038/sj.leu.2403378.

[286] Battelli MG, Polito L, Bolognesi A, Lafleur L, Fradet Y, Stirpe F. Toxicity of ribosome-inactivating proteins-containing immunotoxins to a human bladder carcinoma cell line. *Int J Cancer*. 1996;65(4):485-490. doi:10.1002/(SICI)1097-0215(19960208)65:4<485::AID-IJC16>3.0.CO;2-9.

[287] Ricci C, Polito L, Nanni P, et al. HER/erbB receptors as therapeutic targets of immunotoxins in human rhabdomyosarcoma cells. *J Immunother*. 2002;25(4):314-323. doi:10.1097/00002371-200207000-00003.